Peptides and Peptide Dendrimers as Drug Delivery and Anticancer Agents

Inaugural dissertation

of the Faculty of Science,

University of Bern

presented by

Elena Zakharova

from Russian Federation

Supervisor of the doctoral thesis:

Prof. Dr. Jean-Louis Reymond

Department of Chemistry, Biochemistry

and Pharmaceutical Sciences

University of Bern

Peptides and Peptide Dendrimers as Drug Delivery and Anticancer Agents

Inaugural dissertation

of the Faculty of Science,

University of Bern

presented by

Elena Zakharova

from Russian Federation

Supervisor of the doctoral thesis:

Prof. Dr. Jean-Louis Reymond

Department of Chemistry, Biochemistry

and Pharmaceutical Sciences

University of Bern

Accepted by the Faculty of Science.

Bern, 17.10.2022 The Dean

Prof. Dr. Zoltan Balogh

Dedicated to my grandmother Nadezhda, who raised me, but hasn't managed to observe during her lifetime my Ph.D. thesis defense

«Fais ce que tu dois, advienne que pourra»

Делай, что должен, и будь, что будет

Acknowledgements

In these lines, I would like to acknowledge all the people without whom my research endeavor would not have been possible.

First of all, I would like to express my deepest gratitude to **Prof. Dr. Jean-Louis Reymond** for giving me the opportunity to work in his group at the University of Bern and perform PhD studies under his supervision. I am grateful for his great ideas, helpful suggestions, continuous support, and for providing trust and scientific freedom to perform the work in my way. Thank you for your humanity, empathy, and recognition of my small achievements, which kept me motivated to go on with the projects, even when something was not working.

I'm extremely grateful to **Prof. Dr. Nina Hartrampf** for her precious time evaluating my PhD dissertation and examining by PhD defence, and **Prof. Dr. Francesca Paradisi** for agreeing to chair my PhD defence.

My special thanks to **Dr. Sacha Javor** and **Dr. Kapila Gunasekera** for valuable discussions and scientific advice, which helped me a lot to move the projects forward and to accomplish the thesis. I would like to express my appreciation to my colleagues, including **Dr. Bee Ha Gan** and **Dr. Susanna Zamolo** for sharing their practical experience in cell-based assays, **Xingguang Cai** for showing me bacterial cell culture, **Dr. Thissa Siriwardena** for introduction to peptide synthesis, **PD. Dr. Eduard Babiychuk** for assistance in confocal microscopy. I would like to mention **Alice**, **Markus**, **Hippolyte,** and **Etienne** for the perfect teamwork and collaboration on the projects which contributed to this thesis. Besides, I would like to thank the past and present group members (**Marc**, **Giorgio**, **Daniel**, **Josep**, **Kris**, **Amol**, **Dina**, **Aline**, **Kleni**, **Celine**, **David**, **Ye**, **Thierry**, **Mario**, **Samuel,** and those who I may have forgotten to mention) for a great atmosphere in the lab and for the best time beyond work.

Many thanks to **Sandra Zbinden** and **Beatrice Thönen** for taking care of all the administrative questions and coordinating my relocation to Switzerland. I would be remiss in not mentioning the "Ausgabe"-team for their effective work in ordering the reagents and kits necessary for my research, MS-, "Werkstatt"- and "Hausdienst"-teams for providing excellent service and always maintaining good working conditions.

Sincere gratitude to my parents, **Olga** and **Aleksei** for their endless love and encouragement during my PhD work. Special thanks to my soulmate **Vladimir** (aka "Koshak") for his moral

support and for believing in me. I would like to acknowledge my friends **Dasha**, **Masha**, **Boris**, **Egor**, **Dima**, and **Julia** for being around in good and hard times and for their kindness.

Table of contents

List of abbreviations 9
1. General Introduction 11
1.1. Cancer and problem of drug resistance 11
1.2. Doxorubicin and analogs 13
1.3. Platinum drugs 14
1.4. Drug delivery strategies for small molecules cancer therapeutics 17
1.5. Anticancer peptides 21
1.5.1. Features of cancer cell and bacterial membranes 21
1.5.2. Membranolytic ACPs 23
1.5.2.1. Mechanisms of membrane lysis 23
1.5.3. Other targets of ACPs 25
1.5.4. Databases containing ACPs 26
1.6. Overview of the thesis 28
2. Peptide Dendrimers for Doxorubicin Delivery to Cancer Cells 29
2.1. Abstract 29
2.2. Introduction 29
2.3. Results and discussion 32
2.3.1. Synthesis of Doxorubicin conjugates Z9-Z13 32
2.3.2. Anticancer activity of Z9, Z10, Z13 conjugates 35
2.3.3. Synthesis of Diacetoxy-alkyl doxorubicin conjugates 37
2.4. Conclusion and Outlook 40
3. Peptide Dendrimers for DACHPt Delivery to Cancer Cells 43
3.1. Abstract 43
3.2. Introduction 43
3.3. Results and discussion 45
3.3.1. Synthesis 45
3.3.2. Critical aggregation concentration 50
3.3.3. Cytotoxicity measurements 52
3.4. Conclusion 54
4. Machine Learning Guided Discovery of Non-Hemolytic Membrane Disruptive Anticancer Peptides 55
4.1. Abstract 55

4.2. Introduction 56
4.3. Results and discussion 57
4.3.1. ML-guided design 57
4.3.2. Synthesis and activity of ACPs toward eukaryotic cells 59
4.3.3. Antimicrobial activity 63
4.3.4. Synthesis and activity of D-amino acid substituted peptides 63
4.3.5. Circular dichroism 64
4.3.6. Lipid vesicle leakage assay 65
4.3.7. Cellular entrance and mode of action of AC peptides 66
4.3.7.1. Cellular uptake of fluorescein-labelled peptides 66
4.3.7.2. Propidium iodine (PI) permeabilization. 66
4.3.7.3. ACPs influence mitochondrial function 67
4.4. Conclusion 68
5. Peptide Dendrimers *vs* Isopeptide Dendrimers. Comparison of Antimicrobial and Anticancer Activities. 69
5.1. Abstract 69
5.2. Introduction 69
5.3. Results and discussion 70
5.3.1. Synthesis and structural characteristics of peptide dendrimers 70
5.3.2. Cytotoxicity and Hemolysis 73
5.3.3. Antimicrobial activity at different pH 75
5.4. Conclusion and outlook 76
6. General conclusion and outlook 79
7. Experimental part 81
7.1. Materials and Reagents 81
7.2. Solid-phase peptide synthesis (SPPS) 83
7.2.1. Manual synthesis of peptide dendrimers 83
7.2.2. Automated synthesis of peptide dendrimers 83
7.2.3. Manual synthesis of linear peptides and peptide dendrimers at elevated temperature 83
7.2.4. Synthesis of Fluorescein-labelled peptides 84
7.2.5. Alloc deprotection and fatty acid coupling 84
7.2.6. Cleavage and purification 85
7.3. Synthesis and Characterization of peptide dendrimers 85
7.4. Synthesis and Characterization of linear peptides 87

7.5. Synthesis and Characterization of small molecules, Dox-conjugates, and DACHPt conjugates 96
7.6. Cell- and bacteria-based assays 107
7.6.1. Cell culture conditions 107
7.6.2. Cell viability assay by AlamarBlue® 107
7.6.3. Hemolysis assay (MHC and HC_{50} determination) 107
7.6.4. Antimicrobial activity and MIC determination 108
7.7. Circular dichroism (CD) spectroscopy and helix wheel evaluation 109
7.8. Lipid vesicle leakage assays 109
7.9. Critical Micellar Concentration (CMC) 110
7.10. Acid-base titration 110
7.11. Release kinetics 111
7.12. Confocal microscopy 111
7.12.1. Cellular uptake of Z13 and Doxorubicin 111
7.12.2. Cellular uptake of fluorescein-labelled peptide 111
7.12.3. Colocalization studies 111
7.13. Flow cytometry 112
7.13.1. Cellular uptake 112
7.13.2. Propidium iodine (PI) internalization 112
7.13.3. Mitochondrial membrane depolarization 112
7.13.4. Annexin V-FITC /Propidium iodine (PI) staining 113
8. Supplementary data 115
8.1. Additional data for Chapter 2 115
8.2. Additional data for Chapter 4 119
8.3. Additional data for Chapter 5 125
9. Bibliography 129

List of abbreviations

Natural and unnatural L-amino acids used in this thesis were written in three and one letter code. D-amino acids were written in small letter codes, and the branching units were in *italics*.

C	Degree Celsius
ABC	ATP-binding cassette(transporters)
AcOH	Acetic acid
ACP	Anticancer peptide
ADEPT	Antibody-directed enzyme prodrug therapy
Alloc	Allyloxycarbonyl
AMP	Antimicrobial peptide
APD	Antimicrobial peptide database
Ar	Argon
BAX	Bcl-2-associated X protein
BCL-2	B-cell lymphoma-2 family protein
Boc	*tert*-butyloxycarbonyl
CancerPPD	Anticancer Peptide and Protein Database
CD	Circular dichroism
CHO	Chinese hamster ovary cell line
CMC	Critical micelle concentration
CPPD	Cell penetrating peptide dendrimers
CYP	Cytochrome P450
DACHPt	1,2-Diaminocyclohexane Platinum
DBAASP	Database of antimicrobial activity and structure of peptides
DBU	1,8-Diazabicyclo[5.4.0]undec-7-ene
DCM	Dichloromethane
DIC	Diisopropylcarbodiimide
DIPEA	*N*,*N*-Diisopropylethylamine
DL	Drug loading
DMAP	4-Dimethylaminopyridine
DMEM	Dulbecco's Modified Eagle Medium
DMF	*N*,*N*-Dimethylformamide
DNA	Deoxyribonucleic acid
DODT	3,6-Dioxa-1,8-octandithiol
DOX	Doxorubicin
EMA	European Medicines Agency
EPR	Enhanced permeability and retention
EtOH	Ethanol
FACS	Fluorescence-Activated Cell Sorting
FDA	U.S. Food and Drug Administration
GST	Glutathione *S*-transferase
H69,	Lung cancinoma
H69 AR	Chemoresistant Lung cancinoma
HC_{50}	The half maximal hemolytic concentration
HEK-293	Human embryonic kidney
HOBt	Hydroxybenzotriazole
hRBC	Human red blood cells
HRMS	High-resolution mass spectrometry
IC_{50}	The half maximal inhibitory concentration

ICP MS	Inductively coupled plasma mass spectrometry
LL-III	Lasioglossin III
LPS	lipopolysaccharide
MBA	Oncogenic marker
MCF-10a	Human mammary epithelial cell line
MCF-7	Human mammary adenocarcinoma
MDA-MB-231	Metastatic human breast cancer
MDR	Multidrug resistance
MeCN	Acetonitrile
MeOH	Methanol
MHC	Minimal hemolytic concentration
MIC	Minimum inhibitory concentration
ML	Machine learning
NMR	Nuclear magnetic resonance
NP	Nanoparticle
PA	Phosphatidic acids
PAMAM	Poly(amidoamine)
PB	Phosphate buffer
PC	Phosphatidylcholine
PDGA	Peptide design genetic algorithm
pDOX	2-pyrrolino-Doxorubicin
PEG	Polyethylene glycol
PG	Phosphatidyl glycerol
PI	Phosphatidylinositol
PS	Phosphatidylserine
r.t.	Room temperature
RNN	Recurrent neural network
ROS	Reactive oxygen species
RP-HPLC	Reversed-phase high-performance liquid chromatography
RPMI	Roswell Park Memorial Institute (Medium)
SIL	Self-immolative linker
siRNA	Small interfering RNA
SM	Sphingomyelin
SPPS	Solid-phase peptide synthesis
TBME	Methyl *tert*-butyl ether
TCEP	Tris(2-carboxyethyl)phosphine
TEA	Triethylamine
TFA	Trifluoroacetic acid
THF	Tetrahydrofuran
TIS	Triisopropylsilane
TMRE	Tetramethylrhodamine, ethyl ester
UGT	Uridine 5'-diphospho-glucuronosyltransferase
UV	Ultraviolet
wt	Weight
λ_{ex}	Excitation wavelength (nm)
λ_{em}	Emission wavelength (nm)
δ	Chemical shift
t_R	Retention time

1. General Introduction

1.1. Cancer and problem of drug resistance

Cancer remains one of the leading deadly diseases. In 2020, the World Health Organization reported that every sixth death worldwide is associated with cancer, and the number of diagnosed cancer cases is increasing yearly.[1] Chemotherapy is one of the major approaches to treat cancer by delivering a cytotoxic agent to the cancer cells.

The concept of chemotherapy for cancer treatment goes back to the beginning of the 20th century. In those days, surgery and radiotherapy were dominating approaches, but with time, it became clear that these radical interventions were not effective due to residual malignant tissues progressing to more aggressive cancers. Mechlorethamine was the first chemotherapy drug approved by U.S. Food and Drug Administration (FDA) in 1949.[2] Since then, a lot of effort has been put into developing new anticancer drugs. Although there has been considerable progress in the development of cancer therapies in recent years, problems continue to arise, particularly for chemotherapy, due to drug resistance, low specificity, and side effects of currently available drugs.[3]

Anticancer drug resistance is a complex process that arises from different sources. Several pathways enable or facilitate cancer cells' resistance to pharmaceutical treatment. These mechanisms can occur independently or in combination. The most common mechanisms of drug resistance reported to date are increased drug efflux, decreased drug uptake, drug inactivation, drug target alteration, cell death inhibition, increased DNA damage repair, epigenetic effects, and epithelial-mesenchymal transition (*Figure 1*).[2,4]

One of the well-studied mechanisms involves a physical process of drug elimination by increased efflux. This is achieved by overexpression of ATP-binding cassette (ABC) transporter family proteins, namely MDR1 (Multidrug Resistance Protein 1), MRPs (Multidrug Resistance Related Proteines), and BCRPs (Breast Cancer Resistance Proteins).[5] For compounds depending on active transport to penetrate the cell, resistance is associated with a decrease in expression of the solute carriers transporters (SLCs), resulting in a reduction of drug uptake.[6]

Some anticancer agents undergo chemical modifications making them biologically active in cells. On the other hand, metabolic degradation reduces the drug’s bioavailability which can lead to the development of a tolerance to the drug. The most essential cellular machineries

responsible for drug inactivation include the cytochrome P450 (CYP) system, the glutathione-*S*-transferase (GST) superfamily, and the uridine diphospho-glucuronosyltransferase (UGT) superfamily.[7]

For the alkylating anticancer drugs, which target and damage DNA (for example, cisplatin, and doxorubicin), the mechanism of DNA damage repair plays a crucial role in the development of chemoresistance. For example, platinum-based drugs such as cisplatin form DNA crosslinks, which lead to cell death. But nucleotide excision and homologous recombination repair systems allow to overcome the damages induced by the platinum crosslinks.[8]

Recent developments revealed some protein mutations associated with cancer. Inhibition of mutated oncogenic markers such as MBA, which are key drivers for cancer progression, is another strategy for cancer treatment.[9] Alteration of targets impacts drug binding, reducing or disabling the therapeutic effect. These types of target mutations ultimately lead to drug resistance.

Deregulation of proliferation combined with apoptosis inhibition is a common feature of many cancer cells. This anomaly is considered to precede cancer transformations. Most anticancer drugs aim to induce cancer cell death. Molecular mechanisms, including overexpression of antiapoptotic protein BCL-2 (B-cell lymphoma-2 family protein), downregulation, or mutation of proapoptotic proteins such as BAX (BCL-2-associated X protein), may impact resistance to anticancer drugs.[10]

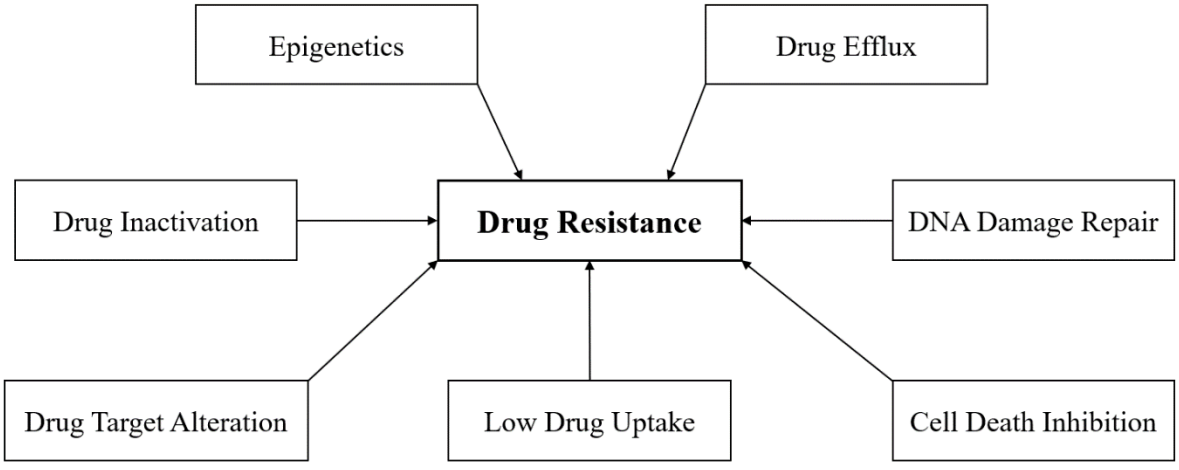

Figure 1. Most common mechanisms of drug resistance in cancer.

1.2. Doxorubicin and analogs

Doxorubicin (DOX), or Adriamycin, is an anthracycline drug first extracted from *Streptomyces peucetius* in the 1970s, and till now, it is broadly used in the treatment of several cancers (*Scheme 1*).[11] It is commonly used to treat some leukemias and Hodgkin's lymphoma but is also effective against breast, bladder, gastric, liver, and kidney cancers as well as Kaposi's sarcoma and neuroblastoma.[12]

The mechanism of action of Doxorubicin (DOX) has been debated since its discovery in the 70s. Several mechanisms have been proposed to explain its toxicity toward cancer cells. DOX can be taken up by cells through active transport with the help of organic cation transporter SLC22A16 or ABCB1 (also known as MDR1 or P-glycoprotein) and by passive diffusion.[13,14] It is reported that DOX can act by nuclei targeting or by indirect formation of reactive oxygen species (ROS), which ultimately lead to cell death. Three independent mechanisms impairing DNA function were observed: a) inhibition of the progression of topoisomerase II, b) intercalation into DNA structure due to the planar aromatic structure and formation of two C-9 hydroxyl-dependent hydrogen bonds with the guanine residue of DNA, c) formation of DNA cross-linking through daunosamine nitrogen in the presence of formaldehyde.[15]

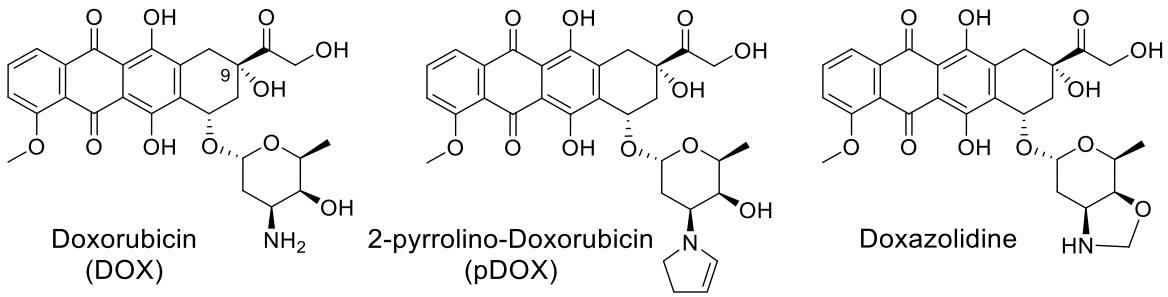

Scheme 1. Chemical structures of Doxorubicin, 2-pyrrolino-Doxorubicin and Doxazolidine.

Unfortunately, the clinical use of Doxorubicin has been limited due to its low selectivity and severe side effects, most common of which are cardiomyopathy, nephrotoxicity, hepatotoxicity, myelosuppression, and skin diseases. In addition to that, Doxorubicin treatment is prone to resistance development.

Therefore, the research on new anthracycline-based drugs with improved pharmacological properties is of great interest. One of the promising analogs of DOX is 2-pyrrolino-Doxorubicin (pDOX)[16]. The structure of pDOX is represented in *Scheme 1*. It showed a 500-fold increase in cytostatic activity for pDOX compared to free DOX.[17,18] It is proposed that introduction of the 5-membered ring plays a crucial role in the increased activity of the drug. The compound's

key feature is the formation of reactive iminium ions in slightly acidic media. Due to the strong electrophilic immonium group, the molecule is able to covalently bind DNA, which dramatically affects DNA function and facilitates the overcoming of DOX resistance (*Scheme 2*).[19]

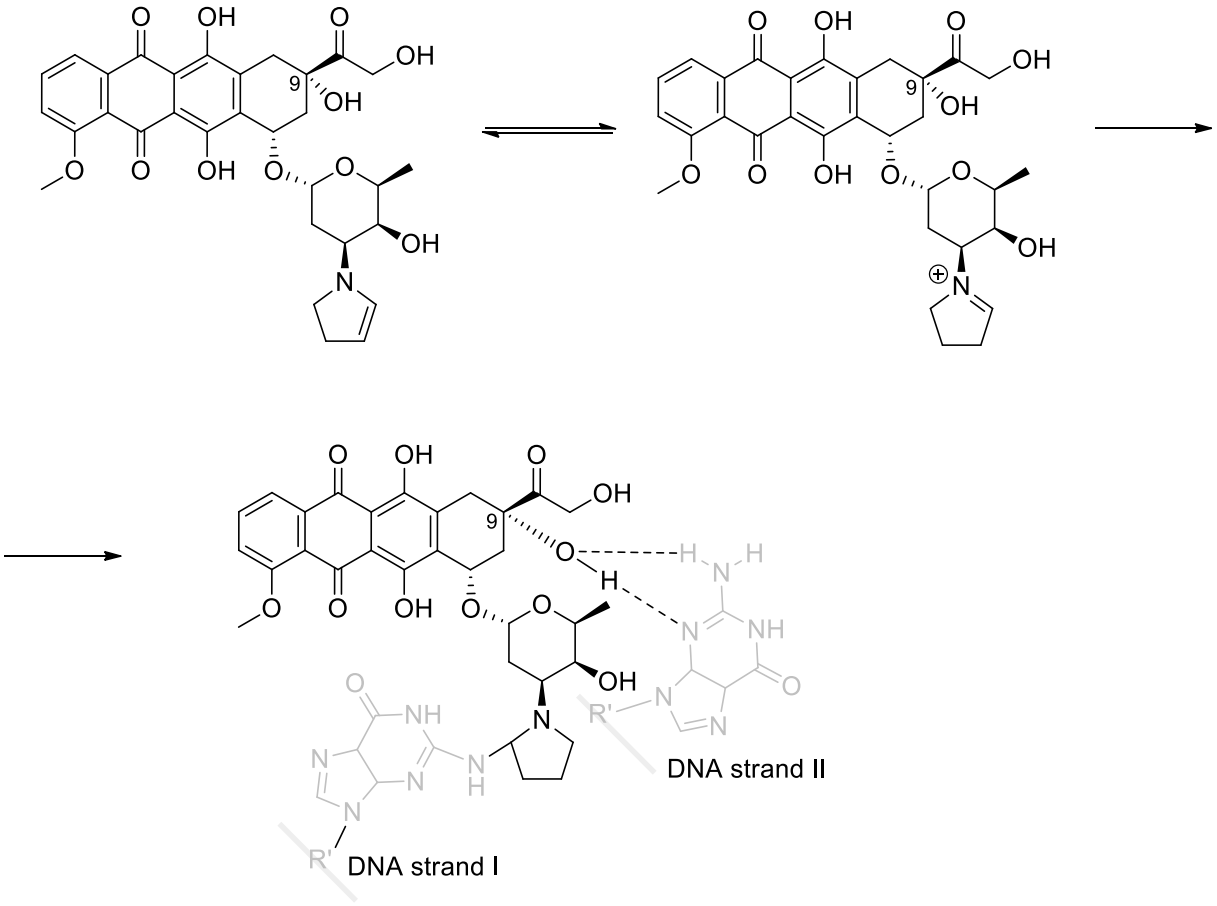

Scheme 2. Formation of pDOX–DNA adducts by reaction between reactive immonium ion and complementary DNA strands (in gray). Figure adapted from reference [19].

Another example of a DOX derivative is known in the literature as Doxazolidine (*Scheme 1*). The compound features an oxazolidine ring instead of a pyrroline moiety in pDOX. In this way, the oxazoline's methylene group in Doxazolidine can form an aminal linkage with the guanine residues of DNA. As a result, Doxazolidine has twice the activity of Doxorubicin and is efficient against DOX-resistant cancer cells.[20]

1.3. Platinum drugs

Platinum anticancer agents represent one of the great success stories in the field of inorganic therapeutics. The history started with the discovery of antiproliferative properties of cisplatin (*Scheme 3*) in the 1970s, following clinical approval in 1978. After more than 40 years,

platinum complexes remain one of the most widely used anticancer drugs in the world.[21] Cisplatin is used to treat testicular, ovarian, bladder, and other carcinomas.

The next generation of Pt(II) drugs include carboplatin and oxaliplatin (*Scheme 2*). Both drugs, together with cisplatin, have global approval, while three other Pt(II) complexes, nedaplatin, heptaplatin, and lobaplatin, are approved only in Asia.

The structures of cisplatin-like drugs generally feature four ligands and planar geometry. Two am(m)ine ligands, called "non-leaving group" ligands, remain bound to the metal center and do not undergo hydrolysis; while "leaving group" ligands, like anionic chloride ligands or chelating dianionic fragments, leave the Pt(II) coordination sphere and can be easily exchanged.

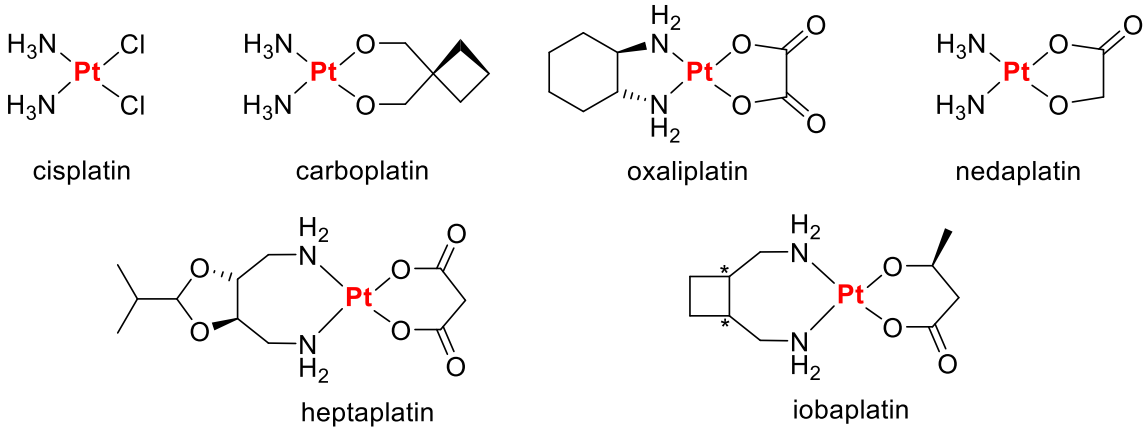

Scheme 3. Chemical structures of clinically approved and marketed Platinum anticancer drugs.

The mechanism of action of cisplatin has been studied for decades. Briefly, cisplatin can penetrate the cell either by passive diffusion or by active transport mediated by membrane proteins.[22] In the cytosol, cisplatin undergoes a transformation into active species by the substitution of chloride ligands and aquation (*Figure 2*). This process occurs preferentially in the cytoplasm because of the Cl^- equilibrium, where chloride ion concentration drops to 10 mM compared to 100 mM in the bloodstream. Positively charged aquatic cisplatin becomes attractive to negatively charged DNA, and nuclear DNA binding takes place. Labile water molecules in cisplatin structure are easily exchanged by nucleophilic nitrogens of the DNA bases, forming intra-strand crosslinks, leading to DNA damage and cell death.[23]

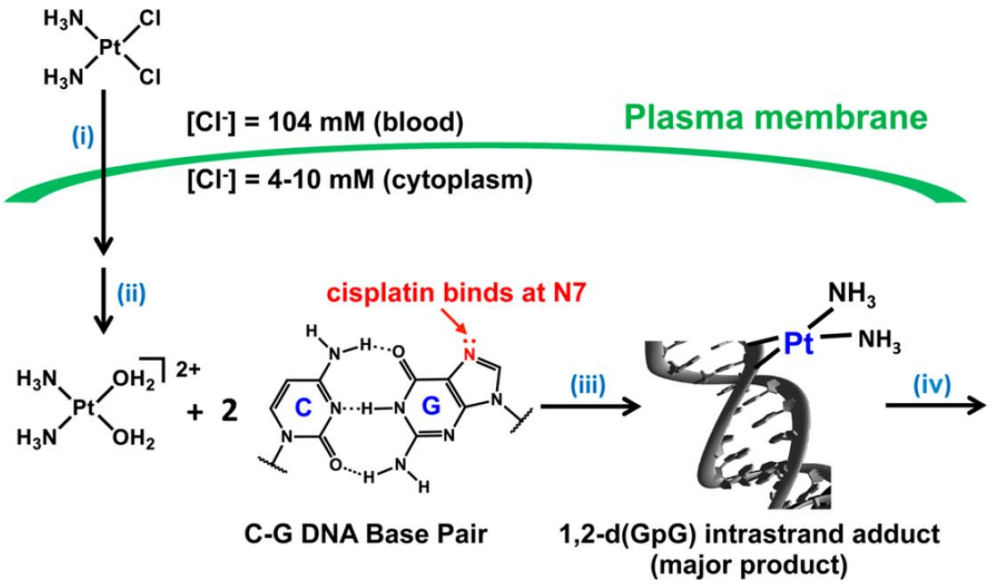

Figure 2. Mechanism of cisplatin activation and DNA binding. Figure reproduced from reference [24].

A feature of chelating ligands of carboplatin and oxaliplatin is that they are substituted by water much more slowly, and solutions of these two drugs are stable to aquation over a period of weeks to months. At the cellular level, cisplatin and oxaliplatin induce distinct cellular responses. For example, in the colorectal cancer cell line HCT116, cisplatin slows down the DNA replication phase and activates the G2–M checkpoint, whereas oxaliplatin activates the G1–S checkpoint and completely blocks the G2–M transition.[25] The mechanism is not fully understood; it is assumed that this difference is linked to the structural characteristics and presence of 1,2-Diaminocyclohexane (DACH) ligand in oxaliplatin. The exceptional activity of oxaliplatin in colon cancer is related to the ability of targeting the organic cation transporters (OCTs), which are overexpressed in this type of cancer.[26]

Pt(IV) complexes are extensively developed as Pt(II) prodrugs. Pt(IV) complexes have a six-coordinate state and adopt octahedral geometries. Additional axial ligands facilitate attachment to drug delivery systems and can optimize the lipophilicity and solubility of the drug.[24] The tetravalent form of Pt is much more kinetically inert, thus increasing stability and minimizing unwanted side reactions with biomolecules prior to DNA binding. Under physiological conditions, Pt(IV) complexes are activated by reductive elimination to release the active Pt(II) form, but in contrast to cisplatin, they are not hydrolyzed or do not undergo a ligand exchange.[27] Ormaplatin represents the first Pt(IV) prodrug, which progressed to clinical trials (*Scheme 4*). Phase I investigations however revealed severe neurotoxicity of Ormaplatin, likely due to the

fact, that chloride ligans in axial position promote fast reduction and release of active Pt(II) species. Next generation Pt(IV) complexes with improved reduction profile such as iproplatin, satraplatin, and LA-12 (*Scheme 4*).are other examples that have undergone clinical trials, but were not approved so far due to the lack of supremacy compared to cisplatin action.[24]

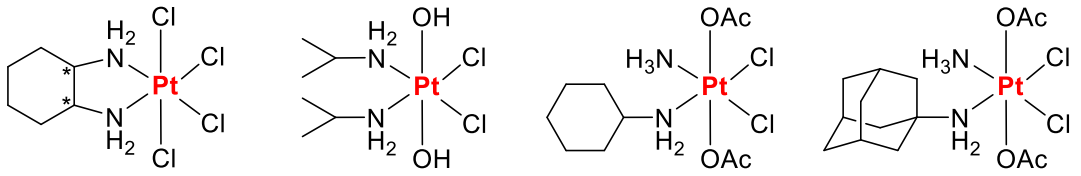

Scheme 4. Chemical structures of Platinum (IV) agents that have undergone clinical trials.

1.4. Drug delivery strategies for small molecules cancer therapeutics

Small molecule cancer therapeutics such as cisplatin, doxorubicin, paclitaxel, and others have been widely used in chemotherapy for decades. While providing a toxic effect to malignant tumors, these drugs simultaneously cause toxicity to healthy organs, lacking selectivity in most cases, which forces the treatment to become dose-limiting. Another rising problem is drug resistance, occurring in different ways (Chapter 1.1.).

In this view, targeted drug delivery is considered a promising option to tackle abovementioned limitations. It allows to minimize side effects without compromising the significant anticancer profile, as well as suppress the development of drug resistance. Several targeting strategies were reported for Pt(II) drugs, including chemical linkages to carbohydrates, steroids, cholesterol, folate, and peptides.[24] DOX-selective delivery can be achieved, *inter alia*, by conjugation to antibodies, hormones, peptides, sugars, nucleic acids, and synthetic polymers.[28,29]

Nanodelivery has been extensively studied and exploited for delivery of anticancer drugs. Nanoparticle (NP) delivery systems improve the therapeutic effect of many chemotherapeutics due to the enhanced permeation and retention (EPR) effect, which results from leaky vasculature and impaired lymphatic drainage in tumors.[30] EPR function of the nano-carries can induce accumulation into tumor tissues and overcome the drug efflux, responsible for reduced efficacy. The main advantages of nanotechnology-based delivery systems are delayed release, prolonged half-life of the drug, and reduced systemic exposure and non-specific toxicity.

Nanoparticle formulations can vary in nature, structure, and size. A great variety of carriers, including organic/inorganic nanoparticles, liposomes, micelles, dendrimers, nanocapsules, and nanotubes have been investigated to facilitate drug delivery and improve activity and selectivity (*Figure 3*).[31] Some of them have demonstrated promising preclinical and clinical results.

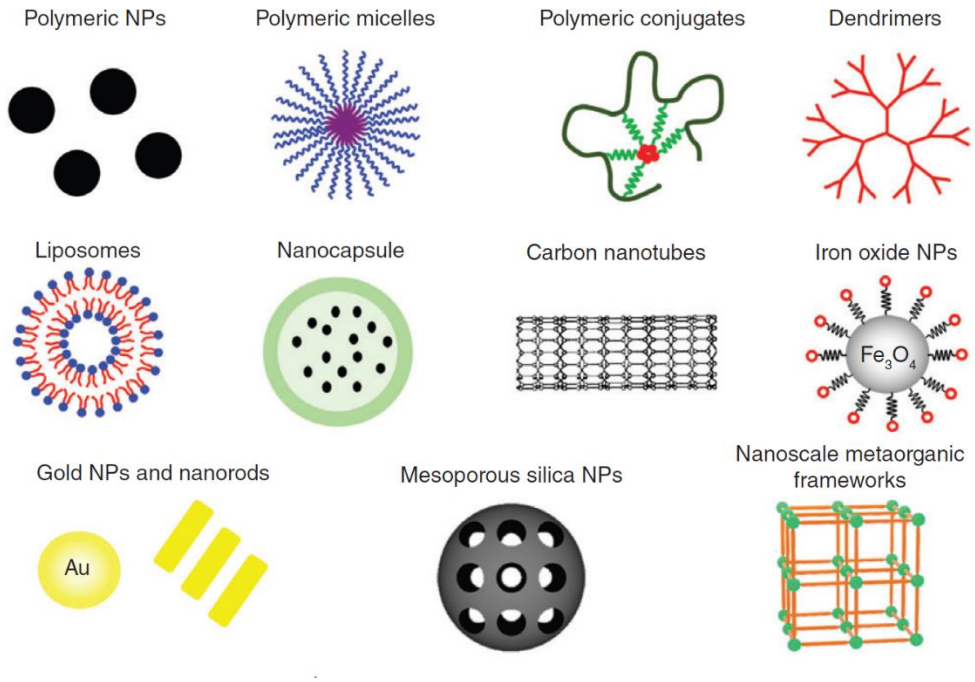

Figure 3. Nanoparticle formulations utilized for anticancer drug delivery. Figure reproduced from reference [31].

Clinical validation of liposomal formulation was first realized for Doxorubicin. Doxil, the first PEGylated liposome encapsulated DOX nanodrug with a particle size of 80-90 nm, was approved by the FDA in 1995 for the treatment of a variety of cancer types, including HIV-associated Kaposi's sarcoma, multiple myelomas, and carcinomas (*Table 1*).[32]

Myocet (produced by Teva Therapeutics UK), the next DOX nanomedicine, represents a non-PEGylated liposomal formulation of DOX and was approved by the European medicine agency (EMA) in 2000 (*Table 1*). It was prescribed for the treatment of metastatic breast cancer.[33] Although Myocet and Doxil encapsulate the same drug DOX, they are different in many aspects such as lipid composition, size, loading method, pharmacodynamics, and pharmacokinetics.

Novel recent DOX formulations such as Thermodox,[34] Aldoxorubicin,[35] Zoptarelin[36] have progressed to Phase III clinical investigations.

Lipoplatin, a PEGylated liposomal form of cisplatin, is another example of a liposome-based drug that has been introduced to Phase III clinical trials in combination with paclitaxel for the treatment of non-small cell lung cancer (NSLC), and has been evaluated in a range of clinical studies for other types of cancer.[37,38] Lipoplatin has a nanoparticle size of 110 nm average diameter and achieves a drug loading of 9 wt%. Such formulation afforded enhanced cisplatin retention in tumor tissue and reduced nephrotoxicity, neuropathy, myelotoxicity, and overall dose-limiting toxicity.[39] Some other cisplatin nanoparticle formulations, such as Nanoplatin,[40] Aroplatin,[41] SPI-077,[42,43] ProLindac (oxaliplatin)[44] demonstrated promising preclinical and clinical results and represent a high interest for cancer research.

Other clinically approved nanoparticles therapeutics for cancer treatment are summarized in *Table 1*.

Table 1. List of clinically approved nanomedicines for cancer treatment. The data has been adapted from reference [45].

Name	Description of carrier	Indication(s)	Approval Year	Company
Untargeted delivery				
Doxil(Caelyx)	Liposomal Doxorubicin (PEGylated)	AIDS-related Kaposi's sarcoma, breast cancer, ovarian cancer	FDA (1995) EMA (1996)	Janssen
DaunoXome	Liposomal daunorubicin (non-PEGylated)	HIV-associated Kaposi's sarcoma (primary)	FDA (1996)	Galen
Myocet	Liposomal Doxorubicin (non-PEGylated)	Metastatic breast cancer (primary)	EMA (2000)	Teva UK
Marqibo	Liposomal vincristine (non-PEGylated)	Philadelphia chromosome-negative acute lymphoblastic leukemia (tertiary)	FDA (2012)	Acrotech
Onivyde(Merrimack)	Liposomal irinotecan (PEGylated)	Metastatic pancreatic cancer (secondary)	FDA (2015)	IPSEN
MEPACT	Liposomal mifamurtide	Osteosarcoma (primary following surgery)	EMA (2009)	Takeda
SMANCS	Poly(styrene-co-maleic acid)-conjugated neocarzinostatin	Hepatoma	Japan (1997)	Astellas
Genexol-PM	Polymeric NP micelle formulation of paclitaxel	Breast cancer and NSCLC	South Korea (2007)	Samyang
Lipusu	Liposomal paclitaxel	NSCLC, ovarian cancer, and breast cancer	China (2006)	Luye Pharma
DepoCyt	Liposomal cytarabine	Lymphomatous meningitis	FDA (1999)	PACIRA Pharma
Abraxane	Albumin-particle bound paclitaxel	Advanced NSCLC (surgery or radiation is not an option) Metastatic breast cancer (secondary) Metastatic pancreatic cancer (primary)	FDA (2005) EMA (2008)	ABRAXIS Bioscience
Oncaspar	PEGylated asparaginase	Acute lymphoblastic leukemia	FDA (1994) EMA (2016)	Sigma Tau
Eligard(Tolmar)	Leuprolide acetate	Advanced prostate cancer	FDA (2002)	Tolmar Therap
Targeted delivery				
Ontak	Engineered protein combining interleukin-2 and diphtheria toxin	Cutaneous T-cell lymphoma	FDA (1999)	Eisai
Combinatorial delivery				
Vyxeos	Liposomal formulation of cytarabine:daunorubicin	Acute myeloid leukemia	FDA (2017) EMA (2018)	Celator Pharms
Hyperthermia				
Nano-therm	Iron oxide nanoparticles	Recurrent glioblastoma, Prostate Cancer	EMA (2010) FDA (2018)	MagForce

1.5. Anticancer peptides

With the progress of molecular biology, a large number of short peptides have been identified from bacteria, fungi, plants, and animals, which possess therapeutic properties.[46] Getting inspired from nature, it created a "new wave" of researching of bioactive peptide–based drugs in different therapeutic areas. Furthermore, the development of chemical peptide synthesis, especially by solid-phase peptide synthesis (SPPS), has significantly accelerated the discovery of therapeutic peptides. In recent years, peptides have been of great interest in oncology and amount of approved peptide drugs is growing. In 2021, out of ten top-seller non-insulin peptide drugs in the market, four (Leuprolide, Octreotide, Lanreotide, Goserelin) are used to treat cancer.

Anticancer peptides (ACPs) represent short peptides, less than 50 amino acids in length, which exhibit toxicity towards cancer cells in a selective manner. The history of the discovery of anticancer peptides goes back to the late 80s when antimicrobial peptides such as defensins and magainins were found to be toxic against a number of cancer cell lines.[47,48] Following that, a growing number of studies reported the anticancer effect of other antimicrobial peptides (AMPs) from different sources, *e.g.*, cecropins, bovine lactoferricin, and others.[49–51] Since then, ACPs have been the subject of extensive studies and became an attractive alternative to small molecule anticancer drugs.

The mechanism of action of ACPs can be classified into two major groups: (i) which oncolytic effect occurs by membrane disruption and (ii) by any other non-membranolytic mechanisms.[52]

1.5.1. Features of cancer cell and bacterial membranes

The plasma membrane of mammalian cells represents a dynamic lipid bilayer and primarily comprises phospholipids, cholesterol, and proteins. Selectivity of ACPs can be achieved through the difference in the membrane structure of cancerous and non-cancerous cells. Healthy cell membranes have sphingomyelin (SM) and zwitterionic phosphatidylcholine (PC) in the outer leaflet and anionic phosphatidylserine (PS) and the phosphatidylethanolamine in the inner leaflet with the asymmetric distribution (*Figure 4*). However, the asymmetry between the inner and outer cytoplasmic membranes is lost in cancer cells, leading to the overexpression of negatively charged PS on the surface of the cell membrane. Moreover, the increased content of other anionic molecules such as *O*-glycosylated mucins, sialylated gangliosides, and heparin sulfates also induces elevated negative charges on cancer cell membrane.[53]

Cholesterol content is essential for maintaining cell fluidity and membrane integrity. Lower cholesterol levels in cancerous cell membranes affect membrane fluidity and lead to susceptibility toward lytic peptides.[54,55] Furthermore, decreased levels of sphingomyelin in the cancer cell membrane is associated with tumorigenesis.[56] In addition, the elevated number and distorted features of microvilli on cancer cells also increase the surface area and contact with ACPs. Extracellular acidity with or without exosome release affects the pH, changing from 7.4 to 6.5 (typical pH of cancer), forming the malignant tumor phenotype.[57]

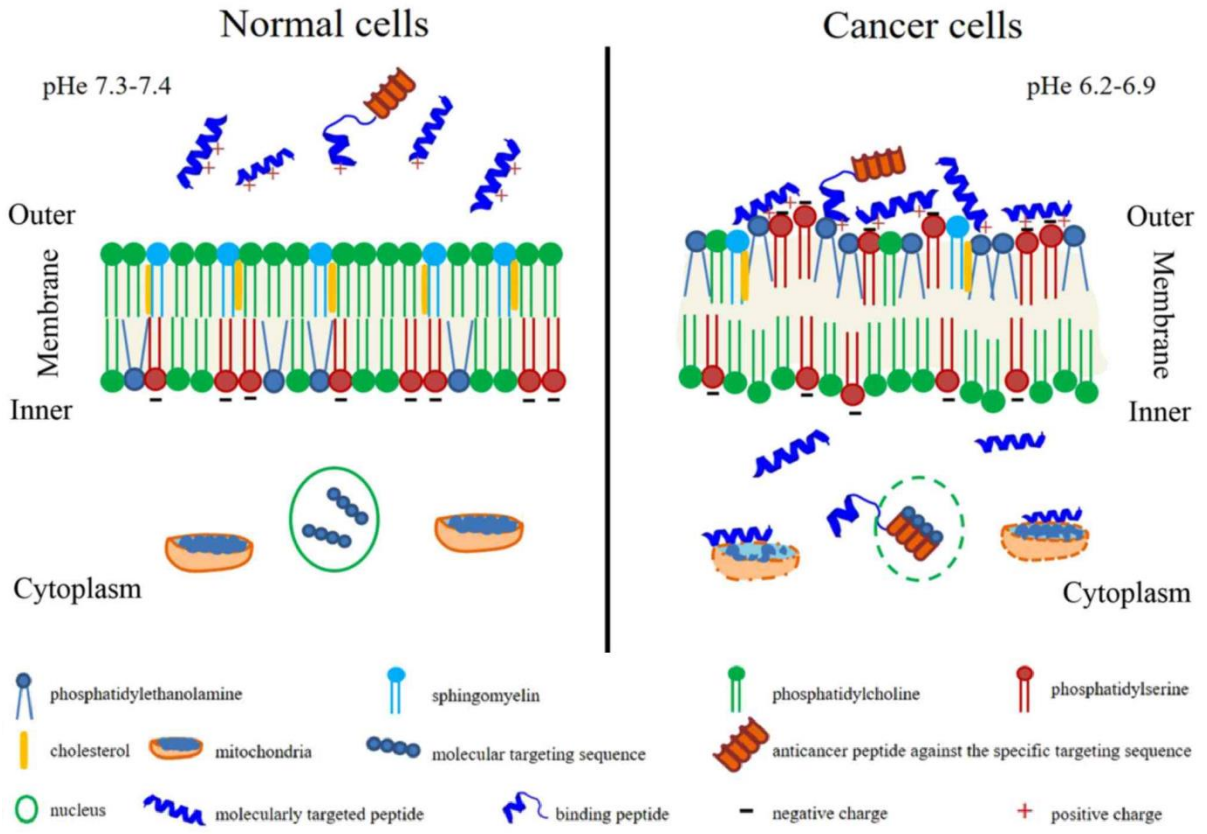

Figure 4. Comparison of a normal cell (left) and a cancer cell (right) membrane composition. Figure reproduced from reference [58].

In contrast, bacteria have a more complex cell wall structure (*Figure 5*).[59,60] The cell wall of Gram-negative bacteria is composed of three layers: the outer membrane, on which lipopolysaccharide (LPS)/endotoxin is anchored, a thin layer of peptidoglycan, and the cytoplasmic (inner) membrane. Gram-positive bacteria's membrane contains many peptidoglycan layers, making it thicker than the one of Gram-negative bacteria. On the outer leaflet of the cytoplasmic membrane are, in general, located high levels of phospholipids with negatively charged head groups such as phosphatidylglycerol (PG), cardiolipin, and phosphatidylserine (PS). Apart from anionic phospholipids, teichoic acid on the surface of

Gram-positive bacteria and lipopolysaccharide (LPS) in the cell wall of Gram-negative bacteria also carry a strong negative charge.[61] Therefore, electrostatic interactions between cationic AMPs and the anionic cell wall of bacteria play a crucial role in antimicrobial activity and selectivity over mammalian healthy cells.

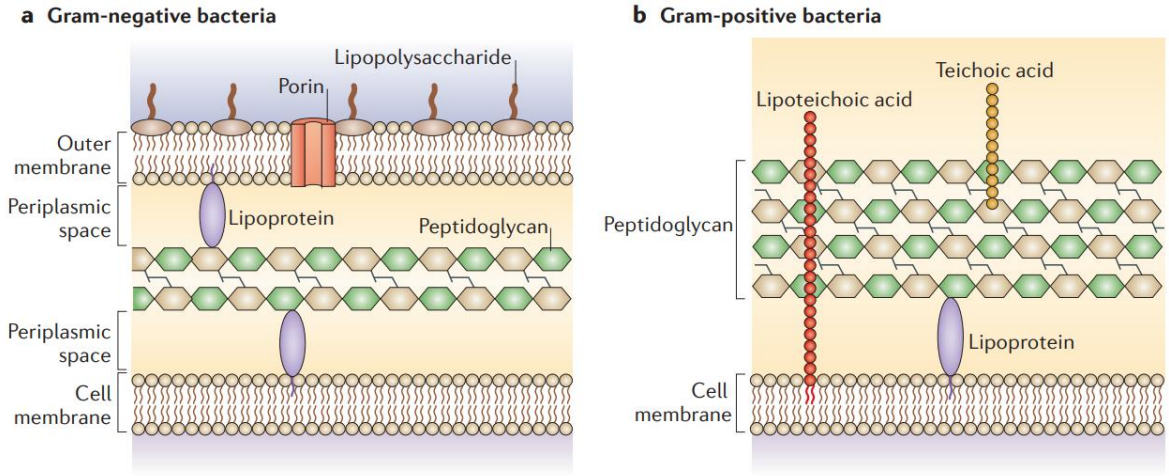

*Figure 5. Gram-negative (**a**) and Gram-positive (**b**) bacterial cell wall structures. Figure reproduced from reference [59].*

1.5.2. Membranolytic ACPs

Membranolytic ACPs are derived from AMPs, and, like the latter, they are characterized by a net positive charge, amphipathic properties, and ordered secondary structure. In the presence of biological membranes, most ACPs adopt an α-helical conformation, but apart from it, there are also reported ACPs folded into β-sheet structure (stabilized by disulfide bond), mixed α-helical and β-sheet structures, ACPs with extended secondary structures, or disordered, proline and/or glycine enriched ACPs.[62,63]

1.5.2.1. Mechanisms of membrane lysis

Membranolytic ACPs and AMPs are thought to share a common mechanistic characteristic: they destroy membrane bilayer integrity either by disruption or by pore formation. Once the cell membrane is disintegrated, the transmembrane electrochemical potential collapses, and cell death occurs rapidly. Many studies have been conducted to investigate the modes of action of ACPs and AMPs, but the results are not always consistent and depend on method chosen.[64] Some peptides can change their mode of action depending on their concentration and lipid membrane composition. The most frequently used models to describe membrane lysis are summarized below (*Figure 6*).[65]

Barrel-stave pore formation. This model is characterized by the formation of transmembrane pores: hydrophobic parts of the peptide interact with the phospholipid acyl chains of the membrane. Peptides are oriented vertically. Melittin and are believed to target membranes by the barrel-stave mechanism at moderate concentration.[66]

Carpet and detergent-like models. Here, the peptides accumulate at the membrane's surface and cover it as a carpet. The peptides interact with the hydrophilic head groups of phospholipids. At a certain critical concentration, the peptides undergo reorientation to the hydrophobic core of the membrane, following the disruption of membrane integrity. Detergent-like or inverted micelle models propose a blebbing of the membrane producing micellar structures at zones with high peptide densities. Some authors consider this mechanism as a late stage of the carpet model. Cecropin P1 is an example of this mode of action.[67]

Toroidal pore formation. This model expands the barrel-stave and carpet model concepts by incorporating the lysis and the pore formation steps. The interaction between the peptides is less tight than in the barrel-stave pore. The main difference with the barrel-stave model is that the peptides mostly interact with the head groups of the bilayer. Magainin is considered to belong to this group.[68]

Shai–Huang–Matsuzaki unifying model (SHM). This recently proposed model unifies the carpet and pore formation mechanisms, suggesting that the action occurs through a multi-stage mechanism. At a low concentration, the peptides accumulate in parallel at the bilayer, as described for the carpet mechanism. Then, as the concentration increases, the curvature strain induces the formation of toroidal pores.[69]

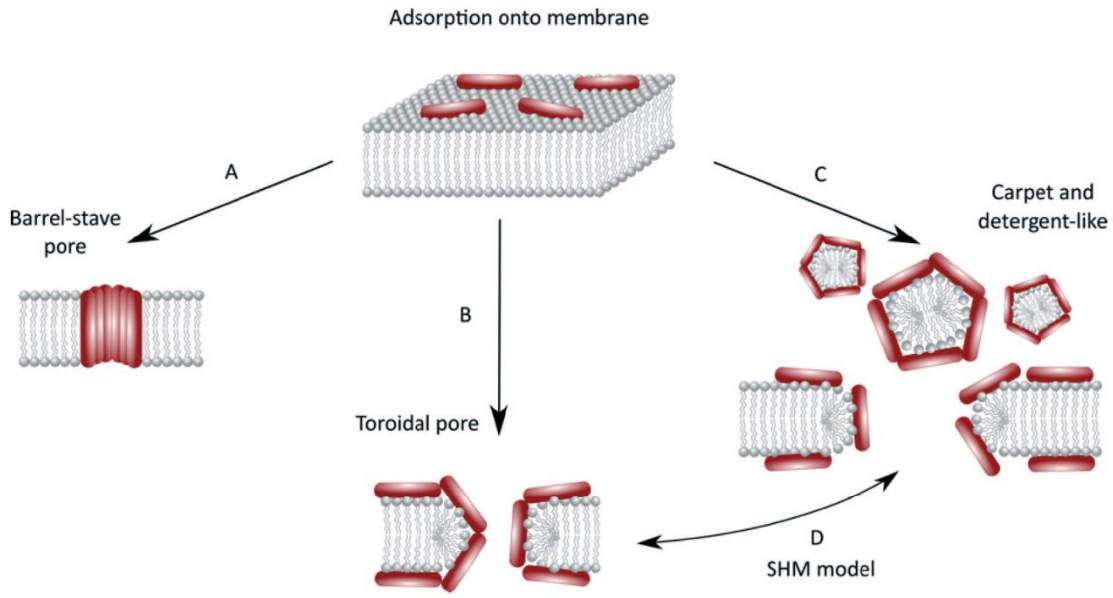

Figure 6. Schematic of membrane's disruption mechanisms. (A) Barrel-stave pore model. (B) Toroidal pore model. (C) Carpet and detergent-like models. (D) Shai–Huang–Matsuzaki unifying model. Figure reproduced from reference [65].

1.5.3. Other targets of ACPs

The modes of action for ACPs are not limited to the disruption of the plasma membranes. Some peptides have dual or multiple modes of action. Mitochondria are another proven target of ACPs, likely due to their negatively charged membrane containing cardiolipin. Both eukaryotic mitochondrial membranes and bacteria cytoplasmic membranes (both the inner and the outer) maintain large transmembrane potentials and have a high content of anionic phospholipids, reflecting the commonality of bacteria and mitochondria, therefore suggesting mitochondria as a possible target for cationic (originated from antimicrobial) ACPs. For example, peptides such as NRC-03 and NRC-07, lactoferricin B, BMAP-28 not only cause membrane disruption but also bind to mitochondria, causing apoptosis.[70–72]

Other existing mechanisms involve alternative pathways such as immunomodulatory effects,[73] effects associated with membrane receptors,[74] DNA synthesis inhibition,[75,76] and anti-angiogenic effects[77] (*Figure 7*).

Some peptides penetrate the cells without membrane perturbation and act on the intracellular targets. Buforin II translocates inside cancer cells, accumulates in nuclei, and causes apoptosis.[78] PR-39, a member of the cathelicidin family, was found to translocate into the cytosol without causing major damage to the membrane and binds to SH3 domains.[79] Peptide

aptamers, which induce apoptosis by inhibition of the heat shock protein 70 (HSP70), have also been described as potential antitumor agents.[80]

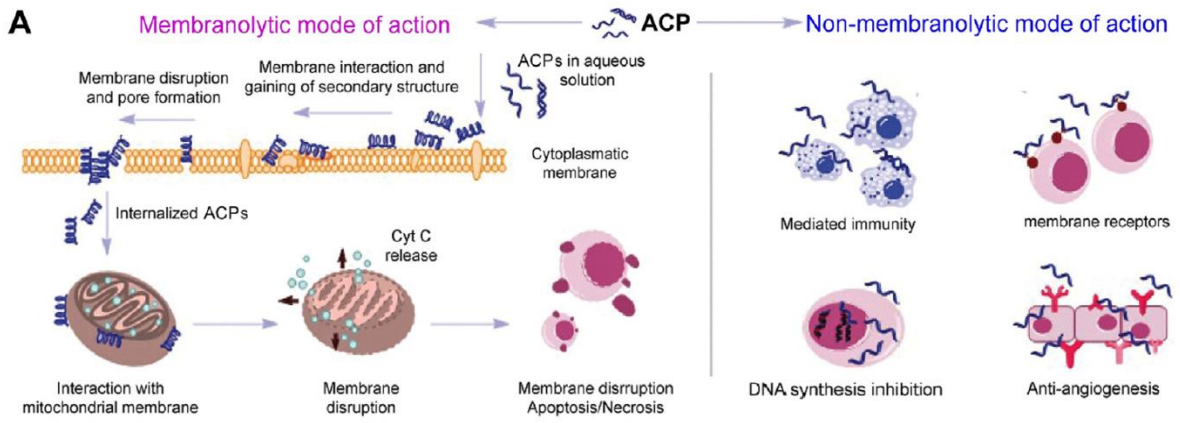

Figure 7. Different acting modes of ACPs. Left: membranolytic mode of action; right: non-membranolytic modes of action. Figure reproduced from reference [81].

1.5.4. Databases containing ACPs

For a better understanding of the structure-activity relationship and rational design of new therapeutic peptides, data analysis of known sequences can provide valuable insights. As the number of bioactive peptides (natural and synthetic) is constantly growing, several databases were developed to summarize and categorize the information from different sources. AMPs and ACPs have been placed into numerous databases, each of which is characterized by specific content (*vide infra*).

The antimicrobial peptide database (APD)[82] contains natural AMPs extracted from different species, covering all six life kingdoms (bacteria, archaea, protists, fungi, plants, and animals). It provides the data on peptide sequence and structure and annotations regarding the respective antibacterial, antifungal, antiviral and anticancer activities. APD subset comprises 262 ACPs (as of 05/2022), but the information about cell lines and types of activities is limited.

Anticancer Peptide and Protein Database (CancerPPD)[83] is a resource focused only on ACPs. It consists of 623 experimentally verified ACPs, including D-enantiomeric and cyclic sequences. The activity data covers 249 cell lines and 21 tissue types. Details such as the origin of the peptide, chemical modifications, chirality, assay time, and type are explicitly annotated. As a limitation, the current version of CancerPPD does not have information on toxicity toward non-cancer cells (e.g., erythrocytes), which would be an important aspect to consider in designing cancer cell-selective ACPs.

Database of antimicrobial activity and structure of peptides (DBAASP)[84] is an extensive collection of both naturally occurring and synthetic AMPs. It contains 18405 monomeric peptide entries, 920 of which are also annotated as ACPs. Not only peptide activities against various cancer cell types are provided, but also the hemolytic effect is annotated when known.

Various calculated physico-chemical properties such as net charge, hydrophobicity, isoelectric point, and amphiphilicity index complement the data on activities.

1.6. Overview of the thesis

My PhD work aimed to study different peptidic modalities for cancer application. The PhD thesis narrative can be divided into two main parts: (i) development of new peptidic carriers for cancer drug delivery (Chapters 2, 3) and (ii) synthesis and activity studies of new anticancer peptides (Chapter 4) and peptide dendrimers (Chapter 5).

(i) In the first part, I looked at stable, non-toxic sequences with high cell-penetrating properties either by active transport or EPR effect. In the first project (Chapter 2), I designed the strategy to deliver Doxorubicin and derivatives to cancer cells. I have synthesized conjugates **Z9**, **Z10**, **Z13** *via* a self-cleavable linker, followed by testing on different cancer cell models, aiming to improve pharmacokinetic features and overcome drug resistance.

In the second project (Chapter 3), I worked on the development of a new macromolecular system, based on peptide dendrimers, able to deliver Pt drug, namely DACHPt. I have performed the synthesis of peptide dendrimers (**C1-C15**), bearing multiple metal coordinating side chains, and optimization of their aggregation properties and drug loading capacity to improve *in vitro* cytotoxicity against HeLa cells.

(ii) For the second part, I focused on the discovery of active, selective, and non-hemolytic peptides acting against cancer directly. I searched for novel bioactive peptide sequences. In the third project (Chapter 4), with the help of machine learning approaches, we have generated 33 new linear peptide sequences with lengths of up to 15 amino acids. Twelve compounds turned out to be active against HeLa cells, and three had low hemolytic properties (**A1**, **B1**, **B2)**. In addition, I have performed mechanistic studies to examine the mode of action of selected peptides.

In the fourth project (Chapter 5), devoted to the development of anticancer peptide dendrimers, I started with elaborating the initial design and screening of around 50 sequences (not included in the final version) by varying the hydrophobicity, charge, and amino acid composition. However, most of the compounds synthesized were either inactive or hemolytic. After several iterations, we revealed a few potent compounds against lung cancer A549 cells, namely **G3KL**, **T7,** and **EZ-282**, which at the same time showed low hemolysis and low toxicity toward non-cancerous HEK-293 cells. Finally, flow cytometry experiments were performed to study the membrane integrity of A549 cells upon peptide dendrimer treatment.

The following chapters should be regarded as independent stories each.

2. Peptide Dendrimers for Doxorubicin Delivery to Cancer Cells

2.1. Abstract

Due to the drug resistance (Chapter 1.1), the development of new vehicles to deliver Doxorubicin-based drugs to cancer cells is of great interest. Targeted delivery of pDOX, a highly cytotoxic derivative of DOX, can be a promising approach toward overcoming multidrug resistance. Here we have designed a new strategy for conjugation of DOX and analogs to peptide carriers by introducing a self-cleavable linker. The conjugation of DOX resulted in compounds **Z9**, **Z10**, and **Z13**, where the latter was the most potent out of the series. The *in vitro* cytotoxic activities of synthesized free pDOX, DOX, and prodrugs **Z14a**, **Z15a** were in accordance with the literature; **Z13** exhibited an overall less potent effect compared to free DOX but restored its activity in the resistant cancer cell line.

Synthesis of conjugates with highly potent derivatives of DOX can be completed following reaction condition optimization.

2.2. Introduction

The design of delivery systems that specifically target cancer cells, that can efficiently cross cell membranes and bring their cargo inside the cell is very challenging. It requires the combination of different functionalities within one molecule. Even though DOX is a well-known anticancer drug, it causes strong side effects due to its lack of selectivity. It is therefore a good candidate to develop drug delivery systems.

In this part of the work, we pursued two main goals: (1) to develop effective, peptide dendrimer-based targeted drug delivery system, and (2) to design a new prodrug strategy for releasing a highly potent Doxorubicin derivative, namely 2-pyrrolino-Doxorubicin (pDOX). One of the major problems of such highly active anticancer agents is off-target toxicity,[85] which is dramatically increasing in line with anticancer potency.

The preliminary investigations were focused on searching for and screening of suitable carriers. The molecular design protocol relies on the expertise acquired over the years by our group in the peptide dendrimer field.[86] Peptide dendrimers represent branched macromolecules consisting of natural or non-natural amino acids as building blocks. Their typical structure includes: (*i*) a central core, allowing different functionalizations, (*ii*) branching units, forming

synthetic generations (G_0-G_3), and (*iii*) surface groups, contributing to physico-chemical properties of the entire molecule (*Figure 8*).

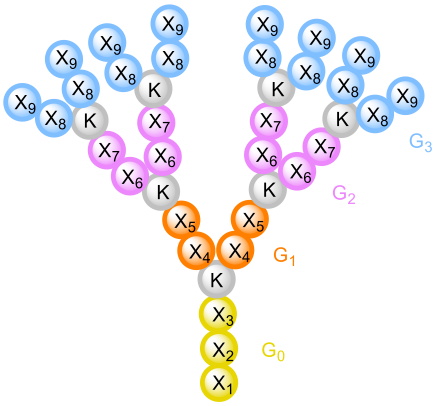

Figure 8. Schematic representation of peptide dendrimer's structure. Gn - generations of peptide dendrimers.

From the synthetic point of view, peptide dendrimers are obtained by SPPS using a branching diamino acid such as lysine at every second or third position in a peptide sequence followed by RP-HPLC purification.[86] The scaffold of a peptide dendrimer offers many advantages compared to linear peptides in terms of stability, multivalency and overcomes the problem of peptide folding and aggregation during synthesis. Moreover, the core of peptide dendrimers can be easily modified with other molecules, expanding the range of applications of these scaffolds.

In particular, our group reviously reported cell-penetrating peptide dendrimers (CPPD), designed to efficiently internalize cytotoxic payloads (Taxol, KLA-peptide) into cells.[87] In this case, clathrin-mediated (energy-dependent) uptake appeared to be the major process of internalization. Having low intrinsic toxicity, CPPDs showed higher cellular uptake compared to their linear analogs. Moreover, a few years earlier, our group has developed glycopeptide dendrimer-colchicine conjugates targeting cancer cells.[88,89]

In 2019, Heitz et al. were able to develop pH-responsive peptide dendrimers for siRNA transfection.[90] These peptide dendrimers consist of polycationic branches connected to a hydrophobic core and form nanoparticles at neutral pH, which undergo endocytosis and disassembly upon acidification of the endosome, resulting in intracellular release and delivery of their cargo.

In the concept of intracellular drug delivery, one interesting approach concerns the self-immolative linkers (SILs), such as redox-active disulfide linkers.[91] This type of linkers was

widely used to design prodrugs for anticancer compounds taking advantage of the high amount of glutathione (GSH) in mammalian cells and the reducing environment of cancer cells.[92]

Getting inspired by the potency of pDOX (Chapter 1.2), we have focused our research efforts on improvement of its general toxicity by development of targeting delivery system. To the best of our knowledge, a limited number of prodrug systems have been reported for pDOX, including photo-controlled delivery,[93] antibody-directed enzyme prodrug therapy (ADEPT),[94] or proteolytic release of antibody-prodrug conjugates.[95]

We have based our strategy on the di-acetoxy prodrugs of pDOX.[96,97] The acetates on this prodrug are cleaved intracellularly by esterase, releasing the latent aldehyde, which undergoes intramolecular cyclization to form pDOX (*Scheme 5*). This strategy possesses efficacy and specificity to the tumor tissues, due to overexpression of various specific enzymes, including esterase, in cancer cells.[98]

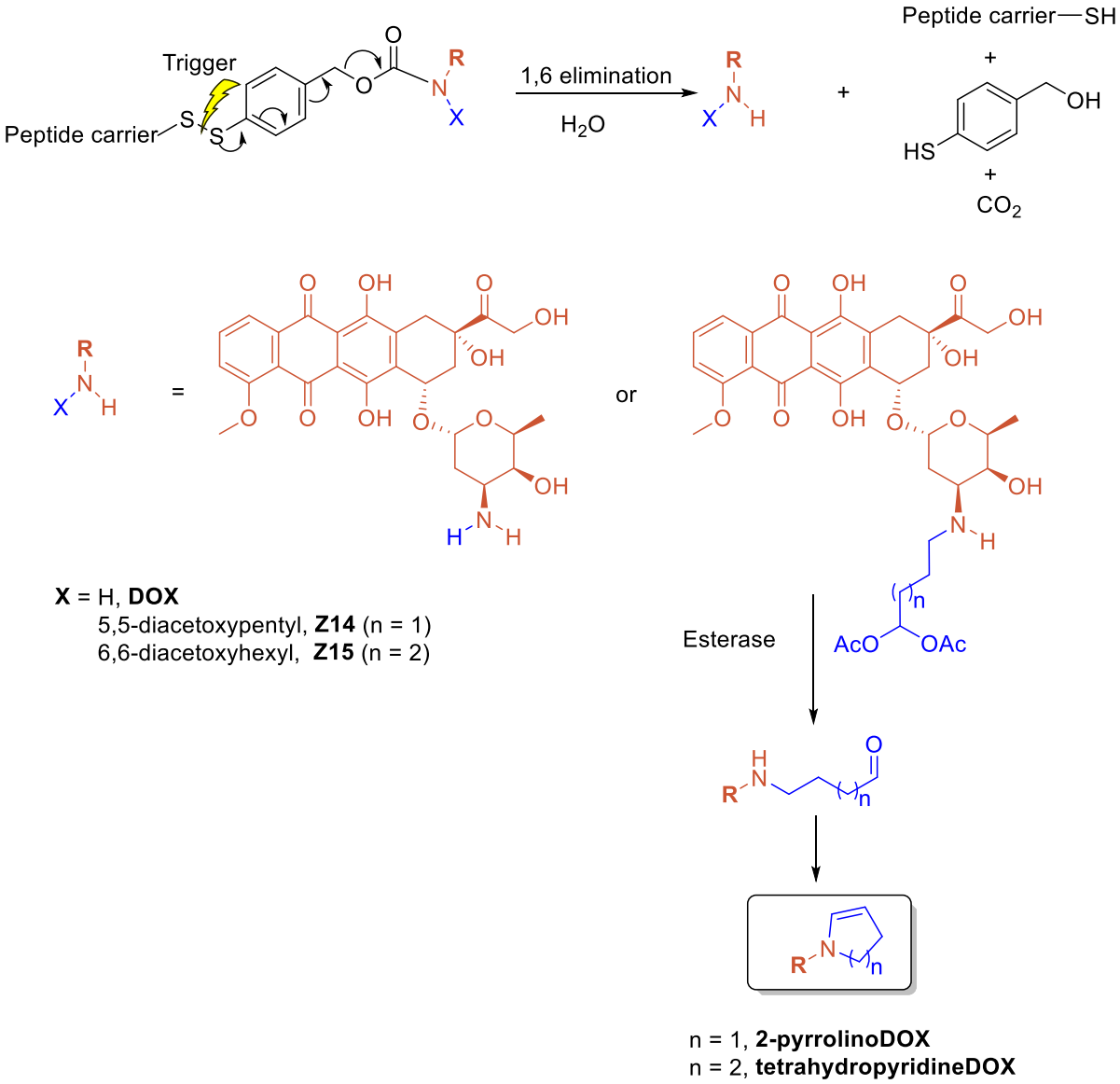

Scheme 5. Representation of the general strategy for delivery of Doxorubicin and its derivatives to cancer cells, applied in this chapter. The self-immolate linker was conjugated to peptide carriers from one side and to a drug from another side. This design allows intracellular drug release under physiological conditions.

2.3. Results and discussion

2.3.1. Synthesis of Doxorubicin conjugates Z9-Z13

For this study, we started with the selection of possible peptide carriers. All selected compounds were synthesized by SPPS, to which a cysteine at the core was added to perform further conjugations, and it yielded to the compounds **Z1**-**Z5** (*Table 2*).

Table 2. Synthesis of peptide carriers by SPPS.

Nr.	Sequence[a]	Yield, mg (%)[b]	MS calc/found[c]
Z1	$(KL)_8(KKL)_4(KLL)_2KCLLLLL$	45.9 (10)	4928.6054/4928.6128
Z2	$(KL)_8(KKL)_4(KLL)_2KCLLLL$	36.3 (8)	4815.5213/4815.5150
Z3	$(RL)_8(KRL)_4(KKK)_2KGYKC$	34.0 (7)	5107.4822 /5107.4901
Z4	$(LI)_8(KRK)_4(KRA)_2KHSKC$	50.6 (11)	4769.2921/4769.3022
Z5	RRRRRRFFERHHMVGSCMRAFHQL	38.5 (21)	3167.6518/3167.6359

[a]One-letter code amino acids are used, *K* is the branched lysine residue. [b]Isolated yields as trifluoroacetate salt after preparative RP-HPLC purification. [c] ESI-MS data.

Targeted drug delivery to cancer tissue in the form of nanoparticles, exploiting the enhanced permeation and retention effect (EPR) is a well-established strategy for cancer therapy.[99] With slight modifications from peptides dendrimers **MH18, MH19**, discovered by Heitz *et al*.,[90] we identified two amphiphilic peptide dendrimers **Z1, Z2** with the best pH-sensitive self-assembly properties (*Figure S1a*). We also chose reported CPPDs,[87] such as **D1** and **D11,** as possible peptide carriers and obtained their cysteine-modified analogs **Z3** and **Z4,** respectively. Linear peptide **Z5**, which was initially designed in our group to mimic 18 residues of the C-terminus end of NSP5 of rotavirus, was selected due to its fast cell-penetrating properties and low toxicity (*Figure S1b*).

For effective conjugation, we have installed a cleavable linker, which would allow us to link peptide carriers on one side and the drug on another side. Self-immolative linkers (SIL) are designed to rapidly decompose as a consequence of a chemical trigger and release an active compound.[100] Disulfide-based self-immolative linker is the known solution for conjugation to peptides through the backbone of cysteine and allows fast release in reducing environment.[101]

We have selected a disulfide benzyl carbonate-based linker, which undergoes 1,6-elimination release mechanism (*Scheme 5*). Synthesis of self-immolative linker **Z7** was performed in two steps by procedures previously described.[102] The commercially available building block includes 4-mercaptobenzyl alcohol, which thiol group was first activated with 2,2'-dithiobispyridine to obtain **Z6**, followed by coupling with 4-nitrobenzyl chloroformate to afford activated carbonate **Z7** with moderate yields (*Scheme 6*). The products were purified by silica gel chromatography and characterized by NMR and HRMS.

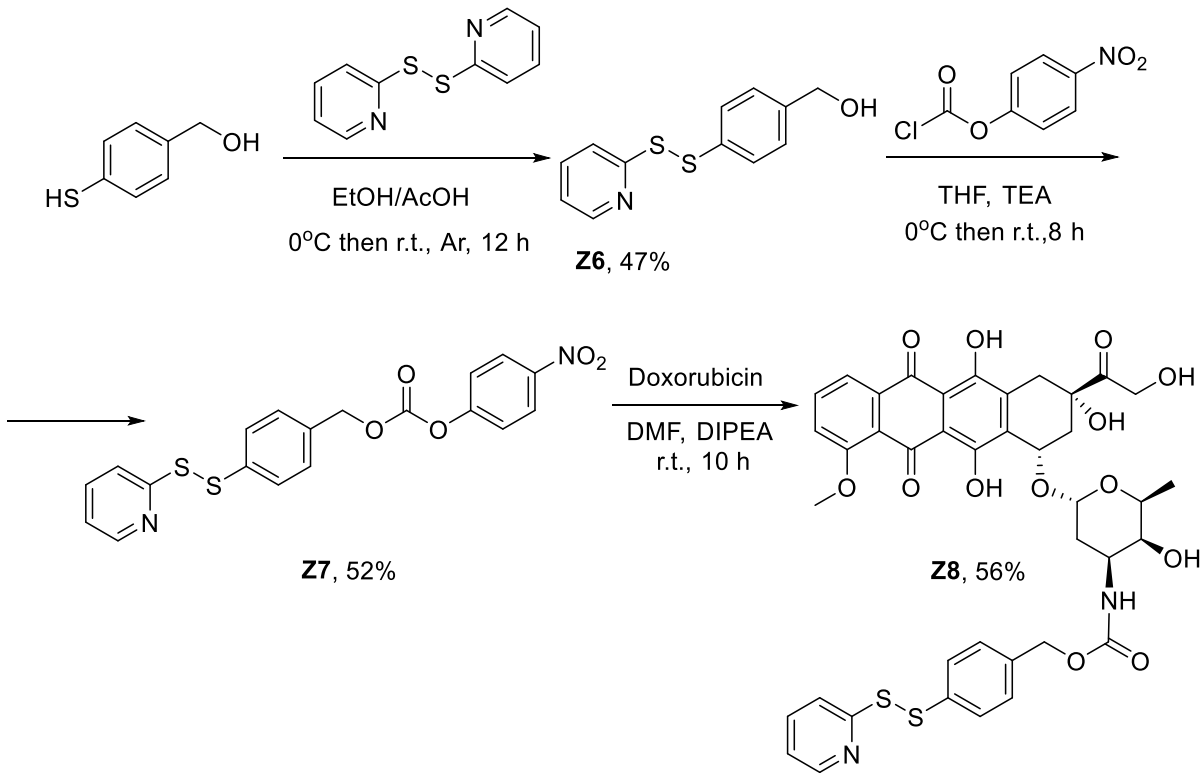

*Scheme 6. Synthetic scheme for heterobifunctional linker **Z7** and carbamate **Z8**.*

The next step involved conjugation of the linker to Doxorubicin at the free amine group to yield carbamate **Z8** (*Scheme 6*). The reaction was performed in DMF, due to poor solubility of DOX in other organic solvents, with the addition of DIPEA to basify the DOX hydrochloride salt. The product **Z8** was purified by RP-HPLC. The last step consisted of the substitution of 2-thiopyridyl group of the linker with cysteine-functionalized peptide and peptide dendrimers in MeCN/H_2O mixture to yield **Z9-Z13** (*Scheme 7*). This reaction was problematic in the case of **Z11** and **Z12** due to solubility issues and low conversion even after 12 h. Exchanging the reaction solvent to DMF did not yield better results. We were further focused on conjugates **Z9**, **Z10**, **Z13**, which were purified by RP-HPLC and obtained in moderate yields (*Table 3*).

*Table 3. Synthesis of Doxorubicin conjugated **Z9-Z13**.*

Nr.	Sequence[a]	Yield, mg (%)[b]	MS calc/found[c]
Z9	$(KL)_8(KKL)_4(KLL)_2KCLLLLL$	4.1 (19)	5635.7726/5635.7810
Z10	$(KL)_8(KKL)_4(KLL)_2KCLLLL$	7.0 (32)	5522.6886/5522.6925
Z11	$(RL)_8(KRL)_4(KKK)_2KGYKC$	-	5820.6964/
Z12	$(LI)_8(KRK)_4(KRA)_2KHSKC$	-	5476.4594/
Z13	RRRRRRFFERHHMVGSCMRAFHQL	5.8 (25)	3874.8191/3874.8341

[a] Sequence of peptide carriers. One-letter code amino acids are used, *K* is the branched lysine residue [b] Isolated yields as trifluoroacetate salt after preparative RP-HPLC purification. [c] ESI-MS data.

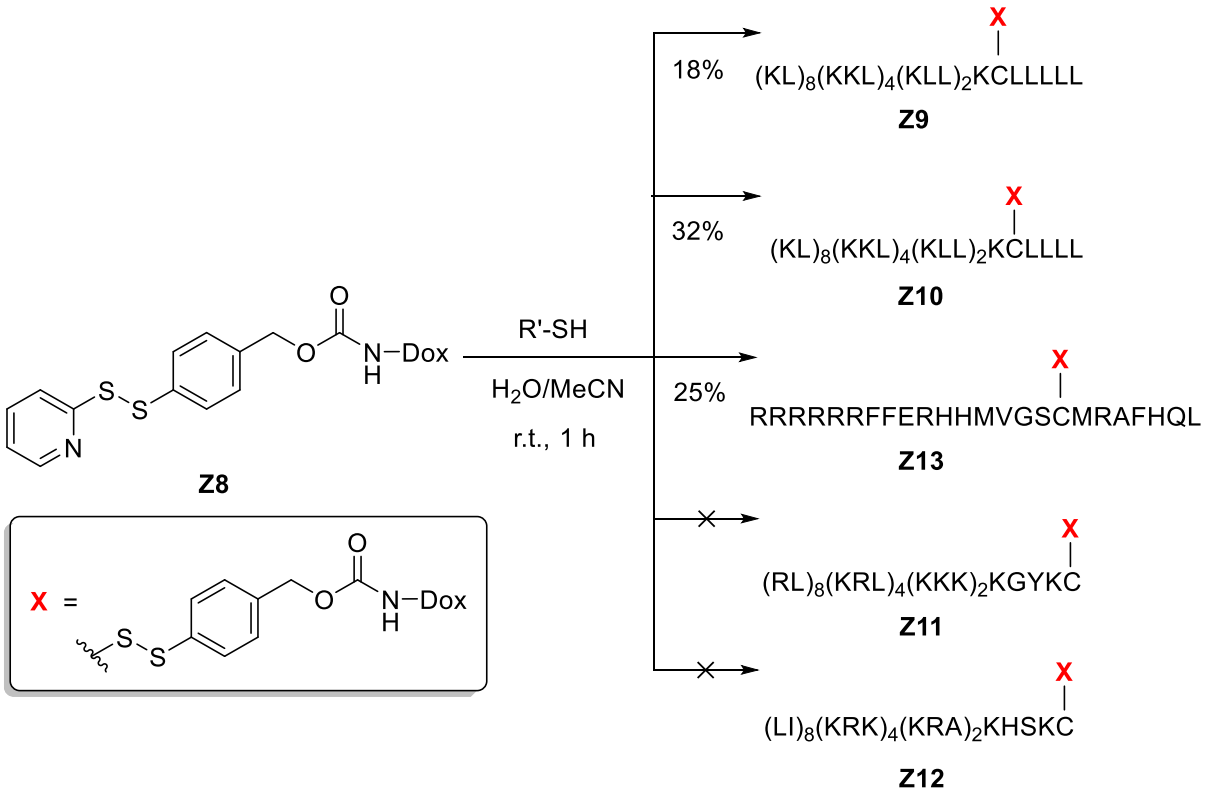

Scheme 7. Synthetic scheme for conjugates **Z9-Z13**.

2.3.2. Anticancer activity of Z9, Z10, Z13 conjugates

We tested the obtained conjugates on a HeLa (cervical cancer) cell line. Free Doxorubicin was used for comparative purposes. Cells were treated with multiple concentrations of the conjugates for 72 h, and then cell viabilities were determined using the alamarBlue™ assay, measuring the cell proliferation. First, HeLa cells showed no significant reduction in cell viability for starting peptide carriers **Z1**, **Z2**, **Z5**. (*Figure S2*). Conjugate **Z13**, bearing the linear peptide carrier, was most potent in the series with IC_{50} value 0.33±0.1 μM, whereas **Z9** and **Z10** showed lower activities with respective IC_{50} values 8.6±3.3 and 13.5±5.0 μM (*Table 4*). Under chosen experimental conditions, DOX alone had a higher activity with IC_{50} value 0.064±0.035 μM.

Table 4. Calculated IC_{50} values for Doxorubicin conjugates on HeLa cells

	Free DOX	Z8	Z9	Z10	Z13
IC_{50}, μM[a]	0.064±0.035	0.18±0.06	8.6±3.3	13.5±5.0	0.33±0.08

[a] IC_{50} was determined after 72 h incubation at 37°C in DMEM high glucose medium supplemented with 10 % FBS.

We questioned what could be the key step responsible for the drastic activity reduction for **Z9** and **Z10**. To check the release speed, we performed recovery kinetics of the Doxorubicin. As an example, the least active **Z10** was triggered by the addition of TCEP and incubated in PBS

at pH 7.0 and at 37°C to mimic physiological conditions (Figure S3Figure S4). The release of Doxorubicin was followed by analytical HPLC by quenching the reaction with 1% TFA and measuring the samples at indicated times (*Figure S4*). The release of Doxorubicin reached about 60% after 60 min of incubation, and the full release was complete in 300 min.

In addition, to test whether the activity is being lost due to hindrance through the linkage of the NH_2 group, which is reported to play a crucial role in DNA binding, we have also tested for cytotoxicity intermediate **Z8** on HeLa cells under the same conditions. The activity of the Doxorubicin-linker (IC_{50} 0.180±0.06) was higher than peptide conjugate **Z13**, indirectly indicating the issue with the peptide carrier (*Table 4*, *Figure S6*).

Decreased activity of peptide conjugates could be caused not only by slow drug release but also by insufficient cellular internalization and accumulation. Confocal imaging of HeLa cells, incubated at 1 μM of compounds for 3, 6, and 12 hours, suggested slower accumulation of **Z13** compared to free Doxorubicin (*Figure S5*). For **Z9**, **Z10**, accumulation was insufficient even after 24 h (data not presented).

Having this information in hand, we further proceeded with **Z13**. Next, **Z13** was tested on a broader panel of cell lines. To compare cytotoxic effects, a viability assay was conducted for MCF-7 (ER-positive) and MDA-MB-231 (triple-negative) breast cancer cell lines and non-cancerous MCF-10a (breast epithelial) and CHO (Chinese hamster ovary) cell lines. The cells were incubated for 72 h, as for the HeLa cell screening and characterized by IC_{50} values (*Table 5*, *Figure S7*, *Figure S8*). **Z13** exhibited cytotoxic properties toward breast cancer cells having IC_{50} 0.57±0.05 μM and 1.33±0.25 μM for MCF-7 and MDA-MB-231 cells, respectively. Overall, **Z13** appeared to be less toxic than the free DOX. Still, nevertheless, the selectivity of **Z13** toward non-cancerous cells was higher compared to unconjugated DOX, which is said by selectivity indices values (SI = IC_{50}non-cancer/IC_{50}cancer) (*Table S1*). The greatest selectivity was achieved when compared to the CHO cell line (SI 4.4 ÷ 22.7). In MCF-10a, a normal human breast epithelial cell line representing a more relevant comparison among breast cell lines, **Z13** was double and a half less toxic compared to breast cancer MCF-7. In contrast, free DOX was only 1.6-fold less toxic (*Table 5*). For the MDA-MB-231 cell line, sufficient selectivity was not achieved.

Table 5. Calculated IC_{50} values on a broad panel of cell lines.

	IC_{50}, μM						
Cpd.	MCF-7[a]	MDA-MB-231[a]	MCF-10a[b]	HeLa[a]	CHO[a]	H69[c]	H69 AR[c]
Z13	0.57±0.05	1.33±0.25	1.4±0.2	0.33 ± 0.08	7.5 ± 2.2	0.86 ± 0.14	1.7 ± 0.5
DOX	0.16±0.02	0.23±0.03	0.26±0.05	0.064 ± 0.015	0.58 ± 0.17	0.12 ± 0.03	2.9 ± 0.4

[a] IC_{50} was determined after 72 h incubation at 37°C in DMEM high glucose medium supplemented with 10 % FBS. [b] IC_{50} was determined after 72 h incubation at 37°C in serum-free HUMEC ready medium. [c] IC_{50} was determined after 72 h incubation at 37°C in RPMI-1640 medium supplemented with 10 % FBS.

Additionally, **Z13** was evaluated for its ability to overcome drug resistance. We compared the potency on selected H69 (lung carcinoma) and H69 AR (DOX resistant lung carcinoma) cell lines. Free Doxorubicin was more potent than **Z13** in the wild type of lung cancer (IC_{50} 0.12 vs 0.86 μM respectively). However, in the H69 AR cell line the potency of DOX alone dropped by 24 times, while **Z13** retained its activity at the low μM range (*Table 5*).

2.3.3. Synthesis of Diacetoxy-alkyl doxorubicin conjugates

2-Pyrrolino-Doxorubicin (pDOX) is a highly potent analog of Doxorubicin.[16] It is active in the low nM range. The homolog of pDOX, tetrahydropyridine-Doxorubicin, *circa* 50 times less active than the five-membered ring counterpart, remains a great advantage in potency compared to Doxorubicin (*Scheme 3*).[16] It was revealed that the extremely high activity of these compounds, even against DOX-resistant tumor cell lines, is a result of its ability to form an aminal adduct with an amino group of a guanine base in DNA. Even though pDOX is very potent, the most significant disadvantage is off-target toxicity. Therefore, pDOX was conjugated to different molecules to enhance targeting and half-life time in the bloodstream.[17,18]

In this part of the work, we have made synthetic attempts to develop a peptide-based prodrug delivery platform (*Scheme 5*). The system's design was based on previous findings with Doxorubicin, where we introduced disulfide self-immolative linker **Z7**. We started with the synthesis of diacetoxy prodrugs **Z14-Z15**. From the retrosynthetic perspective, we considered two possible pathways to obtain diacetoxy prodrugs: (i) by reaction of reductive amination between Doxorubicin and oxobutane/pentane diacetates **Z16**/**Z17**, (ii) by alkylation of Doxorubicin by iodobutane/pentane diacetates (*Scheme 8*).

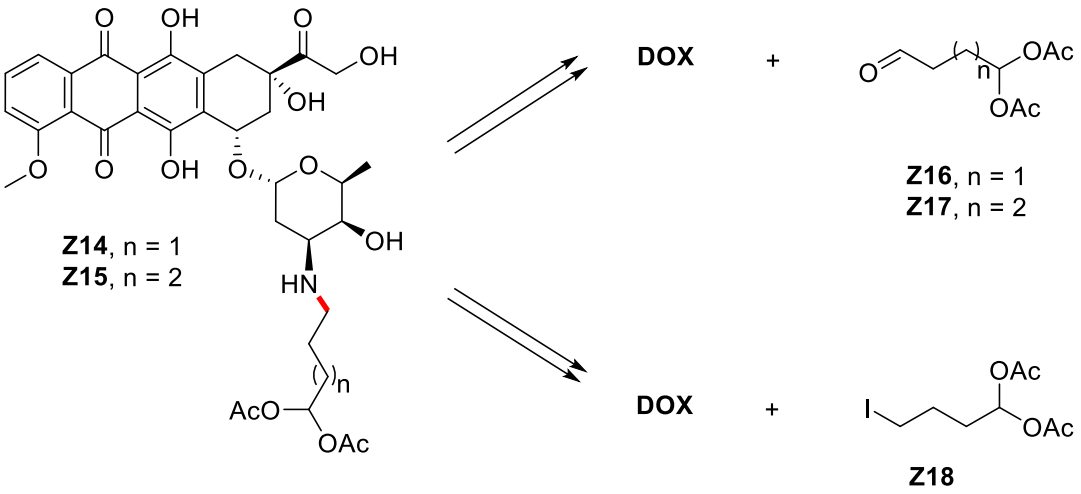

Scheme 8. Retrosynthetic strategies for building diacetoxy-alkyl prodrugs **Z14**-**Z15**.

For the first strategy, the compounds **Z16**, **Z17** were generated in 3 steps, with slight modifications of procedures described in the literature (*Scheme 9*).[96,103] The synthesis started with commercially available alcohols **Z19**, **Z20**, which were oxidized to aldehydes **Z21**, **Z22**, followed by diacetyl acetal protection and ozonolysis and yielded **Z16**, **Z17**.

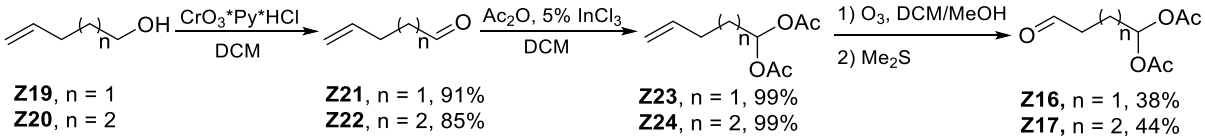

Scheme 9. Synthesis of oxobutane/pentane diacetates **Z16**/**Z17**.

Next, protected aldehydes **Z16, Z17** were introduced to a reaction with DOX with the addition of 0.7 mol. eq of sodium cyanoborohydride. To our surprise, during reaction monitoring, two different products were observed by HPLC-MS for each reaction. In both cases, the side product had [M+2] mass increase, indicating additional reduction transformation in the molecule. The ratio between desired compound and reduced side product was determined by analytical RP-HPLC as 1:2 or 1:1.8 for **Z14** and **Z15,** respectively (*Scheme 10*). We managed to purify the mixture **Z15** and isolate desired compound **Z15a** and side product **Z15b** by RP-HPLC. NMR investigations of **Z15b** confirmed the reduction of the C13 ketone group. Variation of another reducing agent such as $NaBH(OAc)_3$, its concentration and reaction time did not lead to the reaction profile improvement.

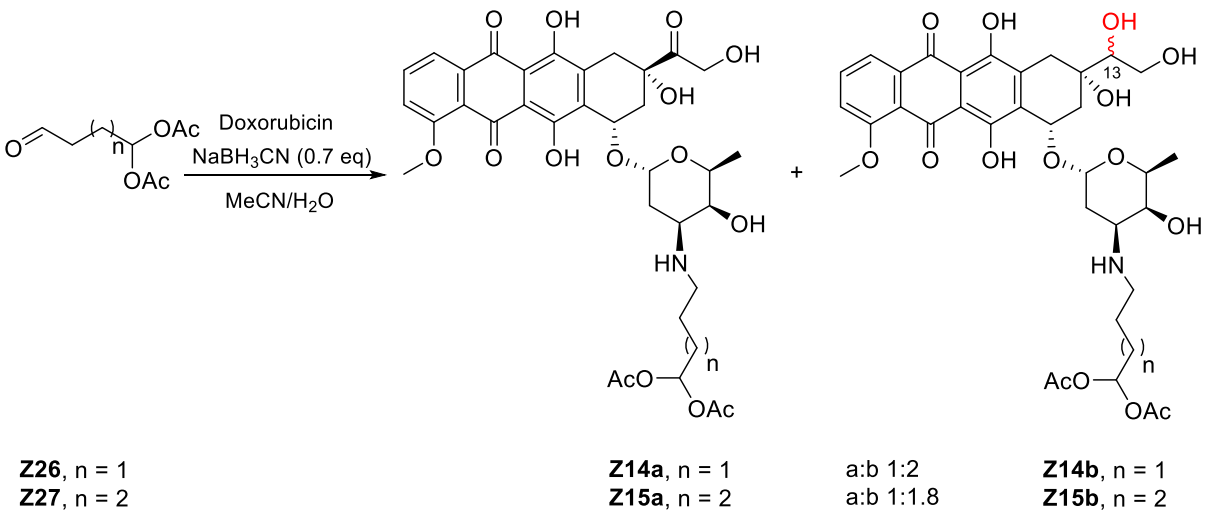

Scheme 10. Conversion of Doxorubicin to diacetoxy-alkyl Doxorubicins via reductive amination.

Due to the low isolated yield of **Z15a** (7%), we were focused on the second strategy to afford diacetoxy prodrug **Z14a** by direct alkylation of Doxorubicin. In this case, the precursor **Z18** was synthesized in 3 steps, starting with building block 2-(3-chloropropyl)-1,3-dioxolane. The conversion to 2-(3-iodopropyl)-1,3-dioxolane **Z25** was performed with 61% yield, followed by dioxolane deprotection (**Z26**) and introduction of a diacetyl protective group to obtain **Z18** in good yield (*Scheme 11*). The next step comprised a nucleophilic substitution with Doxorubicin, which was successfully performed to obtain **Z14a** in 33% yield. The moderate yield is obtained due to the partial double alkylation side reaction, as well as poor solubility during HPLC purification. Reference compound pDOX was synthesized by the addition of 3 mol. excess of 4-iodobutyraldehyde to Doxorubicin in DMF to afford an isolated product with 31% yield.

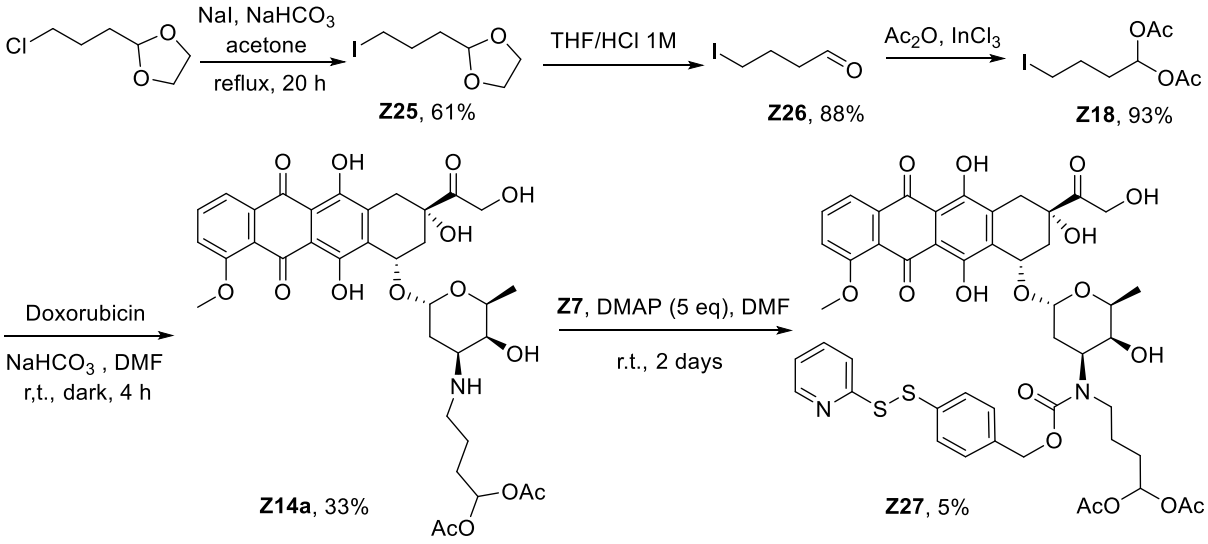

Scheme 11. Synthesis of conjugate **Z27**.

We preliminary examined the cytotoxicity of intermediates **Z14a**, **Z15a**, **Z15b,** and **pDox**. Cytotoxicity assay was conducted on HeLa cells by serial dilution compound treatment and 24 h incubation. In accordance with previously reported observations, pDox displayed higher potency than Dox, with a single digit nM value of IC_{50} (*Table 6*). The prodrugs were toxic in the IC_{50} range 30-41 nM, and the activity of **Z15b** was restored despite the reduced carbonyl group in the structure.

Table 6. Calculated IC_{50} values after 24 hours incubation of HeLa cells.

	DOX	Z14a	Z15a	Z15b	pDOX
IC_{50}, nM[a]	320±25	30±5	38±4	41±3	1.4±0.3

[a] IC_{50} was determined after 24 h incubation at 37°C in DMEM high glucose medium supplemented with 10 % FBS.

Next, we introduced **Z14a** to the reaction with the linker **Z7** (*Scheme 11*). This chemistry was problematic due to the hindered nature of Doxorubicin nitrogen. Initial reaction conditions with pyridine as a basic component afforded only 3% of conversion. Optimization of reaction conditions allowed to improve the conversion up to 15% by using DMAP (*Table 7*). **Z27** was purified by RP-HPLC and isolated with 5% yield. An insufficient amount of intermediate **Z27** did not allow us to proceed with the peptide conjugation step. Nevertheless, further scale-up can afford a successful conjugation completion.

Table 7. Optimization of reaction conditions for **Z27**.

Base[a]	Conversion of **Z27**, %[b]
DMAP	15
Cs_2CO_3	9
Pyridine	3
DBU	0
TBD	0
DIPEA	0

[a] For reaction condition optimization 5 eq of base was used in the reaction [b] Determined by RP-HPLC

2.4. Conclusion and Outlook

In summary, we designed and implemented the synthetic strategy for the conjugation of Doxorubicin and diacetoxy-alkyl prodrugs **Z14**, **Z15** to peptide carriers through the cleavable linker. The linkage of Doxorubicin to peptide carriers was fast and easy, whereas the preparation of **Z14**, **Z15**, followed by linker attachment faced synthetic issues, which can be solved in the future by reaction conditions improvement to successfully afford Prodrug-Peptide conjugates.

The linear peptide-Doxorubicin conjugate **Z13** was most potent in the series. Peptide dendrimer-Doxorubicin conjugates **Z9**, **Z10** were not so effective, probably due to slower cellular uptake. The cytotoxicity of **Z13** was screened on HeLa, MCF-7, MDA-MB-231, H69, H69 AR cancer cell lines, and CHO, MCF-10a non-cancer cell lines. Overall, **Z13** demonstrated lower cytotoxicity level compared to free Doxorubicin. However, it possesses higher selectivity to cancer cell lines compared to non-cancer cell lines CHO and MCF-10a. In terms of drug resistance, **Z13** exhibits similar activities in wild-type H69 and drug-resistant H69 AR cell lines, compared to a 24-fold activity decrease for DOX in H69 AR, which makes **Z13** more promising against multiple drug-resistant cancers.

Despite several difficulties faced during the synthesis, the data suggested that the principle described here can be applied to different drug delivery systems.

3. Peptide Dendrimers for DACHPt Delivery to Cancer Cells

3.1. Abstract

Cis-diammine-Platinum(II) (*cis*Pt) and 1,2-Diaminocyclohexane-Platinum(II) (DACHPt) complexes are used in almost every cancer chemotherapy treatment. However, these metal complexes cause lasting side effects, which might be reduced by targeted delivery to cancer tissue in the form of nanoparticles exploiting the enhanced permeation and retention effect.[31,104] Here, we investigate peptide dendrimers as possible delivery vectors for DACHPt. Our group has developed a reliable solid-phase synthesis access to peptide dendrimers consisting of short dipeptide or tripeptide branches linked by lysine branching points.[105] Heitz et al. recently reported such peptide dendrimers with sequences tailored for siRNA delivery. These dendrimers consist of polycationic branches connected to a hydrophobic core and form nanoparticles at neutral pH, which undergo endocytosis and disassembly upon acidification of the endosome, resulting in intracellular delivery of their siRNA cargo.[90] Thus, we adapted these peptide dendrimers by introducing multiple metal coordinating side chains enabling binding to DACHPt. Optimization of drug loading, hydrophobicity, and charge distribution in the dendrimer structure allowed us to obtain macromolecular systems with improved *in vitro* cytotoxicity against HeLa cells compared to the free drug.

3.2. Introduction

Platinum-based anticancer drugs are one of the most widely used drug classes in cancer therapy. While they are effective, their use is limited by severe, dose-limiting side effects. Additionally, like many small molecule anticancer drugs, Platinum complexes suffer from increasing drug resistance. Toward overcoming these limitations, a wide range of delivery systems have been proposed, including peptide-targeted Pt complexes,[106–110] PAMAM-based dendrimers,[111] polymers,[112–117] and others.[31] Polymeric micelles attracted great attention in cancer research and have been extensively studied for the last three decades as delivery systems for toxic payloads. One of the most successful representatives of polymeric micelles containing platinum-based anticancer complexes, which undergo clinical studies are NC-6004 (Nanoplatin)[40] and NC-4016[118] (*Figure 9*). However, polymer degradation and elimination from the body is a complex process, and the question of safety and good biocompatibility for some polymers, for example, PEG, is still debatable.[119] In this light, amphiphilic peptide

dendrimers can be promising analogs of nanoparticle formulations for Platinum-based cancer therapy. Their defined structure, natural amino acid composition, and straightforward synthesis allow to fine-tune the drug loading, aggregation properties, and biodegradation of the nanoparticles.

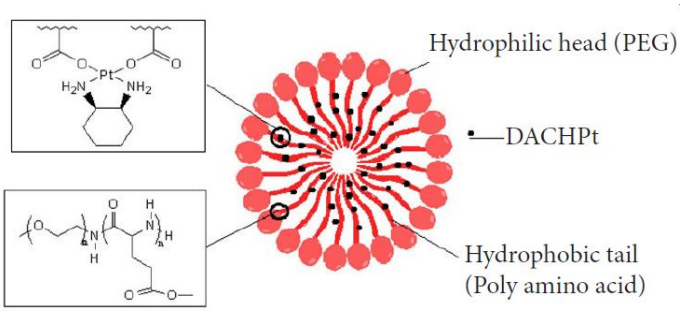

Figure 9. Schematic representation of polymeric micelle NC-4016, undergoing clinical trials. Fgure reproduced from reference [120].

Apart from Pt complexes, other transition metal complexes are reported in the literature as chemotherapeutic agents.[121] Previously, our group has reported cytotoxic peptide conjugates of Ru complexes, which are able to act against cisplatin resistant human ovarian cancer cells A2780R.[122] We proposed, that peptide dendrimers, which are a topic of extensive studies in our group, could also be suitable carriers for metallodrugs.

In this study, we describe new pH-sensitive DACHPt-peptide dendrimer aggregates, which were inspired by the peptide dendrimer sequences, developed for siRNA delivery,[90] capable of self-assembly at neutral pH, and dissociation upon acidification in the endosome, releasing the cargo (*Figure 10*). DACHPt complexation was achieved by introducing multiple metal-coordinating carboxylic side chains in peptide dendrimer structure. To induce amphiphilic properties necessary for aggregation, we performed structure optimization by varying the length of fatty acids and charge distribution among generations. We investigated the aggregation properties of peptide dendrimers alone and complexed with DACHPt by Nile Red CMC assay. We further investigated the activity of DACHPt-peptide dendrimers aggregates against HeLa cells.

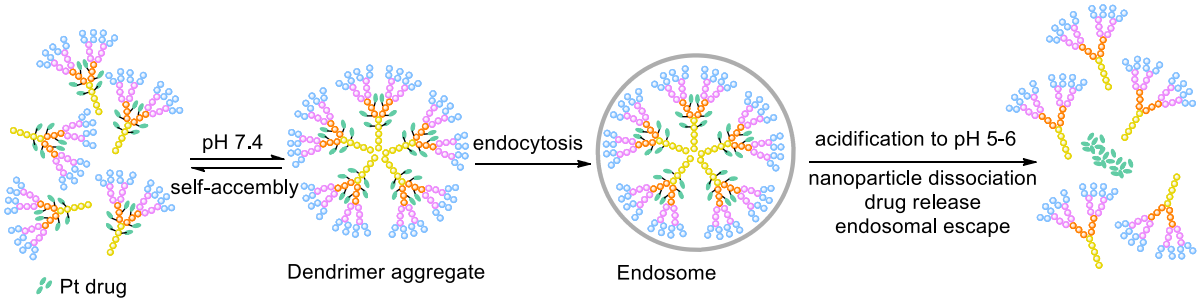

Figure 10. Representation of general strategy for peptide dendrimer-based Pt drug delivery, applied in this chapter.

3.3. Results and discussion

3.3.1. Synthesis

We first performed manual Fmoc-SPPS of designed peptide dendrimers **C1-C15** (*Table 8*) using Tentagel S RAM resin with 0.22 mmol/g loading scale. Peptide dendrimers contained one or two orthogonal protected Lys(Alloc) groups at the core; it was used to introduce lipid tails through acetylation of the Lysine side chain (*Figure 11*). The Alloc-protecting groups were removed after the last coupling, and then fatty acids were added by a standard coupling procedure. Glutamic acid is implied as a Pt complexation source. The overall design of the molecules was performed in a way to balance the amount of negatively charged side chains of Glutamates, positively charged Lysines, and hydrophobic tails. Eventually, the peptide dendrimers were cleaved from the resin with the help of a TFA solution and purified by RP-HPLC to give compounds **C1-C15** with moderate yields.

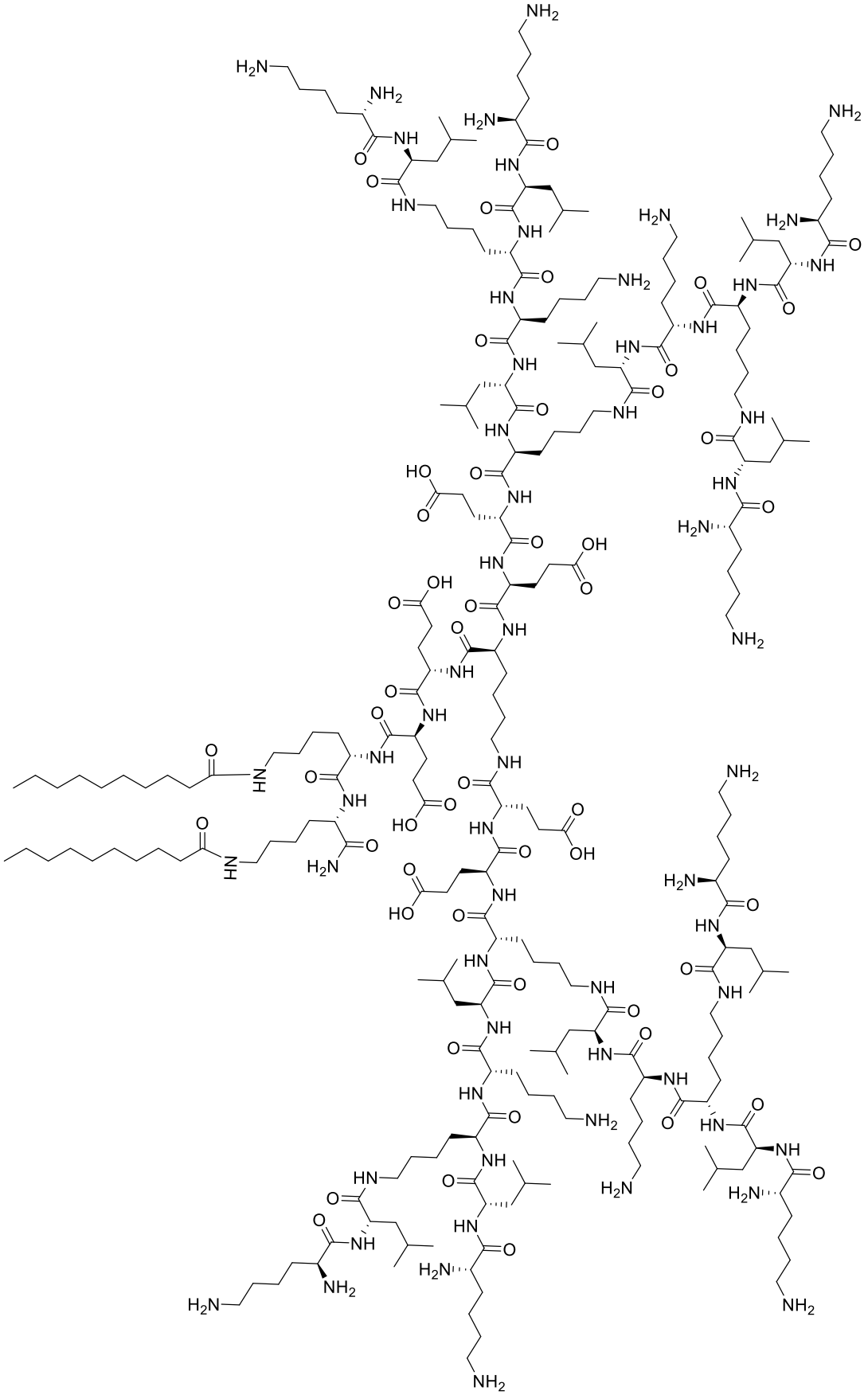

Figure 11. The chemical structure of **C6** *is depicted as an illustrative example of peptide dendrimers used in this chapter.*

Table 8. Synthesis of peptide dendrimers **C1-C15**.

Nr.	Sequence[a]	MS calc/found[b]	Yield, mg (%)[c]
C1	$(KL)_8(KKL)_4(KEEE)_2KK(C_{12})$	4892.3572/4892.3554	40.1 (9.4)
C2	$(KL)_8(KKL)_4(KEEE)_2KK(C_{14})$	4920.3885/4920.3845	20.6 (4.8)
C3	$(KL)_8(KKL)_4(KEE)_2KK(C_{16})$	4690.3346/4690.3332	22.6 (5.3)
C4	$(KL)_8(KKL)_4(KEE)_2KK(C_{18})$	4718.3659/4718.3649	37.0 (8.3)
C5	$(KL)_8(KKL)_4(KEE)_2KEK(C_8),K(C_8)$	4961.4514/4961.4494	40.3 (9.2)
C6	$(KL)_8(KKL)_4(KEE)_2KEEK(C_{10}),K(C_{10})$	5146.5566/5146.5544	58.3 (13.1)
C7	$(KL)_8(KKL)_4(KEEE)_2KEE\ K(C_{10}),K(C_{10})$	5404.6418/5404.6371	37.0 (8.3)
C8	$(KL)_8(KKL)_4(KEE)_2KEK(C_{12}),K(C_{12})$	5073.5766/5073.5562	39.4 (8.8)
C9	$(KL)_8(KKL)_4(KEEE)_2KEEK(C_{14}),K(C_{14})$	5516.7670/5516.7474	36.3 (8.0
C10	$(KL)_8(KKL)_4(KEEEE)_2KEEK(C_{14}),K(C_{14})$	5774.8522/5774.8474	26.6 (5.8)
C11	$(KL)_8(KKLE)_4(KEEE)_2KEEK(C_{14}),K(C_{14})$	6032.9374/6032.9290	33.1 (7.2)
C12	$(KL)_8(KKL)_4(KEE)_2KEK(C_{16}),K(C_{16})$	5185.7018/5185.6970	38.5 (8.5)
C13	$(KL)_8(KKL)_4(KEE)_2KEEK(C_{16}),K(C_{16})$	5314.7444/5314.7376	39.0 (8.6)
C14	$(KL)_8(KKL)_4(KEEEE)_2KEEK(C_{16}),K(C_{16})$	5830.9148/5830.9086	34.3 (7.5)
C15	$(KL)_8(KKLE)_4(KEEE)_2KEEK(C_{16}),K(C_{16})$	6089.0000/6088.9955	22.8 (4.9)

[a] One-letter coded amino acids are used, *K* is the branched lysine residue. Alkyl chains, represented by 'C' followed by their number of carbon atoms, were introduced into the structure through the side chain NH_2 Lysine group. [b] ESI-MS data. [c] Isolated yields as trifluoroacetate salt after preparative RP-HPLC purification.

In the next round, compounds **C1-C8**, **C11**, **C14**, **C15** were selected to prepare complexation with DACHPt. For this, commercially available $DACHPtCl_2$ was transformed into aqueous complex $DACHPt(OH_2)_2^{2+}$, followed by the addition of selected peptide dendrimers and incubation at 25°C for 48 h (*Scheme 12*). Removal of unbound Pt by dialysis at 4ºC yielded in conjugates **C16-C26**.

Platinum content of conjugates was measured by ICP-MS, and drug loading (DL) was calculated according to the following equation:

$$Drug\ loading\ (DL) = \frac{w\ (drug)}{w(drug) + w(nanocarrier)} \times 100\%$$

Overall, the DL decreases with the reduction of the amount of coordination centers in the peptide dendrimer structure (Table 9). However, an increase in the amount of Glu from 8 to 12 did not lead to sufficient DL improvement. The highest DL, 17.6%, was achieved for **C25** when **C14** was used as a carrier. The Pt/peptide dendrimer ratio was in a range from 1.8 to 4.0 for the whole series.

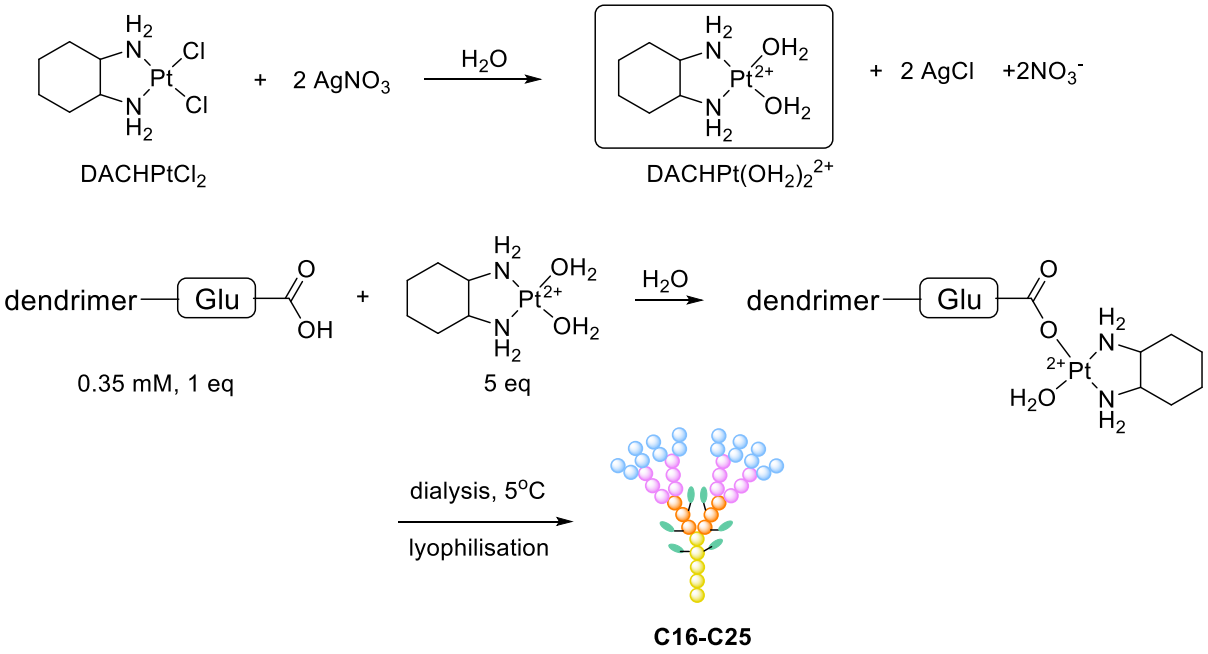

Scheme 12. Synthesis of conjugates ***C16-C25***

Table 9. Synthesis of peptide dendrimer-Pt conjugates **C16-C25**.

Nr.	Structure[a]	Amount of COOH centers[b]	DL, %[c]	Pt/dendrimer ratio[d]
C16	$(KL)_8(\mathit{K}KL)_4(\mathit{K}EEE)_2\mathit{K}K(C_{12})$-DACHPt	6	14.9	2.8
C17	$(KL)_8(\mathit{K}KL)_4(\mathit{K}EEE)_2\mathit{K}K(C_{14})$-DACHPt	6	15.9	3.0
C18	$(KL)_8(\mathit{K}KL)_4(\mathit{K}EE)_2\mathit{K}K(C_{16})$-DACHPt	4	11.7	2.0
C19	$(KL)_8(\mathit{K}KL)_4(\mathit{K}EE)_2\mathit{K}K(C_{18})$-DACHPt	4	12.6	2.2
C20	$(KL)_8(\mathit{K}KL)_4(\mathit{K}EE)_2\mathit{K}EK(C_8),K(C_8)$-DACHPt	5	13.1	2.4
C21	$(KL)_8(\mathit{K}KL)_4(\mathit{K}EE)_2\mathit{K}EEK(C_{10}),K(C_{10})$-DACHPt	6	10.6	2.0
C22	$(KL)_8(\mathit{K}KL)_4(\mathit{K}EEE)_2\mathit{K}EEK(C_{10}),K(C_{10})$-DACHPt	8	16.1	3.4
C23	$(KL)_8(\mathit{K}KL)_4(\mathit{K}EE)_2\mathit{K}EK(C_{12}),K(C_{12})$-DACHPt	5	9.8	1.8
C24	$(KL)_8(\mathit{K}KLE)_4(\mathit{K}EEE)_2\mathit{K}EEK(C_{14}),K(C_{14})$-DACHPt	12	12.1	2.7
C25	$(KL)_8(\mathit{K}KL)_4(\mathit{K}EEEE)_2\mathit{K}EEK(C_{16}),K(C_{16})$-DACHPt	10	17.6	4.0
C26	$(KL)_8(\mathit{K}KLE)_4(\mathit{K}EEE)_2\mathit{K}EEK(C_{16}),K(C_{16})$-DACH Pt	12	14.8	3.4

[a] One-letter coded amino acids are used, *K* is the branched lysine residue. Alkyl chains, represented by 'C' followed by their number of carbon atoms, were introduced into the structure through the side chain ($-NH_2$) of Lysine group. DACHPt - conjugated 1,2-Diaminocyclohexane Platinum. [b] Corresponding to the amount of carboxylic side chain groups of glutamic acid (E) in the structure. [c] Drug loading was determined by ICP-MS. [d] Pt/dendrimer ratio was calculated manually from Pt content.

3.3.2. Critical aggregation concentration

To study the aggregation process of peptide dendrimers alone and complexed with DACHPt, we performed a Nile Red assay at pH 7.4 and pH 5.0, corresponding to the acidified endosome. Nile Red is known to have a higher fluorescence when being surrounded by a hydrophobic environment, and it is a well-known method to determine critical micelle concentration (CMC).[123] CMC is generally calculated by picking the inflection point of the curves. We applied this strategy to our compounds, but we call it critical aggregation concentration (CAC), as peptide dendrimers do not show a real inflection point, and as it is unclear, whether it is a formation of micelles or just aggregates. Nevertheless, we could estimate the aggregation properties and compared them at different pH.

For peptide dendrimers alone, **C1**-**C3**, **C5**, **C7** did not exhibit any aggregation properties at both pH values (*Figure 12*). **C4**, **C6** showed moderate aggregation starting from 0.05 mg/mL at pH 7.4 and no aggregation detectable up to a concentration of 1 mg/mL at pH 5.0. When it comes to more hydrophobic lipidated peptide dendrimers, **C8-C15** showed strong aggregation at pH 7.4, which is in accordance with the rising hydrophobic properties of the sequences due to the presence of different lipid tails. In contrast, at pH 5.0, these peptide dendrimers did not form, or just slightly formed aggregates, thus displaying pH-responsive aggregation character. These effects are probably triggered by the protonation of eight Lysines in the core at lower pH, leading to increased electrostatic repulsion and subsequent disassembly of aggregates.

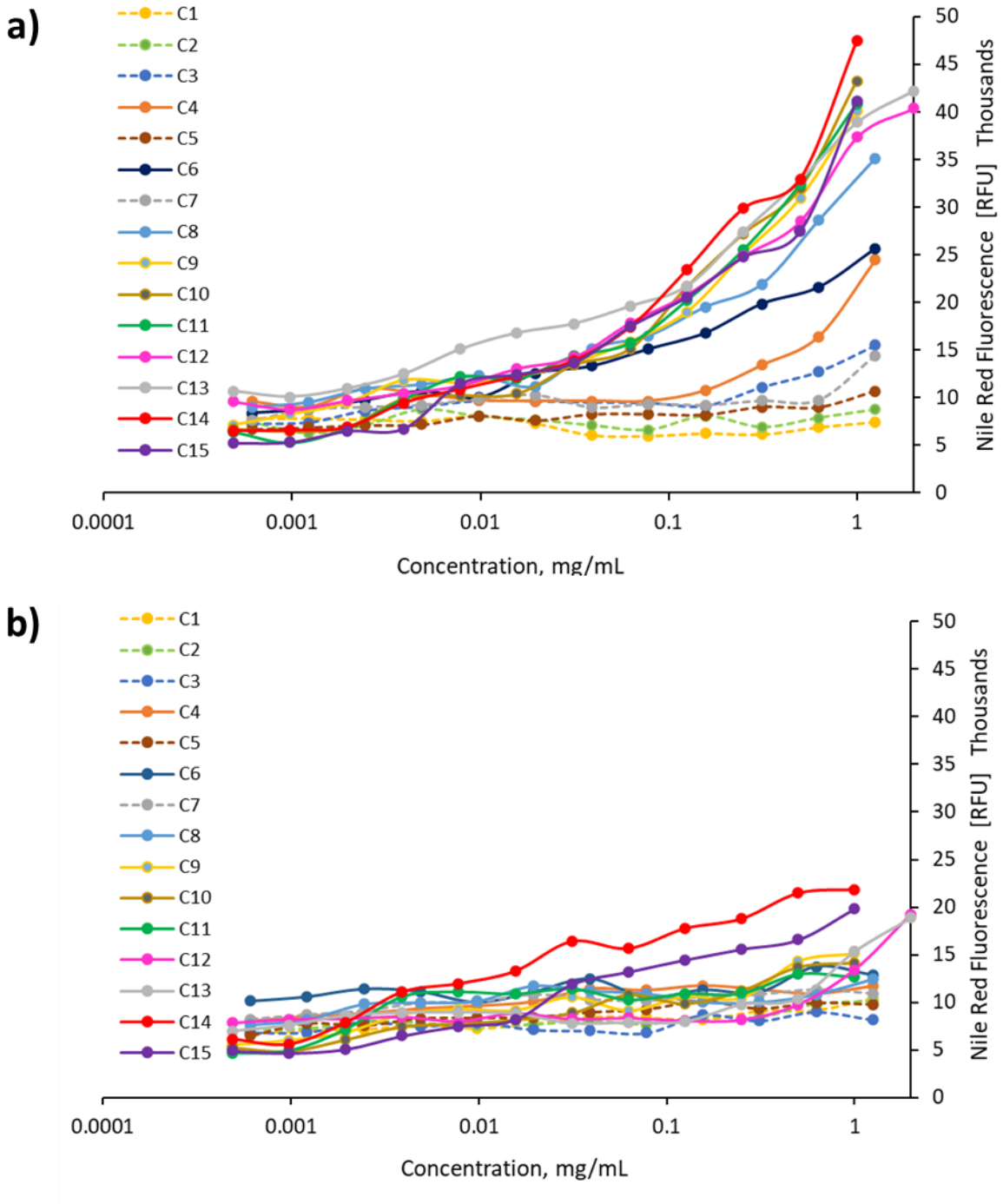

Figure 12. Critical aggregation determination of peptide dendrimers C1-C15 in phosphate buffer at (a) pH 7.4, (b) pH 5.0, performed by serial dilution, followed by treatment of Nile red-coated 96 well plates. Fluorescence is measured at λ_{ex}= 540 nm and λ_{em}= 615 nm.

Next, we performed a similar assay for DACHPt conjugates **C16-C26** (*Figure 13*). By analogy with free peptide dendrimers, compounds **C16**, **C17**, **C18** did not show significant aggregation at both pH values. However, the aggregation properties at pH 5.0 have changed for most of the conjugates compared to free peptide dendrimers. Now, the aggregation was triggered at lower concentrations. It can be explained by hydrophobicity alteration due to the introduction of

hydrophobic diaminocyclohexane scaffolds from the Pt complex. Overall, **C19** turned out to be the most pH-responsive DACHPt conjugate (*Figure 13*).

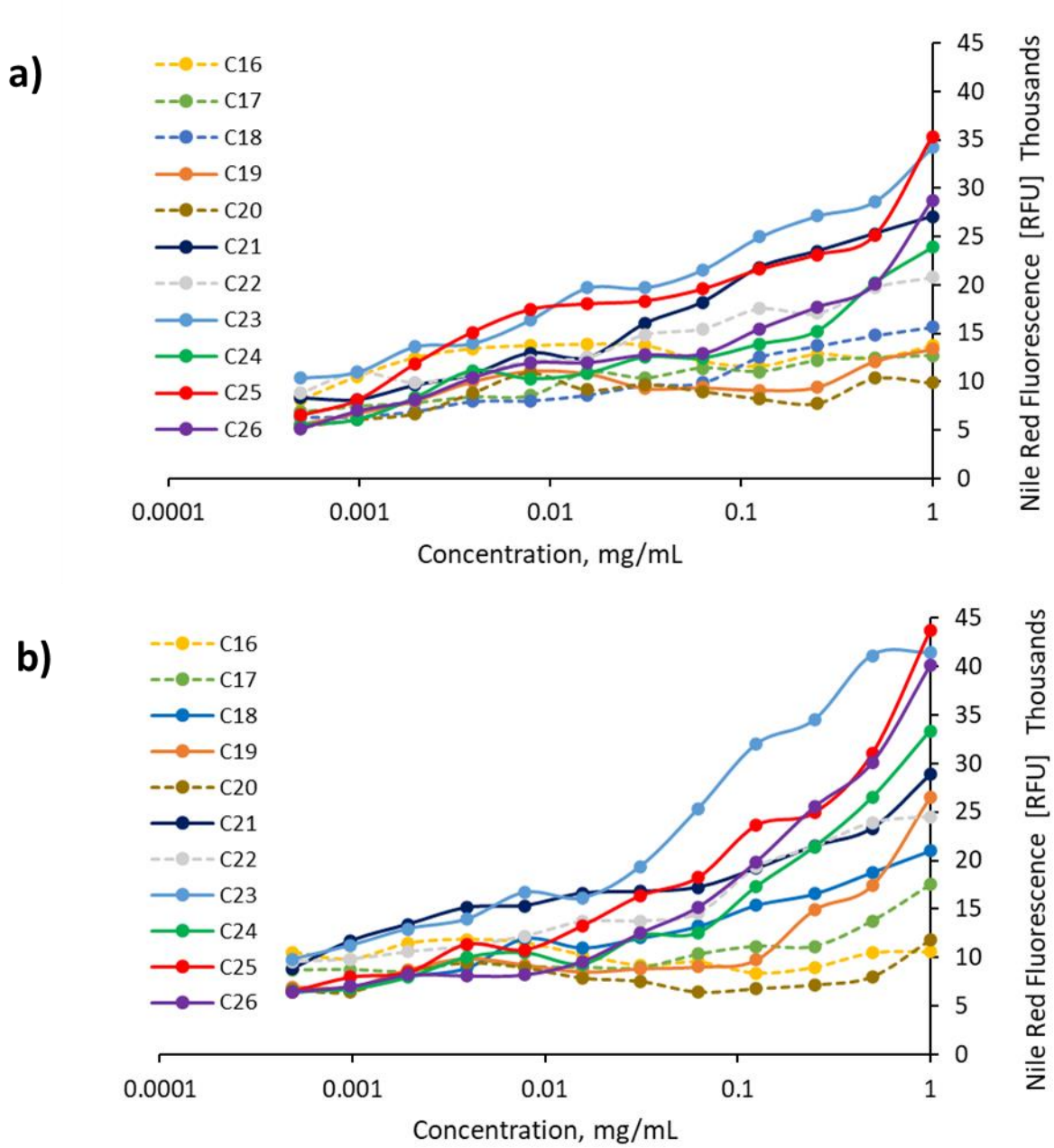

Figure 13. Critical aggregation determination of peptide dendrimers-DACHPt conjugates ***C16-C26*** *in phosphate buffer at (**a**) pH 7.4, (**b**) pH 5.0, performed by serial dilution, followed by treatment of Nile red-coated 96 well plates. Fluorescence is measured at* λ_{ex} *= 540 nm and* λ_{em} *= 615 nm.*

3.3.3. Cytotoxicity measurements

To assess the suitability of peptide dendrimers for further transformations, cytotoxic profiles were studied. The starting peptide dendrimers **C1-C15** were tested on HeLa cells. For this,

HeLa cells were treated with compounds by serial dilution up to 400 μg/mL, incubated for 24 hours at 37ºC in an atmosphere containing 5% CO_2, and cell viability was measured afterward by alamarBlue assay. In general, cell toxicity was satisfactory for most of the analyzed peptide dendrimers, and IC_{50} values were around or above 100 μg/mL, unless **C12**, **C13**, which were most toxic in the series with IC_{50} values 63±5, 51±9 μg/mL, respectively (*Table 10*). Therefore, we excluded **C12**, **C13** for further analysis.

In the next step, we evaluated the cytotoxicity of prepared DACHPt conjugates **C16**-**C26** on HeLa cells. Free DACHPt complex was used for comparison reason. Similarly, HeLa cells were treated with an increased concentration of conjugates and incubated for 24 hours. IC_{50} was further determined and normalized to Pt content in conjugates (*Table 10*).

Table 10. Cytotoxicity data of free peptide dendrimers and DACHPt conjugates for HeLa cells

Peptide Dendrimer	IC_{50}, μg/mL[a]	DACHPt conjugate	IC_{50} (Pt equivalents), μM[b]
C1	>200	C16	9.75±2.6
C2	>200	C17	8.7±3.0
C3	>200	C18	5.9±2.5
C4	>200	C19	3.8 ±1.8
C5	>200	C20	5.4±1.5
C6	~300	C21	6.6±2.0
C7	>100	C22	7.5±1.0
C8	>200	C23	4.7±0.6
C9	~130	-	-
C10	110±14	-	-
C11	>200	C24	5.4±1.1
C12	63±5	-	-
C13	51±7	-	-
C14	99±10	C25	7.4±1.9
C15	~200	C26	7.0±1.1
		DACH Pt[c]	7.1±0.6

[a] IC_{50} was determined after 24 h incubation at 37°C in DMEM high glucose medium supplemented with 10 % FBS. [b] IC_{50} was determined after 24 h incubation at 37°C in DMEM high glucose medium supplemented with 10 % FBS and converted according to Pt content. [b] DACHPt was used for comparison.

In the case of **C1**, **C2**, the cytotoxicity was slightly lower compared to free DACHPt; for **C7**, **C14**, **C15** cytotoxicity was comparable, and the rest of the series showed better potency than

free DACHPt. The most active compound **C19** was two times more potent with IC_{50} value 3.8±1.8 μM than free DACHPt. The increased potency of **C19** could be due to the fact that this macromolecular compound is prone to form pH-sensitive aggregates, which facilitates the cellular uptake and drug release.

3.4. Conclusion

In summary, we designed, synthesized, and characterized peptide dendrimers **C1**-**C15** as new modalities for Platinum drug delivery. We focused our attention on pH-responsive aggregation properties of peptide dendrimers, varying the hydrophobicity and charge distribution among the structure. We further performed DACHPt chelation using well-established carboxylate complexation chemistry. The drug loading was achieved up to 17.6% for **C25**. More than half of the DACHPt-peptide dendrimer exhibited higher cytotoxicity levels compared to free DACHPt in HeLa cell culture. Finally, we identified a hit compound **C19**, which showed pH-responsive aggregation properties and was twice more potent than free DACHPt.

As an outlook, we are planning to asses the toxicity of obtained scaffolds on non-cancer cell models, as well compare the effectivity on cisplatin-resistant cancer cells. We are also interested in study of DACHPt release profile from peptide dendrimers. These results could complete our investigations.

4. Machine Learning Guided Discovery of Non-Hemolytic Membrane Disruptive Anticancer Peptides

All the computations, including the design of recurrent neural network (RNN) models, PDGA implementation, data extraction, filtering, and clustering were performed by Dr. Alice Capecchi and Markus Orsi as a part of their PhD work. The rest of the experimental work (synthesis, physico-chemical analysis, biological evaluation, etc) was performed by myself.

The results presented in this chapter belong to the manuscript «Machine Learning Guided Discovery of Non-Hemolytic Membrane Disruptive Anti-Cancer Peptides», published in *ChemMedChem* Journal.

Zakharova, E.; Orsi, M.; Capecchi, A.; Reymond, J.-L. *ChemMedChem*, **2022**, *n/a*, e202200291.

doi.org/10.1002/cmdc.202200291

4.1. Abstract

Most antimicrobial peptides (AMPs) and anticancer peptides (ACPs) fold into membrane disruptive cationic amphiphilic α-helices, many of which are, however, also unpredictably hemolytic and toxic. Here we exploited the ability of recurrent neural networks (RNN) to distinguish active from inactive and non-hemolytic from hemolytic AMPs and ACPs to discover new non-hemolytic ACPs. Our discovery pipeline involved: 1) sequence generation using either a generative RNN or a genetic algorithm, 2) RNN classification for activity and hemolysis, 3) selection for sequence novelty, helicity, and amphiphilicity, and 4) synthesis and testing. Experimental evaluation of thirty-three peptides resulted in eleven active ACPs, four of which were non-hemolytic, with properties resembling those of the natural ACP lasioglossin III. Mechanistic studies revealed that these ACPs are α-helical amphiphilic peptides, killing cells by membrane disruption as well as by interacting with mitochondria. These experiments show the first example of direct machine learning-guided discovery of non-hemolytic ACPs (*Figure 14*)-

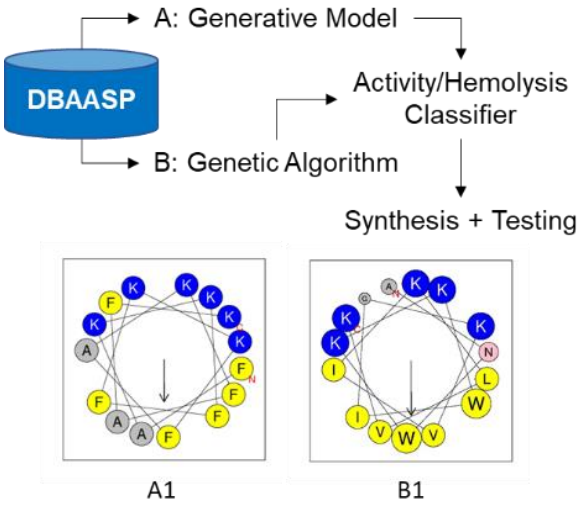

Figure 14. Schematical representation of workflow of the project.

4.2. Introduction

Cancer remains a major cause of death, affecting millions of people. Increasing resistance to chemotherapeutic drugs combined with detrimental side effects complicates cancer treatment.[124] In recent years, therapeutic peptides have been attracting great interest in cancer therapy. Anticancer peptides (ACPs) represent promising anticancer agents due to their high activity, low immunogenicity, good biocompatibility, and easy synthesis.[58,125,126] Moreover, most the ACPs can overcome resistance due to the unique mechanism of action that involves membrane lysis.[127–129] Membranolytic ACPs are derived from antimicrobial peptides (AMPs), and like the latter, they are characterized by the net positive charge, amphipathic properties, and dominated helical structure.[65,130] However, many membranolytic ACPs suffer from toxicity towards non-cancer and red blood cells. Therefore, the design of new selective non-hemolytic anticancer peptides is of great interest.

Machine learning (ML) is ideally suited to assist drug design whenever a large corpus of structure-activity data is available. In the case of peptides, documented to act against various microorganisms, cancer cells, and red blood cells, structure-activity relationships are often difficult to rationalize.[131–133] Most of these ML-guided peptide designs focused on antimicrobial peptides (AMPs), due to the pervasive reported activity data.[16–20] Similar approaches have also been applied to the much less abundant data on anticancer peptides (ACPs),[134–144] however, there are only a few examples of ML *de novo* design of ACPs with experimental validation.[145,146] The ACPs identified with these ML approaches were also hemolytic, and their selectivity had to be improved by iterative mutation and testing. Thus, the

generation of non-hemolytic membrane disruptive ACPs represents a great challenge for ML models, most likely because of the difficulty to distinguish between closely related eukaryotic cells rather than between bacteria and eukaryotes, as well as because of the sparsity of data on ACPs to train ML models.

Herein we report two ML approaches to identify membrane disruptive ACPs supported by data from the database of antimicrobial activity and structure of peptides (DBAASP), which lists sequences and activity information on 18,405 bioactive peptides.[147,148] In our first approach, we generated a set of tentative ACPs by sampling a generative recurrent neural network (RNN). The RNN was trained with active sequences from DBAASP, which lists peptides with various activities comprising antimicrobial and anticancer peptides, and fine-tuned towards ACP generation by transfer learning[149] with a small set of ACPs reported to be active on HeLa cells, an activity which we could easily test experimentally. In a second approach, we used our recently reported PDGA (peptide design genetic algorithm),[150] which evolves random sequences towards any target molecule by rounds of mutation and selection according to a measured similarity, to generate analogs of the known ACP lasioglossin III (LL-III), also with a reported activity on HeLa cells.[151] In both approaches, we filtered the generated peptides using RNN classifiers for activity and hemolysis, which were trained with DBAASP data and were previously shown to have good performance compared to other methods.[152] We finally selected sequences based on novelty as well as on their predicted α-helicity and amphiphilicity to favor the expected membrane disruptive mechanism of action. As detailed below, synthesis and testing of the selected peptides allowed us to identify non-hemolytic membrane disruptive α-helical ACPs from both approaches.

4.3. Results and discussion

4.3.1. ML-guided design

In our first approach, we selected 53 sequences in DBAASP which were reported to be active against HeLa cells, a common type of cancer cells that can be readily assayed. We used these 53 ACPs in a transfer learning step to fine-tune our previously reported general RNN generative prior model,[152] which had been trained with 4,774 peptides reported with any type of bioactivity in the database. We then sampled 50,000 sequences from this fine-tuned generative model. To refine this set, we applied our previously reported RNN activity classifier trained with 6,641 active peptides from DBAASP.[152] This activity classifier labeled approximately 20% of the sampled sequences (11,458) as potentially active. Considering that

46 of the 53 ACPs used for transfer learning were predicted to be hemolytic, we did not apply a hemolysis classifier to this set. Nevertheless, we filtered sequences to be short (≤ 15 residues) as well as novel yet within the classifier's applicability domain (at least five mutations relative to the test set and 6 to 7 mutations from the training set). We further restricted the selection to sequences containing only L-enantiomeric residues and predicted to be > 80% α-helical using helicities predicted by SPIDER3,[153] a neural network trained with data from the Protein Data Bank, and with a calculated hydrophobic moment[154] > 0.3 (corresponding to median values of DBAASP active sequences: 0.83 and 0.31). This procedure retained 202 peptide sequences, from which we selected thirteen by clustering for synthesis and evaluation (*Figure 15a*).

For our second approach, we aimed to select non-hemolytic ACPs directly. Given the sparsity of training data for non-hemolytic ACPs, we focused on LL-III due to its short length (15 residues) and documented non-hemolytic ACP activity below 200 μM.[151,155–157] To generate LL-III analogs, we used PDGA[150] with the molecular fingerprint MAP4 as a similarity measure. This fingerprint is well-suited for virtual screening of molecules of any size range, including peptides.[158] The MAP4-driven PDGA generated 715,658 LL-III analogs, which we then passed through our RNN general activity classifier and our RNN hemolysis classifier, leaving 6,300 sequences (0.88 %) as potentially active and non-hemolytic. Applying the same sequence length, novelty, predicted helicity, and hydrophobic moment criteria as above further reduced the list to 153 peptides, from which we selected 20 sequences by clustering for synthesis and evaluation (*Figure 15b*).

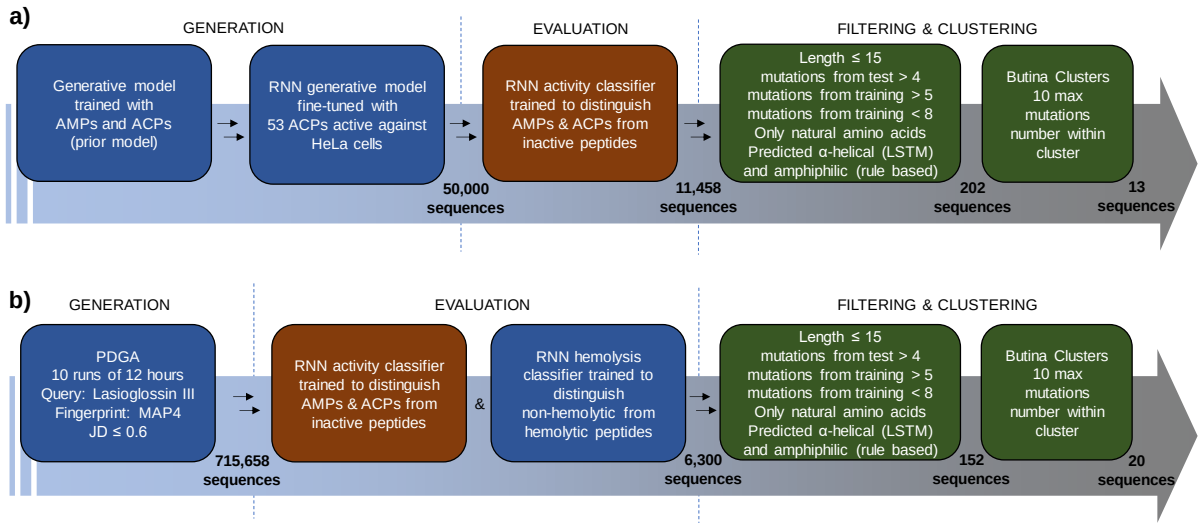

Figure 15. In silico generation, evaluation, filtering, and clustering of ACP-like peptide sequences. ***(a)*** *First approach: a prior generative model trained with AMPs and ACPs was fined-tuned with 53 ACPs active against Hela cancer cells. 50,000 sequences were sampled from the fined-tuned model and evaluated using an RNN classifier trained to distinguish ACPs and AMPs from inactive peptides. The 11,458 sequences predicted to be active were further filtered to be short, novel, within the applicability domain of the classifier, containing only natural amino acids, predicted α-helical and amphiphilic. Finally, the obtained 202 sequences were clustered based on their sequence similarity so that the sequences within each cluster were at a maximum of 10 mutations away from each other, 13 were picked for synthesis.* ***(b)*** *Second approach: PDGA was used to find analogs of LL-III. 10 runs of 12 hours each led to 715,658 unique sequences with a MAP4 Jaccard distance (JD) from the query below or equal to 0.6. The generated sequences were then evaluated using the same activity classifier used in the first approach and a hemolysis classifier trained to distinguish between hemolytic and non-hemolytic peptides. The 6,300 sequences predicted to be active and non-hemolytic were then filtered and clustered as in the first approach, and 20 sequences were selected for further synthesis.*

4.3.2. Synthesis and activity of ACPs toward eukaryotic cells

After manual selection, the series of peptides were synthesized by the standard Fmoc solid phase peptide synthesis method. Compounds **A1-A13** (*Table 11*) and **B1-B20** (*Table 12*) are derived from the first and second ML approaches, respectively. Cytotoxicity screening of compounds was performed on cancerous HeLa and non-cancerous HEK-293 cell lines. Cells were incubated with various concentrations of the peptides for 72 h, and then cell viabilities were determined using the alamarBlue™ assay, measuring the cell proliferation. A hemolysis test as a sign of general toxicity was performed for each peptide on human red blood cells (hRBC) by serial dilution in phosphate buffer and incubation for 4 h at room temperature.

In approach A, seven compounds **A1-A7** out of thirteen (54%) turned out as active against HeLa cells with IC_{50} value range from 8.2 to 19.0 μM (*Table 11*). The compound **A1** demonstrates one of the highest cytotoxicities among the list as well as the best selectivity for HeLa (IC_{50} = 8.2 μM) cells over non-cancer HEK-293 (IC_{50} = 15 μM) cells. Further peptides in the ranking showed less activity distinction between two cell lines; **A2, A5, A6** were even more toxic against HEK-293 cells. At the same time, peptides **A2-A7** were extremely hemolytic ($23 \leq HC_{50} \leq 93$ μM), and only **A1** showed no significant hemolysis. According to the structure, compound **A1** is an analog of Hecate and FLAK peptides, and their toxicity values toward mammalian cells are similar to those obtained for **A1**.[159–161] Compounds **A8-A13** turned out to be neither active nor hemolytic.

In the next approach B, in which generation of sequences was alternatively performed by PDGA, we introduced RNN hemolysis classifier and searched for the analogs of Lasioglossin III (**LL-III**).[151] This short peptide, which originated from wild bee venom, was chosen as a reference due to its potent antimicrobial and anticancer activity, low hemolysis, and proven *in vivo* safety in mice.[151,155–157] It gave us, after manual selection, a library of 20 compounds **B1-B20** which were synthesized and evaluated for the activity (*Table 12*). Three peptides **B1-B3** out of the list have been found to possess activity against mammalian cell lines and low hemolysis, with the best selectivity for **B1**. Compared to reference peptide **LL-III** (IC_{50} = 6.0 μM, HC_{50} > 200 μM), peptide **B1**, in turn, showed also anticancer (IC_{50} = 5.5 μM) and hemolytic (HC_{50} > 200 μM) properties at the same range. Considering the hemolysis threshold of $HC_{50} \geq 100$ μM, compounds **B1-B20** turned out to be non-hemolytic, however, at the same time, the majority of compounds were inactive.

Additional testing of the three most active ACPs identified, namely **A1**, **B1,** and **B2**, as well as **LL-III** showed comparable single-digit micromolar activities against MCF-7 (breast cancer) and MB-MDA-231 (triple-negative breast cancer) cell lines and 2-fold selectivity against MCF-10a (non-cancerous breast) cells line (*Table 13*).

Table 11. Synthesis and activity of peptides from approach A.

Nr.	Sequence[a]	Toxicity[b], IC_{50}/μM		Hemolysis[c], HC_{50}/μM	MIC[d], μg/mL		CD[e]	% Vesicle leakage[f]	
		HeLa	HEK-293	hRBC	*PAO1*	*A. baumannii*	% α-helix	PC	PG
A1	FAKKFFKKFAKFAFK	8.2±0.5	15±0.7	>200	8	8	72	79	43
A2	WFKRILKYLKKLV	8.4±0.5	7.8±0.2	60±8	8	4	66	78	29
A3	WLNALKKILGHLIRH	8.2±0.8	13±0.7	30±5	16	4	79	100	37
A4	KYLKYLVRLVGRLYR	12±1.4	13±1.1	61±10	16	4	68	96	56
A5	WKRIVRIIRWIRKYY	18±0.2	14±0.6	93±4	>16	>16	74	100	46
A6	FAARILRAWFRFLRR	11±2	7.5±0.5	23±2	>16	16	75	93	35
A7	SISRLWHSLLRHLLH	19±1	19±4	23±3	>16	4	76	100	100
A8	KNFKKLMKKVASVL	>50	>50	>400	8	4	51	16	97
A9	SFSKWMGKLKNIFKK	>50	>50	>400	8	8	50	18	32
A10	LLRHCLRRIRDRLV	>50	>50	>400	16	8	70	56	67
A11	KWRSKIKKIMRTFK	>50	>50	>400	16	16	46	11	32
A12	GLLGRLAKLLANS	>50	>50	>400	16	16	49	1	3
A13	VFRQWQKIMRRLVRR	>50	>50	>400	>16	16	49	2	5

[a] All peptides were synthesized with C-terminal amidation. [b] IC_{50} was determined after 72 h incubation at 37°C in DMEM high glucose medium supplemented with 10 % FBS. [c] HC_{50} was measured on human red blood cells in 10 mM phosphate buffer saline, pH 7.4, 25°C. Triton X-100 was used as a positive control. [d] MIC was determined after incubation for 16–20 h at 37°C in MH medium. [e] Circular Dichroism spectra were measured at concentration 100 μg/mL of peptides in 10 mM phosphate buffer, pH 7.4 in a presence of 5 mM DPC. Percentage of α-helical structure was calculated by DichroWeb. [f] Fluorescein leakage from phosphatidyl choline (PC) or phosphatidyl glycerol (PG) vesicles was measured in buffer (10 mM TRIS, 107 mM NaCl, pH 7.4) in the presence of 10 μg/mL of peptides. 0.012% Triton in buffer was used as positive control.

Table 12. Synthesis and activity of peptides from approach B.

Nr.	Sequence[a]	Toxicity[b], IC_{50}/μM		Hemolysis[c], HC_{50}/μM	MIC[d], μg/mL		CD[e]	% Vesicle leakage[f]	
		HeLa	HEK-293	hRBC	*PAO1*	*A. baumannii*	% α-helix	PC	PG
LL-III[g]	VNWKKILGKIIKVVK	6.0±0.5	15±3	>200	4-8	4	74	99	72
B1	ANWKKWIGKVIKLVK	5.5±0.8	12±2	>200	4	4	70	99	77
B2	NWKKILGKILDHLAC	7.0±1.4	6.7±0.5	322±27	>16	8	68	94	100
B3	ANWKKILKRLCDI	22±0.5	28±5	166±4	>16	16	71	62	99
B4	NWKKILGKICR	>50	>50	>400	4	4	49	51	99
B5	KNWKKIIKKVVK	>50	>50	>400	4	16	35	11	99
B6	VNVWKKIGRLVKIVK	>50	>50	>400	8	4	60	50	74
B7	NEWKKIKKIIKIVK	>50	>50	>400	16	16	49	24	28
B8	KWRQLGKKIIKVAK	>50	>50	>400	16	16	51	12	99
B9	NWKKIRKLGKVVKKI	>50	>50	>400	16	16	40	28	80
B10	VVNNWKKKIIKVIK	>50	>50	>400	>16	>16	48	3	66
B11	DWHKIGKKVIKVIK	>50	>50	>400	>16	>16	53	14	99
B12	KWNNILGKLGKLAR	>50	>50	>400	>16	>16	46	4	14
B13	NVVGRLGKIVKIVK	>50	>50	>400	>16	>16	46	1	30
B14	NPKVFLKKIIKVVK	>50	>50	>400	>16	>16	54	0	0
B15	ADVWKKVIKVIK	>50	>50	>400	>16	>16	42	2	16
B16	WRGKIGKIIKAVK	>50	>50	>400	>16	>16	60	16	21
B17	NWKKILGRLGEKG	>50	>50	>400	>16	>16	26	0	13
B18	KNWKKIVHDIKNS	>50	>50	>400	>16	>16	38	1	14
B19	NWKKILGKVIDDMKM	>50	>50	>400	>16	>16	58	16	95
B20	DKFSEKLGKIIKIVK	>50	>50	>400	>16	>16	62	5	51

[a] All peptides were synthesized with C-terminal amidation. [b] IC_{50} was determined after 72 h incubation at 37°C in DMEM high glucose medium supplemented with 10 % FBS. [c] HC_{50} was measured on human red blood cells in 10 mM phosphate buffer saline, pH 7.4, 25°C. Triton X-100 was used as a positive control. [d] MIC was determined after incubation for 16–20 h at 37°C in MH medium. [e] Circular Dicroism spectra were measured at concentration 100 μg/mL of peptides in 10 mM phosphate buffer, pH 7.4 in a presence of 5 mM DPC. Percentage of α-helical structure was calculated by DichroWeb. [f] Fluorescein leakage from phosphatidyl choline (PC) or phosphatidyl glycerol (PG) vesicles was measured in buffer (10 mM TRIS, 107 mM NaCl, pH 7.4) in the presence of 10 μg/mL of peptides. 0.012% Triton in buffer was used as a positive control. [g] Parent peptide *lasioglossin* III (LL-III) used for PDGA was synthesized for comparison.

Table 13. Extended IC_{50} profiling.

Nr.	Sequence	HeLa[a]	MCF-7[a]	MB-MDA-231[a]	MCF-10a[b]	HEK-293[a]
A1	FAKKFFKKFAKFAFK	8.2±0.5	6.0 ±0.5	6.4±0.5	17.3±3.5	15.2±0.7
B1	ANWKKWIGKVIKLVK	5.5±0.8	6.1±1.0	5.0±0.6	19.5±2.8	12.1±1.6
B2	NWKKILGKILDHLAC	7.0±1.4	5.4±0.3	5.4±1.2	11.7±0.4	6.7±0.5
LL-III[a]	VNWKKILGKIIKVVK	6.0±0.5	7.1±0.3	5.9±0.4	14.8±2.1	15.0±3.0

[a] IC_{50} was determined after 72 h incubation at 37°C in DMEM high glucose medium supplemented with 10 % FBS. [b] IC_{50} was determined after 72 h incubation at 37°C in serum-free HUMEC ready medium.

4.3.3. Antimicrobial activity

The fact that the RNN activity classifier was beside ACP trained on AMP data, suggested us to test compounds in a broader context. Compounds **A1**-**A13**, **B1**-**B20** were evaluated for antibacterial activity toward two Gram-negative strains *P. aeruginosa (PAO1)* and *A. baumannii* by determining minimum inhibitory concentrations (MIC) against bacteria in broth microdilution assay in Muller–Hinton medium (*Table 11*, *Table12*). Considering an activity threshold of MIC ≤ 16 μg·mL^{-1}, 9 of 13 peptides (69%) from group A and 7 of 20 peptides (35%) from group B were active against *P. aeruginosa;* 12 of 13 (92%) peptides from group A and 9 of 20 peptides (45%) from group B were active against *A. baumannii,* showing substantial antibacterial activities independent of their hemolytic activities.

Interestingly, inactive against mammalian cells peptides **A8**-**A13** were able to kill bacteria *P. aeruginosa* and/or *A. baumannii* with MIC range 4-16 μg·mL^{-1}. Similarly, six inactive for eucaryotic cells peptides from group B were also active on bacteria.

Thus, implementation of ML models allowed us to find peptides with either dual (anticancer and antibacterial) activity or with selective antibacterial activity, but not *vice versa*, supporting the fact that *in silico* prediction of selective ACPs may require a more sophisticated ML model compared to AMPs. Several ML model training iterations with obtained bioactivity data can improve further predictions.

4.3.4. Synthesis and activity of D-amino acid substituted peptides

To further investigate the influence of peptidic structure on activity, we decided to synthesize peptides **DA1**, **DB1,** and **DLL-III -** analogs of hit peptides, consisting of D-amino acids (*Table 14*). We have found that toxicity toward mammalian cells as well as hemolysis remain analogous for both L-and D-stereoisomeric forms; therefore, the activity is not related to the chirality. These results align with reported activities for stereoisomers of macropin, lasioglossins, and halictine.[155] Concerning antibacterial activity, switching the chirality to D-amino acids had an impact on *P. aeruginosa* and/or *A. baumannii* by showing 2-fold reduction

in MIC for tested peptides. Increased activity of D-stereoisomers was previously observed with other AMPs against various fungal and bacterial strains.[162] It can be explained by increased stability of D- over L-stereoisomers in a bacterial environment.

Table 14. Synthesis and activity D-amino acid substituted peptides.

		Toxicity[b], IC_{50}/µM		Hemolysis[c], HC_{50}/µM	MIC[d], µg/mL		CD[e]
Nr.	Sequence[a]	HeLa	HEK-293	hRBC	*PAO1*	*A. baumannii*	% α-helix
DLL-III	vnwkkilgkiikvvk	5.0±0.7	14.5±2.0	>200	4	2	74
DA1	fakkffkkfakfafk	7.9±0.3	15.0±2.3	>200	4	4	71
DB1	anwkkwigkviklvk	6.2±1.1	13.1±2.8	>200	4	2	71

[a] All peptides were synthesized from D-amino acids with C-terminal amidation. [b] IC_{50} was determined after 72 h incubation at 37°C in DMEM high glucose medium supplemented with 10 % FBS. [c] HC_{50} was measured on human red blood cells in 10 mM phosphate buffer saline, pH 7.4, 25°C. Triton X-100 was used as a positive control. [d] MIC was determined after incubation for 16–20 h at 37°C in MH medium. [e] Circular Dicroism spectra were measured at concentration 100 µg/mL of peptides in 10 mM phosphate buffer, pH 7.4 in a presence of 5 mM DPC. Percentage of α-helical structure was calculated by DichroWeb.

4.3.5. Circular dichroism

In view of the selection procedure applied, we anticipated that our peptides would behave as membrane disruptive α-helices similar to most known ACPs.[65,127,163] Although the activities of the synthesized peptides varied strongly, an inspection of helix-wheel models showed that all the synthesized sequences could indeed be expected to form amphiphilic and potentially membrane disruptive α-helices, in line with our selection for high predicted hydrophobic moment (*Figure 16a* and *S9*). To investigate whether this was the case, we measured circular dichroism (CD) spectra in neutral phosphate buffer, with an optional addition of 5 mM dodecyl phosphocholine (DPC), which mimics the membrane surface and induces folding of α-helical amphiphilic peptides.

The peptides indeed behaved as typical α-helical amphiphiles by showing an unordered conformation in neutral phosphate buffer but a substantial α-helical fraction in the presence of 5 mM DPC (*Figure 16b, S10-11, Tables 11-12*). However, contrary to the predicted α-helicity, which was equally high for all synthesized peptides, experimental helicity varied strongly between the different peptides and was correlated with ACP and AMP activity. For instance, helicity was higher in sequences with anticancer activity (66 - 79% α-helix) compared to those showing only antibacterial effects (35 - 70% α-helix) and those lacking any activity (26 - 60% α-helix).

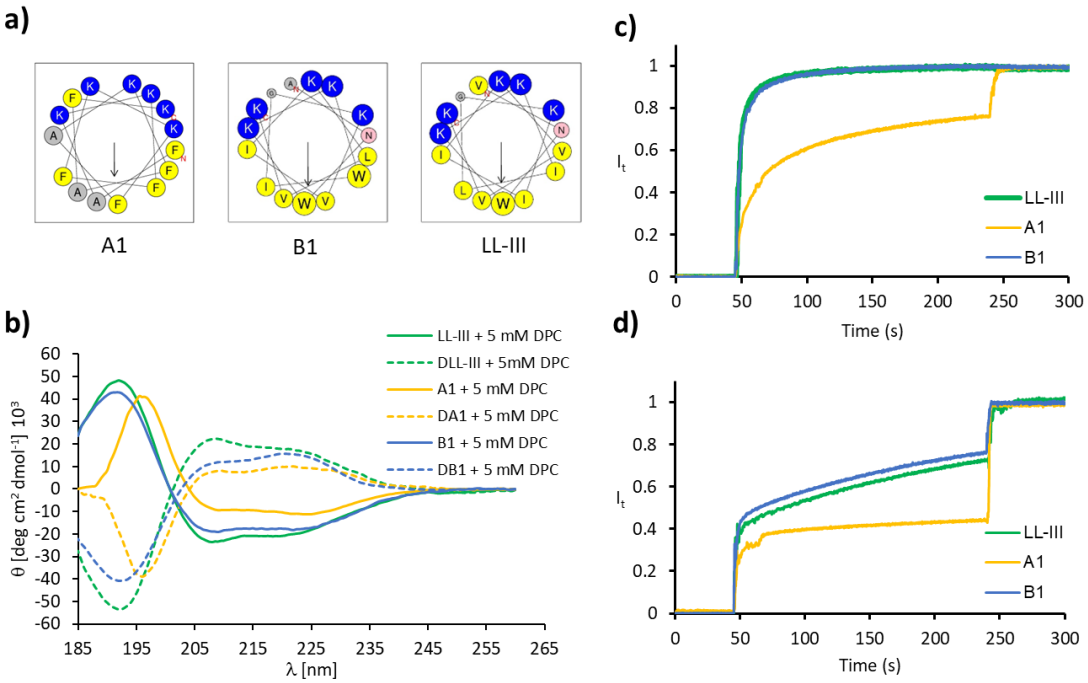

*Figure 16. Helical properties of ACPs A1, B1 and LL-III. (**a**) Helix properties predicted by HeliQuest.[164] Circle size proportional to side-chain size, blue indicates cationic residues, red indicates anionic residues, yellow indicates hydrophobic residues, grey indicates alanine and glycine, pink indicates asparagine. Arrows represent the helical hydrophobic moment. (**b**) CD spectra of hit peptides (100 µg/mL) in 10 mM phosphate buffer pH 7.4 in the presence of 5 mM DPC. (**c**) Vesicle leakage experiment using 5(6)-carboxyfluorescein, induced by selected peptides at 10 µg/mL. Fluorescein leakage assay from egg yolk phosphatidyl choline (PC) lipid vesicles. (**d**) Fluorescein leakage assay from egg yolk phosphatidyl glycerol (PG) lipid vesicles. Vesicles were suspended in buffer (10 mM TRIS, 107 mM NaCl, pH 7.4) and compounds were added after 45 sec. After 240 seconds 1.2% Triton X-100 was added for the full release of fluorescein.*

4.3.6. Lipid vesicle leakage assay

To measure membrane disruptive activities directly, we performed fluorescein leakage assays with vesicles made from either phosphatidyl glycerol (PG) as an anionic lipid mimicking bacterial and cancer cell membranes, or phosphatidyl choline (PC) as a zwitterionic lipid mimicking the neutral membrane of healthy eukaryotic cells (*Figure 16c/d, S11-S12, Tables 11-12*). In approach A, all active ACPs showed strong leakage activity at 10 µg/mL on PC vesicles. Furthermore, all peptides from this series except the least active **A12** and **A13** were also active on PG vesicles. In approach B, only the most active ACPs (**LL-III**, **B1** and **B2**) showed intense activity against PC vesicles, while activity on PG vesicles was visible in the most active AMPs (**LL-III**, **B1**-**B9**) as well as in two inactive peptides (**B10** and **B11**). Overall, these data showed that the experimental percentage of α-helix also varied with membrane disruptive effects on vesicle model systems. The fact that the most active ACPs discovered,

peptides **A1** and **B1**, were among the most α-helical and showed very strong vesicle leakage activity was consistent with a membrane disruptive mechanism of action.

4.3.7. Cellular entrance and mode of action of AC peptides

4.3.7.1. Cellular uptake of fluorescein-labelled peptides

To understand the behavior of our peptides toward mammalian cells, we investigated their cellular uptake. Most active peptides (L- and D- versions) were coupled with 5/6-carboxyfluorescein at N-terminus, giving **FA1** and **FDA1, FB1** and **FDB1, FLL-III** and **FDLL-III,** respectively. Flow cytometry experiments, performed with fluorescent peptides on HeLa cells within 3 h at 10 μM, showed that the peptides bound to or internalize HeLa cells (Fluorescein-positive cells > 70%) (*Figure 17a*).

Furthermore, confocal microscopy images of fixed HeLa cells treated with 10 μM of **FB1** and **FDB1, FLL-III** and **FDLL-III** showed the accumulation of fluorescent peptides in the cytosol with some density in the nucleoli after 2 h, the most visible for **FLL-III** (*Figure S14*). Evidences of DNA interaction with lasioglossins were already mentioned in the literature, suggesting DNA as a possible alternative intracellular target.[165,166]

4.3.7.2. Propidium iodine (PI) permeabilization.

Additionally, cell membrane disruption was studied by Propidium Iodine (PI) internalization assay. PI cannot cross intact plasma membrane and, therefore, will only be present in the DNA of cells where the plasma membrane has been compromised. PI internalization was observed by flow cytometry upon HeLa cells treatment with peptides **A1**, **DA1**, **B1**, **DB1**, **LL-III**, **DLL-III** at 10 μM. In 15 min the number of PI-positive cells reached a level between ~23 % and ~48 % (*Figure 17b, S15*). Thus, we can conclude that the tested peptides' mechanism of action involves initial permeabilization of the cell membrane.

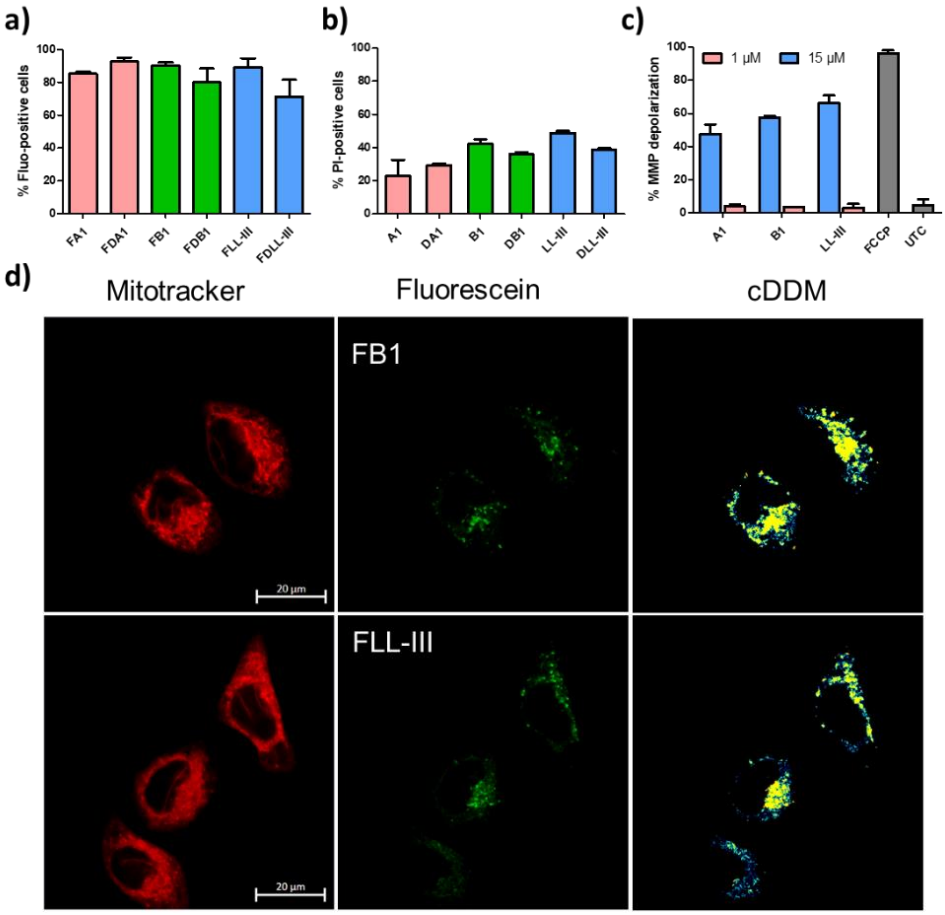

*Figure 17. Interaction of ACPs with HeLa cells. (**a**) Cellular internalization of fluorescein-labelled peptides. HeLa cells were treated with 10 µM of fluorescein-labelled peptides, incubated for 3 h and analyzed by flow cytometry. (**b**) Propidium Iodine (PI) entrance to HeLa cells, treated with 10 µM of peptides and incubated for 15 min, was detected by flow cytometry. (**c**) Mitochondrial Membrane Potential (MMP) depolarization as detected by flow cytometry. HeLa cells were treated by 1 µM (pink),15 µM (blue) of peptides and incubated for 120 min and 15 min, respectively. UTC – untreated cells, Carbonyl cyanide-p-trifluoromethoxyphenylhydrazone (FCCP) 50 µM was used as a positive control. (**d**) Colocalization analysis of fluorescein-labelled peptides with mitochondria (live cells). HeLa cells were treated with 10 µM of peptide-fluorescein and incubated for 1h. Images were taken on a Zeiss LSM 880 confocal microscope with Oil compatible lens x63/1.3. cDDM: Co-Density Distribution Map, built by coDDMaker software.*[167]

4.3.7.3. ACPs influence mitochondrial function

Positively charged amphiphilic peptides have also been shown to interact with intracellular components, which may augment their cytotoxic activity.[163] One of the proven targets of such anticancer peptides are mitochondria, likely due to their negatively charged membrane containing cardiolipin. Both eukaryotic mitochondrial membranes and bacteria cytoplasmic membranes (both the inner and the outer) maintain large transmembrane potentials and have a high content of anionic phospholipids, reflecting the commonality of bacteria and

mitochondria. Existed antimicrobial activity of our best peptides suggested us to consider mitochondria as a possible intracellular target.

Mitochondria function of HeLa cells was evaluated using TMRE-Mitochondrial Membrane Potential Assay by flow cytometry. At low concentration (1 μM), there were no visible changes in mitochondria function within 2 hours. However, after the addition of higher concentrations of the peptides (15 μM), mitochondria started to lose their membrane potential already by 15 min, and more than 50% of cells lacked TMRE fluorescence (evidence of mitochondria membrane depolarization) (*Figure 17c, S16*).

Furthermore, we performed live cell imaging of HeLa cells treated with 10 μM of fluorescein-labelled peptides for 1h and stained with mitochondrial dye Mitotracker (*Figure 17d*). Co-Density Distribution Map, built by coDDMaker software,[167] demonstrates overlapping of two channels – Mitotracker and Fluorescein, which can indicate cellular colocalization of mitochondria and fluorescent peptides.

4.4. Conclusion

Despite the many previous reports showing that ML methods can classify bioactive peptides, including membrane disruptive ACPs, experimental ML-based searches reported to date yielded hemolytic ACPs, requiring additional optimization to reduce their hemolysis.[145,146] Here, we showed that combining an RNN generative model or a genetic algorithm with activity and hemolysis classifiers allows identifying of new non-hemolytic ACPs directly. Detailed investigations showed that these new ACPs formed amphiphilic α-helices and displayed membrane disruptive activities on model vesicles. The subsequently selected hit-compounds **A1** and **B1** showed IC_{50} activities with low micromolar range against several cancer cell lines. Further biological evaluations revealed membranolytic and mitochondria targeting properties, thereby reproducing the properties of **LL-III**, a known and typical natural ACP.

5. Peptide Dendrimers *vs* Isopeptide Dendrimers. Comparison of Antimicrobial and Anticancer Activities.

The preliminary anticancer activity of **G3KL** and **T7** on A549 cells was discovered by Xingguang Cai. Antimicrobial and Hemolytic activity determinations were performed by Hippolyte Personne and Etienne Bonvin in a collaboration framework.

5.1. Abstract

Peptide dendrimers are a versatile tool in medicinal chemistry and possess different biological properties, depending on the structure. In this work, we investigate the applicability of Lysine- or Isolysine-containing peptide dendrimers for cancer and antimicrobial treatments. We were able to reveal selective toward A549 cells anticancer properties of reported peptide dendrimers **G3KL** and **T7** (IC_{50} 2.38±0.21 and 1.43±0.13 μM respectively) and newly discovered **EZ-282** (IC_{50} 1.53±0.31 μM), retaining the hemolytic properties at a low level. Flow cytometry studies on A549 cells demonstrated that peptide dendrimers permeabilize the cell membrane and kill A549 cells by membrane disruption, partially causing apoptosis. Moreover, **EZ-282** partially adopts α-helical confirmation in the presence of 5 mM DPC micelles and exhibits antimicrobial properties. At neutral pH **EZ-282** shows better activity against *E. coli* and *A. baumannii* bacterial strains than hit **G3KL** and **T7**. Isopeptide dendrimers did not show expected potency against either bacteria or cancer cells.

5.2. Introduction

Peptide dendrimers are a topic of extensive studies in our group. We have already demonstrated various applications of peptide dendrimers as gene transfection reagents,[90,168,169] with immunomodulatory[170] and cell-penetrating properties,[87] as artificial enzymes or protein models with catalytic activity.[171–175] However, the primary research focus is investigations of their antimicrobial activities.[176–179] Antimicrobial resistance is a severe human threat that is proliferating every year. In this light, peptide dendrimers, such as **G3KL**[176] and **T7**[178] can become promising antimicrobials as they show potency even for resistant bacterial strains.

Peptidic molecules can be easily modified to create new compounds, for example, D-enantiomeric, stereorandomized,[180] or mixed chirality[181] analogs, many of which preserve antimicrobial activity.

In this work were interested in designing a new class of peptide dendrimers containing isopeptide bonds through the side chains of Lysines (*Scheme 13*), namely isopeptide dendrimers. This design can change the conformation as well as the protonation state of peptide dendrimers due to the difference in pKa values of α-ammonium ion and side chain group (8.95 and 10.53 respectively) on Lysines and, therefore a total pKa. Moreover, our group recently showed that the antimicrobial activity of peptide dendrimers could be altered at elevated pH values.[182] We were interested the behavior of isopeptide dendrimers against bacteria at different pH values compared to their original analogs.

Additionally, we intended to investigate the anticancer properties of selected peptide dendrimers. We have chosen A549 (human lung cancer) as a cancerous and HEK-293 (human embryo kidney) as non-cancerous cell models. **G3KL**, **T7,** and **EZ-282** turned out to be extremely potent against A549 cells with more than 10-fold-selectivity over HEK-293. Annexin V-FITC/Propidium Iodine (PI) flow cytometry studies on A549 gave us a sign of a cell membrane disruption caused by peptide dendrimers.

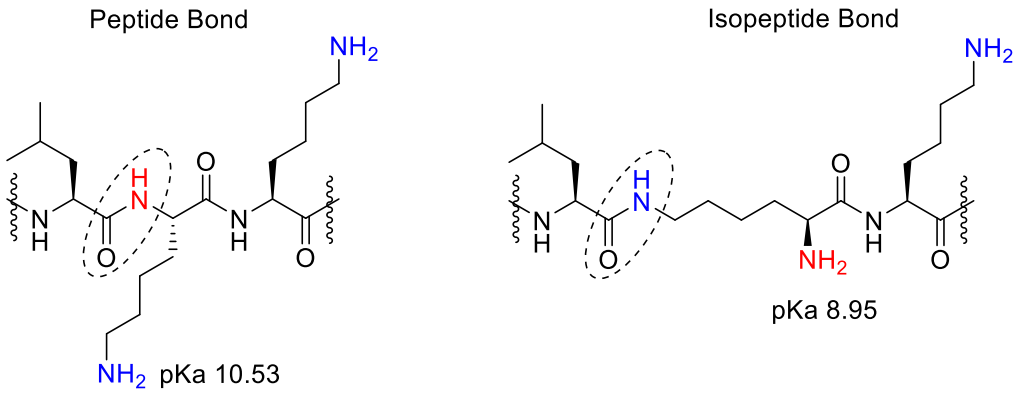

Scheme 13. A general illustration of peptide and isopeptide bonds.

5.3. Results and discussion

5.3.1. Synthesis and structural characteristics of peptide dendrimers

We started our work by synthesizing a small library of compounds (*Table 15*) by either manual or automated solid phase peptide synthesis. Isopeptide dendrimers **EZ-209**, **EZ-211**, **EZ-212** were synthesized by using inverted Boc-Lys(Fmoc)-OH as a building block (*Figure 18*). Afterward, the compounds were cleaved from the resin by TFA/TIS/H_2O solution treatment and purified by RP-HPLC to yield 6 peptide dendrimers.

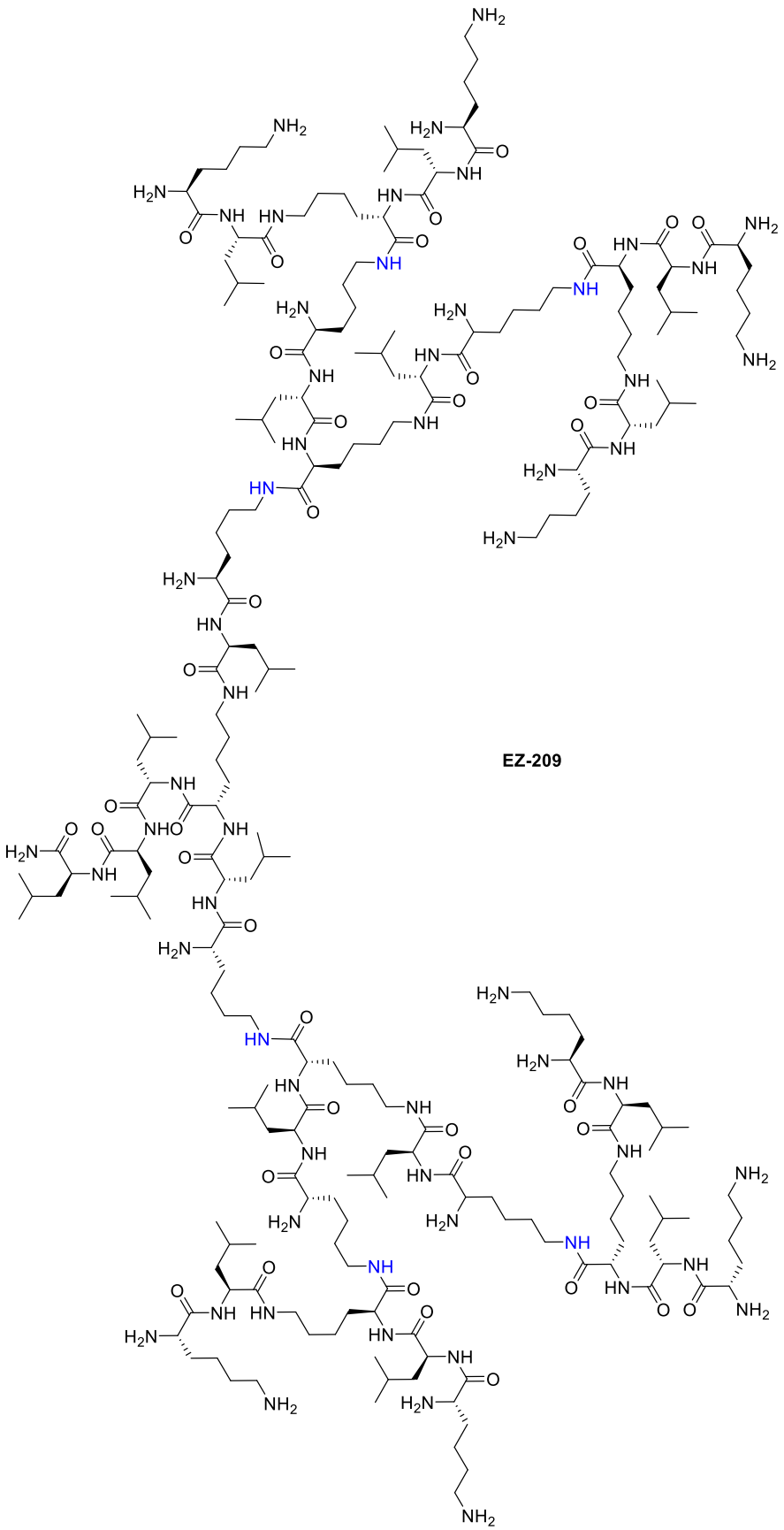

Figure 18. The chemical structure of **EZ-209**, *illustrated as an example of isopeptide dendrimers synthesized in this chapter.*

Table 15. Synthesis of peptide dendrimers by SPPS

Cpd.	Sequence[a]	Yield, mg (%)[b]	MS calc/found[c]
EZ-282	$(KL)_8(KKL)_4(KKL)_2KLLL$	131 (21.1)	4629.45/4629.45
G3KL	$(KL)_8(KKL)_4(KKL)_2KKL$	107 (23.0)	4631.38/4631.38
T7	$(KL)_8(KKL)_4(KKLL)_2KKKL$	142 (26.4)	4885.64/4885.65
EZ-209	$(KL)_8(KK^*L)_4(KK^*L)_2KLLL$	20 (3.4)	4629.45/4629.46
EZ-211	$(KL)_8(KK^*L)_4(KK^*L)_2KK^*L$	31 (5.3)	4531.38/4531.38
EZ-212	$(KL)_8(KK^*L)_4(KK^*LL)_2KK^*K^*L$	85.9 (12.9)	4885.64/4885.64

[a] One-letter code amino acids are used, *K* are representing branching lysines and K* indicates isopeptide residue. [b] Isolated yields as trifluoroacetate salt after preparative RP-HPLC purification. [c] ESI-MS data.

We further performed acid-base titration of isopeptide dendrimers to ensure the proper chemical structure. As expected, the titration curves had an extended plateau at around pH 6.5, compared to reported **G3KL**[179] and **T7**[182]; NaOH equivalents corresponded to titrated α-NH_2 groups (*Figure S17*).

To investigate the conformation of peptide dendrimers in the solution, we performed circular dichroism (CD) in PB buffer at pH 5.0, 7.4, and 8.0 in the absence and presence of 5 mM dodecyl phosphocholine (DPC), mimicking membrane environment (*Figure 19, Table S2*). Isopeptide dendrimers displayed random coil conformations at all pH values measured, regardless of DPC addition. Non-natural peptide conjunction does not allow to adopt secondary structures. For the sake of consistency, we remeasured CD and reevaluated obtained results for the previously reported **G3KL** and **T7**. All compounds **G3KL**, **T7**, and **EZ-282** showed their partial transition from a random coil in the aqueous buffer to an α-helical state upon the addition of 5 mM dodecylphosphocholine (DPC).

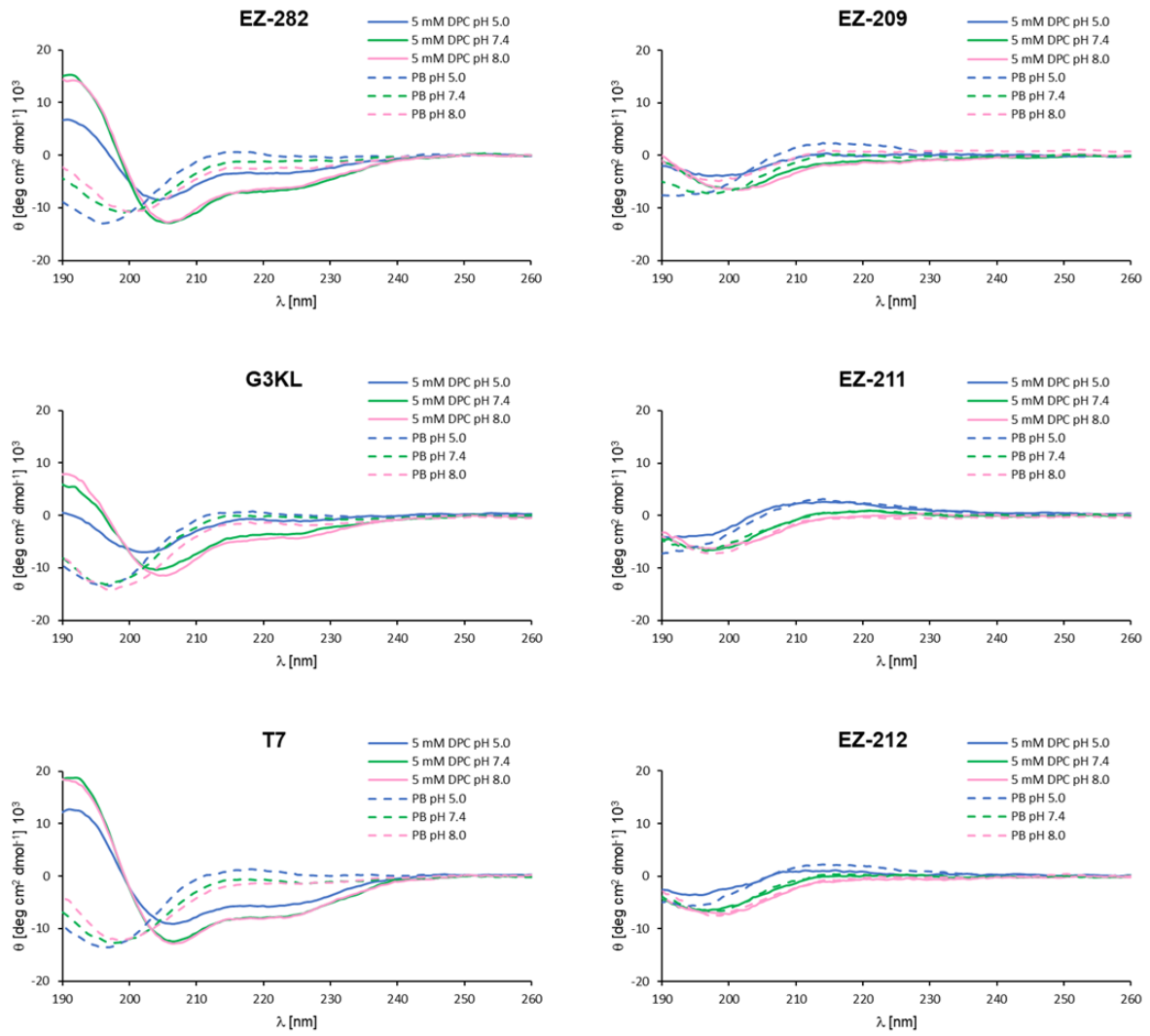

*Figure 19. Circular dichroism spectra in the presence of 5 mM DPC (solid lines) and in phosphate buffer 10 mM alone (dashed lines) at pH 5.0 (blue), 7.4 (green), and 8.0 (pink) for **EZ-282**, **EZ-209**, **G3KL**, **EZ-211**, **T7**, and **EZ-212**.*

5.3.2. Cytotoxicity and Hemolysis

Next, we evaluated the cytotoxicity on A549 (lung cancer) and HEK-293 (human embryo kidney) by treating the cells with compounds at different concentrations and 72 h incubation. The cell viabilities were assessed by alamarBlue™ assay. The data were processed, and IC_{50} was identified. As a general toxicity test, we also measured the viability of isolated erythrocytes (human red blood cells), determined by the minimal hemolytic concentration (MHC).

Isopeptide dendrimers **EZ-209, EZ-211, EZ-212** showed decreased activity against A549 and no activity against HEK-293 (*Table 16, Figure S18*). In contrast, peptide dendrimers with the normal structure were extremely potent with single-digit micromolar activities against lung cancer. **G3KL** turned out to be the most potent in the series, possessing the highest selectivity.

Interestingly, the same peptide dendrimers showed much lower potency on other cancer cell lines such as HeLa or MCF-7 under the same conditions (*Table S3*). None of the compounds showed significant hemolytic properties, suggesting their further *in vivo* applicability.

Table 16. Toxicity of peptide dendrimers against A549, HEK-293, and red blood cells.

Cpd.	Sequence[a]	IC_{50} (μM)[b]		MHC (μg/mL)[c]
		A549	HEK-293	hRBC
EZ-282	$(KL)_8(KKL)_4(KKL)_2KLLL$	1.53 ± 0.31	17.7 ± 1.1	500
G3KL	$(KL)_8(KKL)_4(KKL)_2KKL$	2.38 ± 0.21	> 50	> 1000
T7	$(KL)_8(KKL)_4(KKLL)_2KKKL$	1.43 ± 0.13	17.2 ± 1.5	1000
EZ-209	$(KL)_8(KK^*L)_4(KK^*L)_2KLLL$	≈22	> 50	> 1000
EZ-211	$(KL)_8(KK^*L)_4(KK^*L)_2KK^*L$	≈35	> 50	> 1000
EZ-212	$(KL)_8(KK^*L)_4(KK^*LL)_2KK^*K^*L$	≈45	> 50	> 1000

[a] One-letter code for amino acids. *K* are representing branching lysines and K* indicates isopeptide residue. [b] IC_{50} was determined after 72 h incubation at 37°C in RPMI-1640 medium (for A549) or in DMEM high glucose medium (for HEK-293) supplemented with 10% FBS. [c] Minimum hemolytic concentration on human red blood cells (hRBCs) in 10 mM phosphate buffer, 150 mM NaCl, pH 7.4, 25°C.

To investigate the tested peptide dendrimers' mechanism of action, A549 cells were incubated for 3 hours with 10 μM of the active compound. To detect cell death, Annexin V-FITC/ propidium iodide (PI) double staining was performed, and cells were analyzed by flow cytometry. The Annexin V corresponding signal provides a very sensitive method for detecting cellular apoptosis, while propidium iodide (PI) is used to detect necrotic or late apoptotic cells, characterized by the loss of the integrity of the plasma membranes. Annexin V binds to the phosphatidylserine (PS), which is overexpressed on the outer membrane of the apoptotic cells. Scatter plots, illustrated in *Figure 20*, showed that peptide dendrimers, after 3-hour incubation, mostly induce necrosis but also partially apoptosis, affecting half of the cells in case of **EZ-282** and **T7** and one-third in case of **G3KL**. The positive apoptosis signal can also be attributed to the non-specific Annexin V bunding inside the cells after membrane disintegration.

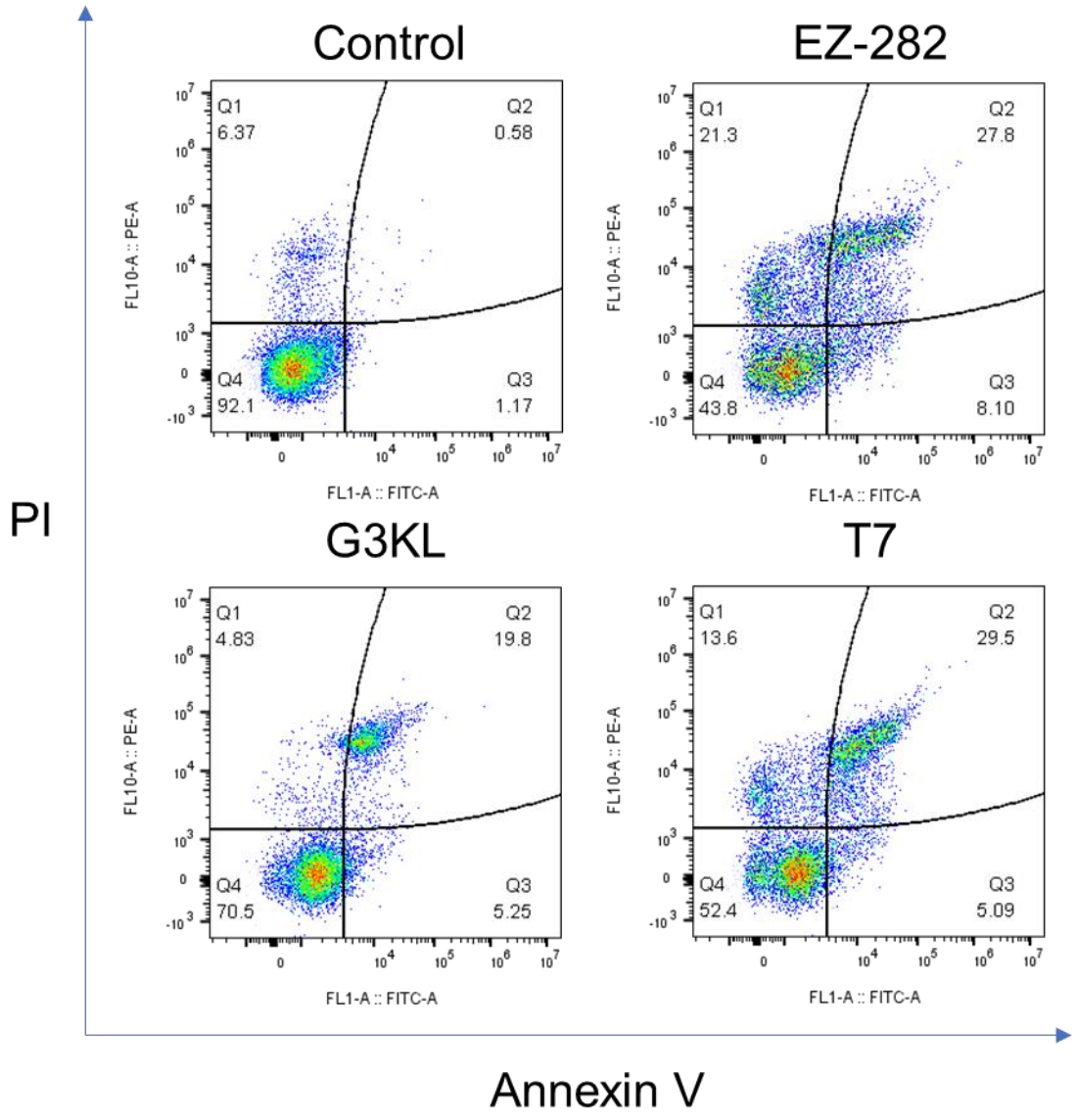

Figure 20. Flow cytometry analysis of Annexin V-FITC and propidium iodide (PI) staining of A549 cells after 3 hours incubation with 5 μM of the compound. Q1 = dead cells. Q2= late-stage apoptotic/dead cells. Q3 = early-stage apoptotic cells. Q4 = viable cells.

5.3.3. Antimicrobial activity at different pH

As the potent antimicrobial activities of **G3KL** and **T7** were already known, we sought to compare these peptide dendrimers data as a reference to newly synthesized **EZ-282** and isopeptide dendrimers **EZ-211**, **EZ-212**, **EZ-209**. We assessed the antimicrobial activities on clinically significant four gram-negative and one gram-positive (Methicillin-resistant Staphylococcus aureus (MRSA)) bacterial strains by measuring minimal inhibitory concentrations (MIC). We were curious to see the effect at different pH values; therefore, we determined the MIC values at pH 5.0, 7.4, and 8.0 (*Table 17*). In the standard broth microdilution method, **EZ-282** showed comparable to **G3KL** and **T7** antimicrobial activities,

with the increased activities at elevated pH, the behavior is in accordance with one for already reported reference peptide dendrimers.[182] To our surprise, isopeptide dendrimers (except for a few conditions) did not show expected activity on a panel of bacterial strains. This indicates that not only multivalency of peptide dendrimers but also structure and conformation are essential to cause the antimicrobial effect.

Table 17. Antibacterial activities of peptide dendrimers at different pH.

	MIC (μg/mL) pH 5.0 / 7.4 / 8.0				
Cpd.	P. aeruginosa PAO1[a]	K. pneumoniae NCTC418[a]	A. baumannii ACTC19606[a]	E. coli W3110[a]	S. aureus COL (MRSA)[a]
G3KL	16-32 / 4 / 4	>64 / 32 / 8	32 / 4 / 2	>64 / 4 / 2	>64 / >64 / 8
T7	8-16 / 4 / 4	>64 / 8 / 8	8 / 4 / 2-4	64 / 4 / 2	>64 / >64 / 8
EZ-282	4-8 / 4 / 4	32-64 / 8 / 4	8 / 2 / 2	16 / 2 / 2	>64 / >64 / 8
EZ-211	>64 />64 />64	>64 />64 />64	>64 / 64 />64	>64 />64 />64	>64 />64 / >64
EZ-212	>64 />64 />64	>64 />64 />64	>64 / 64 /32-64	>64 />64 / >64	>64 />64 / >64
EZ-209	>64 / 16 / >64	>64 />64 />64	>64 / 4 / 8	>64 / 4 / 8	>64 />64 / >64

[a] Minimum inhibitory concentration in μg/mL was determined on bacteria in Mueller-Hinton (MH) broth after incubation for 16-20 hours at 37°C. Values represent at least two different duplicates.

5.4. Conclusion and outlook

The experiments above show a comparative study of peptide dendrimers with a normal peptide bond structure and isopeptide dendrimers. We investigated the antimicrobial and anticancer properties of the selected compounds, as well as their general toxicity on HEK-293 or erythrocytes. The data did not show any potential effect of the isopeptide dendrimers.

However, in this work, for the first time, we demonstrated the selective properties of peptide dendrimers against A549 lung cancer cells. Flow cytometry analysis of Annexin V-FITC/PI stained A549 cells revealed that peptide dendrimers exhibit a membranolytic mode of action and kill the cell primarily by affecting the integrity of the cell membrane.

The high sensitivity of A549 cells toward peptide dendrimer treatment can be attributed to the difference of the cell membrane composition. Lipid homeostasis is a very complex process that is essential for the health of the normal cells.[183] One of the most significant properties of cancer cells is the altered lipid metabolism and, consequently, the abnormal cell membrane composition.[184] Though there is no solid connection between the cell membrane composition and its exposure to membrane lysis, but it is generally known that an increased number of unsaturated over saturated phospholipids in the cell membrane increases cell fluidity and, therefore, susceptibility to disruption. In particular, the A549 cell line has significantly increased levels of phosphatidylinositol 18:0_20:4, sphingomyelin 42:2, and

phosphatidylethanolamine 16:0_20:4 and decreased levels of phosphatidic acids 34:2 and C18:2.[185] The extensive study of lipid imbalance in cancer cells can help to answer our question, which is beyond the scope of current work.

6. General conclusion and outlook

This thesis has dealt with the use of peptides and peptide dendrimers as (*i*) drug delivery systems and (*ii*) anticancer agents.

(*i*) In the first part, we intended to synthesize peptide dendrimers for delivery of Doxorubicin derivative (pDOX) (Chapter 2) and Pt complexes (Chapter 3) to cancer cells.

We based our Doxorubicin (and derivatives) conjugation chemistry on a well-known approach with the help of a self-cleavable linker. Such conjugation to linear peptide **Z5** allowed slower Doxorubicin accumulation and increased sensitivity of multidrug-resistant cancer cells upon treatment compared to free Doxorubicin. The conjugation to selected peptide dendrimers did not show the expected potency. The question of conjugation to more potent Doxorubicin derivatives remains open, in this way, additional synthetic optimization pathways by varying Doxorubicin-derivative's nature or reaction conditions, in general, might be probed.

In Chapter 3, we aimed to establish a pH-sensitive nanodelivery system based on the different aggregation properties of peptide dendrimers at pH 7.4 and 5.0. Pt complexation was achieved by introducing Glutamic acid residues into the structure, and different fatty acid tails were added to maintain the hydrophobicity necessary for appropriate aggregation. Such design allowed us to obtain macromolecular scaffolds with up to 17.6% of Pt content for **C25**. Still, the highest *in vitro* cytotoxicity was achieved for **C19**, possessing the best pH-sensitive aggregation in CMC Nile Red assay. These findings suggest, that pH-triggered dissociation of nanocarrier and drug release can play a crucial role for activity inside the cells.

(*ii*) In the second part, we sought to develop potent peptides and peptide dendrimers against cancer.

Membranolytic peptides represent a promising anticancer agent as, due to the receptor-free mechanism, they can tolerate resistance. We showed that even with the help of machine learning methods the generation of active and non-hemolytic anticancer peptides stays a big challenge. We identified 3 (out of 33) new sequences with similar activities as reference lasioglossin III and proved their membrane-disruptive behavior in a range of assays.

The manual design of peptide dendrimers with anticancer properties led us to a new research offshoot. Peptide dendrimers **G3KL** and **T7** reported for their potent antimicrobial activities were checked for anticancer activities. We reported for the first time, that **EZ-282** and **T7** showed a high potency for lung cancer A549 cells, whereas **G3KL** showed better selectivity

compared to non-cancer HEK-293 cells. The further flow cytometry investigations with the Annexin V/PI staining revealed a primarily necrotic mode of action, which affect the membrane integrity, similar to linear peptides from Chapter 4.

As an outlook for Chapter 5, we introduced active peptide dendrimers to NCI-60 Human Tumor Cell Lines Screen, which can bring more insights into the biological response triggered by selected compounds.

In summary to the second part, these results could lead to new potent anticancer agents based on peptidic structures.

7. Experimental part

7.1. Materials and Reagents

All reagents, salts, and buffers were used as purchased from commercial suppliers: Sigma Aldrich, Thermo Fisher, Fluorochem Ltd, , TCI (Tokyo Chemical Company), Avanti Polar Lipids Inc. Dichloro(1,2 diaminocyclohexane)platinum (II) was purchased from Sigma Aldrich. Doxorubicin hydrochloride was purchased from Fluorochem Ltd (Hadfield, UK). Dialysis cassettes were purchased from Thermo Fisher Scientific.

Amino acids were purchased from Space Peptides Pharmaceutical AG/ Iris Biotech GmbH and used as the following derivatives: Fmoc-Ala-OH, Fmoc-Arg(Pbf)-OH, Fmoc-Asn(Trt)-OH, Fmoc-Asp(OtBu)-OH, Fmoc-Cys(Trt)-OH, Fmoc-Gln(Trt)-OH, Fmoc-Glu(OtBu)-OH, Fmoc-Gly-OH, Fmoc-His(Trt)-OH, Fmoc-Ile-OH, Fmoc-Leu-OH, Fmoc-Lys(Boc)-OH, Fmoc-Met-OH, Fmoc-Phe-OH, Fmoc-Ser(tBu)-OH, Fmoc-Thr(tBu)-OH, Fmoc-Trp(Boc)-OH, Fmoc-Tyr(tBu)-OH, Fmoc-Val-OH. Rink Amide AM LL resin was purchased from Novabiochem (loading: 0.29 mmol·g−1). Tentagel S RAM was purchased form Rapp Polymere GMBH.

Materials for biological assays: 0.05% Trypsin-EDTA, FluoroBrite DMEM were purchased from Gibso, Thermo Fisher Scientific (Reinach, CH). Hoechst 33258, Mitotracker Red, Propidium Iodine/Annexin V-FITC staining solutions were purchased from Invitrogen, Thermo Fisher Scientific (Reinach, CH). Dulbecco's modified Eagle medium (DMEM) high glucose, Roswell Park Memorial Institute 1640 medium (RPMI 1640), Poly L-Lysine, Fetal Bovine Serum (FBS), AlamarBlue® were purchased from Sigma Aldrich (Buchs, CH). TMRE-Mitochondrial Membrane Potential Assay Kit was purchased from Abcam (Cambridge, UK).

Analytical RP-HPLC was performed with an Ultimate 3000 Rapid Separation LC-MS System (DAD-3000RS diode array detector) using an Acclaim RSLC 120 C18 column (2.2 μm, 120 Å, 3×50 mm, flow 1.2 mL/min) from Dionex. Data recording and processing were done with Dionex Chromeleon Management System Version 6.80 (analytical RP-HPLC). All RP-HPLC were using HPLC-grade acetonitrile and Milli-Q deionized water. The elution solutions were: A Milli-Q deionized water containing 0.05% TFA; D Milli-Q deionized water/acetonitrile (10:90, v/v) containing 0.05% TFA.

Preparative RP-HPLC (if not specified) was performed with a Waters automatic Prep LC Controller System containing the four following modules: Waters2489 UV/Vis detector,

Waters2545 pump, Waters Fraction Collector III, and Waters2707 Autosampler. A Dr. Maisch GmbH Reprospher column (C18-DE, 100×30 mm, particlesize 5 μm, pore size 100 Å, flow rate 40 mL/min) was used. Compounds were detected by UV absorption at 214 nm using a Waters 248 Tunable Absorbance Detector. Data recording and processing were performed with Waters ChromScope version 1.40 from Waters Corporation. All RP-HPLC were performed using HPLC-grade acetonitrile and Milli-Q deionized water. The elution solutions were: A: Milli-Q deionized water containing 0.1% TFA; D: Milli-Q deionized water/acetonitrile (10/90, v/v) containing 0.1% TFA.

Preparative RP-HPLC for **EZ-282** and **EZ-212** were performed with a Waters automatic Prep LC Controller system containing the four following modules: Waters 515 HPLC pump, Waters 2489 UV/vis detector, SQ Detector 2 (single quadrupole mass detcector and Waters 2767 Sample Manager, Injector and Collector. A Dr. Maisch GmbH Reprospher column (C18-DE, 100×30 mm, particle size 5 μm, pore size 100 Å, flow rate 40 mL/min) was used. Compounds were collected according to their mass using SQ Detector 2. Data recording and processing was performed with MassLynx software version 4.2. The elution solutions were: A MilliQ deionized water containing 0.05% TFA; D Acetonitrile containing 0.05% TFA. Method used was a gradient from 2% to 50% of solvent D in 14 minutes with a total runtime of 20 minutes.

HRMS spectra, recorded on a Thermo Scientific LTQ OrbitrapXL, were provided by the MS analytical service of the Department of Chemistry, Biochemistry and Pharmaceutical Sciences at the University of Bern (group PD Dr. Stefan Schürch).

NMR spectra (^{1}H, ^{13}C). NMR spectra were recorded at 22°C unless otherwise stated. Chemical shifts (δ) are reported in ppm relative to the signal of tetramethylsilane (TMS) and residual solvent signals in 1H and 13C NMR spectra were used as internal reference. Coupling constants (*J*) are given in Hz. The apparent resonance multiplicity is described as s (singlet), d (doublet), t (triplet), q (quartet), p (quintet), m (multiplet), or combinations thereof and broad signals are indicated as br (broad). 1H and 13C-NMR spectra were measured either on a Bruker Avance 300 spectrometer (at 300 MHz and 75 MHz, respectively) or on a Bruker Avance II 400 spectrometer (at 400 MHz and 101 MHz, respectively).

7.2. Solid-phase peptide synthesis (SPPS)

7.2.1. Manual synthesis of peptide dendrimers

Peptide dendrimers **Z1-Z4**, **C1-C15** from Chapter 2, 3 were synthesized by the method described below.

Peptide dendrimers were synthesized by placing 300 mg Tentagel S RAM resin (0.22 mmol/g) in a 10 mL polypropylene syringe fitted with a polypropylene frit, a teflon stopcock and a stopper. Stirring of the reaction mixture at any given step was performed by attaching the closed syringes to a rotating axis. The synthesis was started with resin swelling by addition of DCM (5 mL, 20 min). After removal of the DCM, the Fmoc-protecting group of the resin was removed by using a solution of 20% piperidine in NMP (5 mL, 2×10 min). Between all steps, the resin was washed with NMP (3×4 mL), MeOH (3×4 mL), and DCM (3×4 mL). Coupling of amino acids was performed by using Fmoc-protected amino acids (5 eq), Oxyma (5 eq) and DIC (5 eq) in NMP (5 mL). Coupling steps were carried out according to the dendrimer generations with 1×1 h for the 0th generation, 2×2 h for the 1st generation, 3×2 h for the 2nd generation and 4×2 h for the 3rd generation.

7.2.2. Automated synthesis of peptide dendrimers

Peptide dendrimers **EZ-211** and **EZ-209** from Chapter 5 were synthesized by CEM Liberty Blue Microwave peptide synthesizer. The synthesis was carried out by using 150 mg of Rink Amide LL resin (100-200 mesh), unloaded (0.33 mmol/g). The resin was swollen in DMF/DCM 1:1 at r.t. for 15 min. Removal of the Fmoc protecting group – at each step the Fmoc protecting group was removed with 3 mL of piperidine/DMF (1:4, v/v) for 2 min at 75 °C. After filtration, the resin was washed 3 times for 7 sec with DMF. Coupling of the Fmoc-protected amino acids – 5 eq of Fmoc-protected amino acid with a concentration of 0.2 M, 5 eq of Oxyma and 6 eq of DIC, both with a concentration of 0.2 M, were used as coupling reagents in 4.5 mL of DMF. The resin was then washed with DMF for 3 times.

7.2.3. Manual synthesis of linear peptides and peptide dendrimers at elevated temperature

Linear peptides **Z5** from Chapter 2**, A1-A13**, **B1-B20** from Chapter 4, peptide dendrimers **G3KL**, **T7**, **EZ-282** and **EZ-212**, were synthesized by the method described below.

Peptides were synthesized manually using 150-300 mg of Rink Amide AM LL resin (0.29 mmol/g) by standard 9-fuorenylmethoxycarbonyl (Fmoc) Solid Phase Peptide Synthesis at 60°C under nitrogen bubbling. The resin was swollen in DMF for 10 min. Double deprotection of the Fmoc group was performed using a solution containing 5% w/v piperazine, 2% v/v 1,8-diazabicyclo(5.4.0)undec-7-ene (DBU), 10% v/v of 2-butanol in DMF during 1 min and 4 min respectively. The resin was washed with DMF (5×8 mL DMF) after deprotection. Coupling step (2×8 min) was performed with 3 mL of amino acid (0.2 M), 2 mL of DIC (0.8 M) and 1.5 mL of Oxyma (0.8 M) in DMF. Resin was washed with DMF between couplings (2×8 mL) and after second coupling (3×8 mL).

For sequences containing aspartic or glutamic acid deprotection solution was exchanged to 20% v/v piperidine + 0.7% v/v formic acid in DMF to avoid aspartimide, glutamide and side products formation.

7.2.4. Synthesis of Fluorescein-labelled peptides

The reaction with 5/6-carboxyfluorescein (5/6-CF) was carried out manually in a polypropylene syringe, fitted with a polypropylene frit, a teflon stopcock and a stopper. Last amino acid was deprotected to have free N-terminus. Coupling was performed by using 5/6-CF (7 eq, relative to resin loading), HOBt (7 eq, relative to resin loading) and DIC (7 eq, relative to resin loading) in DMF (5 mL). The resin was stirred at r.t. (2×2 h) and protected from light by covering the syringe with aluminum foil. The resin was washed with DMF, MeOH and DCM (3×4 mL each). A solution of 20% piperidine in DMF (8×5 mL, until the supernatant was colorless) was added to the resin to remove the excess of free 5/6-CF and the resin was finally washed with DCM (5×4 mL).

7.2.5. Alloc deprotection and fatty acid coupling

All the manipulations were performed under inert atmosphere. The resin was located to the syringe with filter and dried *in vacuo* from solvents, then dry DCM (8 mL) was added and the resin was bubbled under N_2 flow for 5 min. DCM was removed and to the swollen resin solutions of $Pd(PPh_3)_4$ (0.1 eq, 10 mg) in dry DCM (3 mL) and $(CH_3)_2NH{\cdot}BH_3$ (25 eq, 100 mg) in dry DCM (3 mL) were added and the mixture was bubbled with N_2 flow for 1 h . The resin was washed with dry DCM (3×8 mL) and the reaction was repeated once for 2 h. The resin was washed with sodium diethyldithiocarbamate (0.02 M in DMF, 10 mL) for 20 min and NMP, MeOH and DCM (2×10 mL each). Then, the fatty acids were coupled according to the general solid phase manual procedure.

7.2.6. Cleavage and purification

After the final Fmoc deprotection, the cleavage from resin was carried out by treating the resins with 7 mL of a TFA/TIS/DODT/H_2O (95/2/2/1, v/v/v/v) solution for 3 h. The peptide solutions were precipitated with 30 mL of cold terbutylmethyl ether (TBME), centrifuged for 10 min at 3500 rpm (twice), evaporated from TBME excess and dried in high vacuum for 60 min. The crude was then dissolved in a H_2O/MeCN (15/1, v/v) mixture, some drops of MeOH added when needed and purified by preparative RP-HPLC. The fractions of the crude peptides were then lyophilized. Yields are given as SPPS total yields. In all cases, yields are calculated for the corresponding TFA salts (assuming TFA complexation to each cationic residue).

7.3. Synthesis and Characterization of peptide dendrimers

M: monoisotopic reconstituted mass

Z1 $(KL)_8(KKL)_4(KLL)_2KCLLLLL$ was obtained after manual synthesis as a white foamy solid after preparative RP-HPLC purification (45.9 mg, 9.6%). Analytical RP-HPLC: t_R = 1.56 min (100% A to 100% D in 3.5 min, λ= 214 nm). MS (ESI+): $C_{243}H_{467}N_{61}O_{41}S$ calc./found 4928.6054/4928.6128 [M].

Z2 $(KL)_8(KKL)_4(KLL)_2KCLLLL$ was obtained after manual synthesis as a white foamy solid after preparative RP-HPLC purification (36.3 mg, 7.7%). Analytical RP-HPLC: t_R = 1.50 min (100% A to 100% D in 3.5 min, λ= 214 nm). MS (ESI+): $C_{237}H_{456}N_{60}O_{40}S$ calc./found 4815.5213/4815.5150 [M].

Z3 $(RL)_8(KRL)_4(KKK)_2KGYKC$ was obtained after manual synthesis as a white foamy solid after preparative RP-HPLC purification (34.0 mg, 6.5%). Analytical RP-HPLC: t_R = 1.28 min (100% A to 100% D in 3.5 min, λ= 214 nm). MS (ESI+): $C_{230}H_{440}N_{88}O_{40}S$ calc./found 5107.4822 /5107.4901 [M].

Z4 $(LI)_8(KRK)_4(KRA)_2KHSKC$ was obtained after manual synthesis as a white foamy solid after preparative RP-HPLC purification (50.6 mg, 11%). Analytical RP-HPLC: t_R = 1.28 min (100% A to 100% D in 3.5 min, λ= 214 nm). MS (ESI+): $C_{222}H_{422}N_{72}O_{40}S$ calc./found 4769.2921/4769.3022 [M].

C1 $(KL)_8(KKL)_4(KEEE)_2KK(C_{12})$ was obtained after manual synthesis as a white foamy solid after preparative RP-HPLC purification (40.1 mg, 9.4%). Analytical RP-HPLC: t_R = 1.42 min (100% A to 100% D in 3.5 min, λ= 214 nm). MS (ESI+): $C_{234}H_{439}N_{59}O_{51}$ calc./found 4892.3572/4892.3554 [M].

C2 $(KL)_8(KKL)_4(KEEE)_2KK(C_{14})$ was obtained after manual synthesis as a white foamy solid after preparative RP-HPLC purification (20.6 mg, 4.8%). Analytical RP-HPLC: t_R = 1.47 min (100% A to 100% D in 3.5 min, λ= 214 nm). MS (ESI+): $C_{236}H_{443}N_{59}O_{51}$ calc./found 4920.3885/4920.3845 [M].

C3 $(KL)_8(KKL)_4(KEE)_2KK(C_{16})$ was obtained after manual synthesis as a white foamy solid after preparative RP-HPLC purification (22.6 mg, 5.3%). Analytical RP-HPLC: t_R = 1.53 min (100% A to 100% D in 3.5 min, λ= 214 nm). MS (ESI+): $C_{228}H_{433}N_{57}O_{45}$ calc./found 4690.3346/4690.3332 [M].

C4 $(KL)_8(KKL)_4(KEE)_2KK(C_{18})$ was obtained after manual synthesis as a white foamy solid after preparative RP-HPLC purification (37.0 mg, 8.3%). Analytical RP-HPLC: t_R = 1.59 min (100% A to 100% D in 3.5 min, λ= 214 nm). MS (ESI+): $C_{230}H_{437}N_{57}O_{45}$ calc./found 4718.3659/4718.3649 [M].

C5 $(KL)_8(KKL)_4(KEE)_2KEK(C_8),K(C_8)$ was obtained after manual synthesis as a white foamy solid after preparative RP-HPLC purification (40.3 mg, 9.2%). Analytical RP-HPLC: t_R = 1.43 min (100% A to 100% D in 3.5 min, λ= 214 nm). MS (ESI+): $C_{239}H_{450}N_{60}O_{50}$ calc./found 4961.4514/4961.4494 [M].

C6 $(KL)_8(KKL)_4(KEE)_2KEEK(C_{10}),K(C_{10})$ was obtained after manual synthesis as a white foamy solid after preparative RP-HPLC purification (58.3 mg, 13.1%). Analytical RP-HPLC: t_R = 1.52 min (100% A to 100% D in 3.5 min, λ= 214 nm). MS (ESI+): $C_{248}H_{465}N_{61}O_{53}$ calc./found 5146.5566/5146.5544 [M].

C7 $(KL)_8(KKL)_4(KEEE)_2KEE\ K(C_{10}),K(C_{10})$ was obtained after manual synthesis as a white foamy solid after preparative RP-HPLC purification (37.0 mg, 8.3%). Analytical RP-HPLC: t_R = 1.52 min (100% A to 100% D in 3.5 min, λ= 214 nm). MS (ESI+): $C_{258}H_{479}N_{63}O_{59}$ calc./found 5404.6418/5404.6371 [M].

C8 $(KL)_8(KKL)_4(KEE)_2KEK(C_{12}),K(C_{12})$ was obtained after manual synthesis as a white foamy solid after preparative RP-HPLC purification (39.4 mg, 8.8%). Analytical RP-HPLC: t_R = 1.63 min (100% A to 100% D in 3.5 min, λ= 214 nm). MS (ESI+): $C_{247}H_{466}N_{60}O_{50}$ calc./found 5073.5766/5073.5562 [M].

C9 $(KL)_8(KKL)_4(KEEE)_2KEEK(C_{14}),K(C_{14})$ was obtained after manual synthesis as a white foamy solid after preparative RP-HPLC purification (36.3 mg, 8.0%). Analytical RP-HPLC:

t_R = 1.80 min (100% A to 100% D in 3.5 min, λ= 214 nm). MS (ESI+): $C_{266}H_{495}N_{63}O_{59}$ calc./found 5516.7670/5516.7474 [M].

C10 $(KL)_8(KKL)_4(KEEEE)_2KEEK(C_{14}),K(C_{14})$ was obtained after manual synthesis as a white foamy solid after preparative RP-HPLC purification (26.6 mg, 5.8%). Analytical RP-HPLC: t_R = 1.75 min (100% A to 100% D in 3.5 min, λ= 214 nm). MS (ESI+): $C_{276}H_{509}N_{65}O_{65}$ calc./found 5774.8522/5774.8474 [M].

C11 $(KL)_8(KKLE)_4(KEEE)_2KEEK(C_{14}),K(C_{14})$ was obtained after manual synthesis as a white foamy solid after preparative RP-HPLC purification (33.1 mg, 7.2%). Analytical RP-HPLC: t_R = 1.76 min (100% A to 100% D in 3.5 min, λ= 214 nm). MS (ESI+): $C_{286}H_{523}N_{67}O_{71}$ calc./found 6032.9374/6032.9290 [M].

C12 $(KL)_8(KKL)_4(KEE)_2KEK(C_{16}),K(C_{16})$ was obtained after manual synthesis as a white foamy solid after preparative RP-HPLC purification (38.5 mg, 8.5%). Analytical RP-HPLC: t_R = 1.96 min (100% A to 100% D in 3.5 min, λ= 214 nm). MS (ESI+): $C_{255}H_{482}N_{60}O_{50}$ calc./found 5185.7018/5185.6970 [M].

C13 $(KL)_8(KKL)_4(KEE)_2KEEK(C_{16}),K(C_{16})$ was obtained after manual synthesis as a white foamy solid after preparative RP-HPLC purification (39.0 mg, 8.6%). Analytical RP-HPLC: t_R = 1.98 min (100% A to 100% D in 3.5 min, λ= 214 nm). MS (ESI+): $C_{260}H_{489}N_{61}O_{53}$ calc./found 5314.7444/5314.7376 [M].

C14 $(KL)_8(KKL)_4(KEEEE)_2KEEK(C_{16}),K(C_{16})$ was obtained after manual synthesis as a white foamy solid after preparative RP-HPLC purification (34.3 mg, 7.5%). Analytical RP-HPLC: t_R = 1.90 min (100% A to 100% D in 3.5 min, λ= 214 nm). MS (ESI+): $C_{280}H_{517}N_{65}O_{65}$ calc./found 5830.9148/5830.9086 [M].

C15 $(KL)_8(KKLE)_4(KEEE)_2KEEK(C_{16}),K(C_{16})$ was obtained after manual synthesis as a white foamy solid after preparative RP-HPLC purification (22.8 mg, 4.9 %). Analytical RP-HPLC: t_R = 1.91 min (100% A to 100% D in 3.5 min, λ= 214 nm). MS (ESI+): $C_{290}H_{531}N_{67}O_{71}$ calc./found 6089.0000/6088.9955 [M].

7.4. Synthesis and Characterization of linear peptides

Z5 RRRRRRFFERHHMVGSCMRAFHQL, from Rink Amide resin (150 mg, 0.29 mmol/g) was obtained after manual synthesis as a white foamy solid after preparative RP-HPLC

purification (38.5 mg, 21.5%). Analytical RP-HPLC: t_R = 1.32 min (100% A to 100% D in 3.5 min, λ= 214 nm). MS (ESI+): $C_{135}H_{218}N_{56}O_{28}S_3$ calc./found 3167.6518/3167.6359 [M].

A1 (FAKKFFKKFAKFAFK-NH_2) was obtained after manual synthesis from Rink Amide AM resin LL (150 mg, 0.29 mmol/g), the peptide was obtained as a white foamy solid after preparative RP-HPLC purification (20 mg, 18.0%). Analytical RP-HPLC: t_R = 1.40 min (100% A to 100% D in 3.5 min, λ= 214 nm). MS (ESI+): $C_{99}H_{144}N_{22}O_{15}$ calc./obs. 1881.12/1881.12 [M].

A2 (WFKRILKYLKKLV-NH_2) was obtained after manual synthesis from Rink Amide AM resin LL (150 mg, 0.29 mmol/g), the peptide was obtained as a white foamy solid after preparative RP-HPLC purification (14 mg, 14.0%). Analytical RP-HPLC: t_R = 1.60 min (100% A to 100% D in 3.5 min, λ= 214 nm). MS (ESI+): $C_{88}H_{144}N_{22}O_{14}$ calc./obs. 1733.12/1733.13 [M].

A3 (WLNALKKILGHLIRH-NH_2) was obtained after manual synthesis from Rink Amide AM resin LL (300 mg, 0.29 mmol/g), the peptide was obtained as a white foamy solid after preparative RP-HPLC purification (33 mg, 17.6%). Analytical RP-HPLC: t_R = 1.65 min (100% A to 100% D in 3.5 min, λ= 214 nm). MS (ESI+): $C_{86}H_{143}N_{27}O_{16}$ calc./obs. 1810.12/1810.12 [M].

A4 (KYLKYLVRLVGRLYR-NH_2) was obtained after manual synthesis from Rink Amide AM resin LL (300 mg, 0.29 mmol/g), the peptide was obtained as a white foamy solid after preparative RP-HPLC purification (33 mg, 13.7%). Analytical RP-HPLC: t_R = 1.51 min (100% A to 100% D in 3.5 min, λ= 214 nm). MS (ESI+): $C_{93}H_{155}N_{27}O_{18}$ calc./obs. 1938.20/1938.20 [M].

A5 (WKRIVRIIRWIRKYY-NH_2) was obtained after manual synthesis from Rink Amide AM resin LL (300 mg, 0.29 mmol/g), the peptide was obtained as a white foamy solid after preparative RP-HPLC purification (35 mg, 14.2%). Analytical RP-HPLC: t_R = 1.48 min (100% A to 100% D in 3.5 min, λ= 214 nm). MS (ESI+): $C_{105}H_{166}N_{32}O_{17}$ calc./obs. 2147.31/2147.31[M].

A6 (FAARILRAWFRFLRR-NH_2) was obtained after manual synthesis from Rink Amide AM resin LL (300 mg, 0.29 mmol/g), the peptide was obtained as a white foamy solid after preparative RP-HPLC purification (32 mg, 15.5%). Analytical RP-HPLC: t_R = 1.61 min (100%

A to 100% D in 3.5 min, λ= 214 nm). MS (ESI+): $C_{95}H_{148}N_{32}O_{15}$ calc./obs. 1977.18/1977.18 [M], $C_{99}H_{150}F_6N_{32}O_{19}$ calc./obs. 2205.16/2205.17 $[M+H+2CF_3COOH]^+$

A7 (SISRLWHSLLRHLLH-NH_2) was obtained after manual synthesis from Rink Amide AM resin LL (150 mg, 0.29 mmol/g), the peptide was obtained as a white foamy solid after preparative RP-HPLC purification (18 mg, 19.9%). Analytical RP-HPLC: t_R = 1.64 min (100% A to 100% D in 3.5 min, λ= 214 nm). MS (ESI+): $C_{86}H_{139}N_{29}O_{18}$ calc./obs. 1866.09/1866.08 [M].

A8 (KNFKKLMKKVASVL-NH_2) was obtained after manual synthesis from Rink Amide AM resin LL (150 mg, 0.29 mmol/g), the peptide was obtained as a white foamy solid after preparative RP-HPLC purification (16 mg, 16.8%). Analytical RP-HPLC: t_R = 1.42 min (100% A to 100% D in 3.5 min, λ= 214 nm). MS (ESI+): $C_{76}H_{137}N_{21}O_{16}S$ calc./obs. 1632.03/1632.03 [M].

A9 (SFSKWMGKLKNIFKK-NH_2) was obtained after manual synthesis from Rink Amide AM resin LL (150 mg, 0.29 mmol/g), the peptide was obtained as a white foamy solid after preparative RP-HPLC purification (25 mg, 23.9%). Analytical RP-HPLC: t_R = 1.48 min (100% A to 100% D in 3.5 min, λ= 214 nm). MS (ESI+): $C_{88}H_{141}N_{23}O_{18}S$ calc./obs. 1840.05/1840.06[M].

A10 (LLRHCLRRIRDRLV-NH_2) was obtained after manual synthesis from Rink Amide AM resin LL (300 mg, 0.29 mmol/g), the peptide was obtained as a white foamy solid after preparative RP-HPLC purification (36 mg, 18.2%). Analytical RP-HPLC: t_R = 1.32 min (100% A to 100% D in 3.5 min, λ= 214 nm). MS (ESI+): $C_{78}H_{144}N_{32}O_{16}S$ calc./obs. 1817.12/1817.11[M].

A11(KWRSKIKKIMRTFK-NH_2) was obtained after manual synthesis from Rink Amide AM resin LL (150 mg, 0.29 mmol/g), the peptide was obtained as a white foamy solid after preparative RP-HPLC purification (23 mg, 20.0%). Analytical RP-HPLC: t_R = 1.29 min (100% A to 100% D in 3.5 min, λ= 214 nm). MS (ESI+): $C_{86}H_{149}N_{27}O_{16}S$ calc./obs. 1848.14/1848.14 [M].

A12 (GLLGRLAKLLANS-NH_2) was obtained after manual synthesis from Rink Amide AM resin LL (300 mg, 0.29 mmol/g), the peptide was obtained as a white foamy solid after preparative RP-HPLC purification (31 mg, 23.0%). Analytical RP-HPLC: t_R = 1.66 min (100%

A to 100% D in 3.5 min, λ= 214 nm). MS (ESI+): $C_{59}H_{109}N_{19}O_{15}$ calc./obs. 1323.84/1323.83[M].

A13 (VFRQWQKIMRRLVRR-NH_2) was obtained after manual synthesis from Rink Amide AM resin LL (150 mg, 0.29 mmol/g), the peptide was obtained as a white foamy solid after preparative RP-HPLC purification (29 mg, 24.2%). Analytical RP-HPLC: t_R = 1.45 min (100% A to 100% D in 3.5 min, λ= 214 nm). MS (ESI+): $C_{93}H_{159}N_{35}O_{17}S$ calc./obs. 2070.24/2070.24 [M].

LL-III (VNWKKILGKIIKVVK-NH_2) was obtained after manual synthesis from Rink Amide AM resin LL (300 mg, 0.29 mmol/g), the peptide was obtained as a white foamy solid after preparative RP-HPLC purification (41 mg, 20.2%). Analytical RP-HPLC: t_R = 1.63 min (100% A to 100% D in 3.5 min, λ= 214 nm). MS (ESI+): $C_{86}H_{153}N_{23}O_{16}$ calc./obs. 1764.19/1764.20 [M].

B1 (ANWKKWIGKVIKLVK-NH_2) was obtained after manual synthesis from Rink Amide AM resin LL (300 mg, 0.29 mmol/g), the peptide was obtained as a white foamy solid after preparative RP-HPLC purification (30 mg, 14.5%). Analytical RP-HPLC: t_R = 1.56 min (100% A to 100% D in 3.5 min, λ= 214 nm). MS (ESI+): $C_{89}H_{148}N_{24}O_{16}$ calc./obs. 1809.15/1809.15 [M].

B2 (NWKKILGKILDHLAC-NH_2) was obtained after manual synthesis from Rink Amide AM resin LL (300 mg, 0.29 mmol/g), the peptide was obtained as a white foamy solid after preparative RP-HPLC purification (25 mg, 14.5%). Analytical RP-HPLC: t_R = 1.65 min (100% A to 100% D in 3.5 min, λ= 214 nm). MS (ESI+): $C_{81}H_{135}N_{23}O_{18}S$ calc./obs. 1750.01/1750.00 [M].

B3 (ANWKKILKRLCDI-NH_2) was obtained after manual synthesis from Rink Amide AM resin LL (300 mg, 0.29 mmol/g), the peptide was obtained as a white foamy solid after preparative RP-HPLC purification (51 mg, 30.2%). Analytical RP-HPLC: t_R = 1.57 min (100% A to 100% D in 3.5 min, λ= 214 nm). MS (ESI+): $C_{73}H_{126}N_{22}O_{16}S$ calc./obs. 1598.94/1598.94 [M].

B4 (NWKKILGKICR-NH_2) was obtained after manual synthesis from Rink Amide AM resin LL (300 mg, 0.29 mmol/g), the peptide was obtained as a white foamy solid after preparative RP-HPLC purification (22 mg, 14.0%). Analytical RP-HPLC: t_R = 1.42 min (100% A to 100% D in 3.5 min, λ= 214 nm). MS (ESI+): $C_{62}H_{108}N_{20}O_{12}S$ calc./obs. 1356.82/1356.82 [M].

B5 (KNWKKIIKKVVK-NH_2) was obtained after manual synthesis from Rink Amide AM resin LL (300 mg, 0.29 mmol/g), the peptide was obtained as a white foamy solid after preparative RP-HPLC purification (37 mg, 19.4%). Analytical RP-HPLC: t_R = 1.26 min (100% A to 100% D in 3.5 min, λ= 214 nm). MS (ESI+): $C_{73}H_{131}N_{21}O_{13}$ calc./obs. 1510.02/1510.02 [M].

B6 (VNVWKKIGRLVKIVK-NH_2) was obtained after manual synthesis from Rink Amide AM resin LL (300 mg, 0.29 mmol/g), the peptide was obtained as a white foamy solid after preparative RP-HPLC purification (36 mg, 17.6%). Analytical RP-HPLC: t_R = 1.47 min (100% A to 100% D in 3.5 min, λ= 214 nm). MS (ESI+): $C_{85}H_{151}N_{25}O_{16}$ calc./obs. 1778.18/1778.17 [M].

B7 (NEWKKIKKIIKIVK-NH_2) was obtained after manual synthesis from Rink Amide AM resin LL (300 mg, 0.29 mmol/g), the peptide was obtained as a white foamy solid after preparative RP-HPLC purification (54 mg, 26.6%). Analytical RP-HPLC: t_R = 1.37 min (100% A to 100% D in 3.5 min, λ= 214 nm). MS (ESI+): $C_{85}H_{151}N_{23}O_{17}$ calc./obs. 1766.17/1766.17 [M].

B8 (KWRQLGKKIIKVAK-NH_2) was obtained after manual synthesis from Rink Amide AM resin LL (300 mg, 0.29 mmol/g), the peptide was obtained as a white foamy solid after preparative RP-HPLC purification (41 mg, 23.2%). Analytical RP-HPLC: t_R = 1.24 min (100% A to 100% D in 3.5 min, λ= 214 nm). MS (ESI+): $C_{80}H_{143}N_{25}O_{15}$ calc./obs. 1694.12/1694.12 [M].

B9 (NWKKIRKLGKVVKKI-NH_2) was obtained after manual synthesis from Rink Amide AM resin LL (300 mg, 0.29 mmol/g), the peptide was obtained as a white foamy solid after preparative RP-HPLC purification (28 mg, 12.2%). Analytical RP-HPLC: t_R = 1.26 min (100% A to 100% D in 3.5 min, λ= 214 nm). MS (ESI+): $C_{87}H_{157}N_{27}O_{16}$ calc./obs. 1836.23/1836.23 [M].

B10 (VVNNWKKKIIKVIK-NH_2) was obtained after manual synthesis from Rink Amide AM resin LL (300 mg, 0.29 mmol/g), the peptide was obtained as a white foamy solid after preparative RP-HPLC purification (33 mg, 16.6%). Analytical RP-HPLC: t_R = 1.33 min (100% A to 100% D in 3.5 min, λ= 214 nm). MS (ESI+): $C_{82}H_{145}N_{23}O_{16}$ calc./obs. 1708.12/1708.12 [M].

B11 (DWHKIGKKVIKVIK-NH_2) was obtained after manual synthesis from Rink Amide AM resin LL (300 mg, 0.29 mmol/g), the peptide was obtained as a white foamy solid after preparative RP-HPLC purification (29 mg, 14.7%). Analytical RP-HPLC: t_R = 1.31 min (100% A to 100% D in 3.5 min, λ= 214 nm). MS (ESI+): $C_{81}H_{139}N_{23}O_{16}$ calc./obs. 1690.08/1690.08 [M].

B12 (KWNNILGKLGKLAR-NH_2) was obtained after manual synthesis from Rink Amide AM resin LL (300 mg, 0.29 mmol/g), the peptide was obtained as a white foamy solid after preparative RP-HPLC purification (23 mg, 12.8%). Analytical RP-HPLC: t_R = 1.45 min (100% A to 100% D in 3.5 min, λ= 214 nm). MS (ESI+): $C_{74}H_{128}N_{24}O_{16}$ calc./obs. 1609.00/1609.00 [M].

B13 (NVVGRLGKIVKIVK-NH_2) was obtained after manual synthesis from Rink Amide AM resin LL (300 mg, 0.29 mmol/g), the peptide was obtained as a white foamy solid after preparative RP-HPLC purification (60 mg, 34.9%). Analytical RP-HPLC: t_R = 1.40 min (100% A to 100% D in 3.5 min, λ= 214 nm). MS (ESI+): $C_{70}H_{132}N_{22}O_{15}$ calc./obs. 1521.02/1521.02 [M].

B14 (NPKVFLKKIIKVVK-NH_2) was obtained after manual synthesis from Rink Amide AM resin LL (300 mg, 0.29 mmol/g), the peptide was obtained as a white foamy solid after preparative RP-HPLC purification (36 mg, 18.6%). Analytical RP-HPLC: t_R = 1.42 min (100% A to 100% D in 3.5 min, λ= 214 nm). MS (ESI+): $C_{81}H_{145}N_{21}O_{15}$ calc./obs. 1652.12/1652.12 [M].

B15 (ADVWKKVIKVIK-NH_2) was obtained after manual synthesis from Rink Amide AM resin LL (300 mg, 0.29 mmol/g), the peptide was obtained as a white foamy solid after preparative RP-HPLC purification (55 mg, 35.8%). Analytical RP-HPLC: t_R = 1.39 min (100% A to 100% D in 3.5 min, λ= 214 nm). MS (ESI+): $C_{69}H_{120}N_{18}O_{14}$ calc./obs. 1424.92/1424.92 [M].

B16 (WRGKIGKIIKAVK-NH_2) was obtained after manual synthesis from Rink Amide AM resin LL (300 mg, 0.29 mmol/g), the peptide was obtained as a white foamy solid after preparative RP-HPLC purification (25 mg, 13.9%). Analytical RP-HPLC: t_R = 1.28 min (100% A to 100% D in 3.5 min, λ= 214 nm). MS (ESI+): $C_{71}H_{126}N_{22}O_{13}$ calc./obs. 1494.99/1494.99 [M].

B17 (NWKKILGRLGEKG-NH_2) was obtained after manual synthesis from Rink Amide AM resin LL (300 mg, 0.29 mmol/g), the peptide was obtained as a white foamy solid after preparative RP-HPLC purification (26 mg, 16.3%). Analytical RP-HPLC: t_R = 1.34 min (100% A to 100% D in 3.5 min, λ= 214 nm). MS (ESI+): $C_{68}H_{116}N_{22}O_{16}$ calc./obs. 1496.89/1496.89 [M].

B18 (KNWKKIVHDIKNS-NH_2) was obtained after manual synthesis from Rink Amide AM resin LL (300 mg, 0.29 mmol/g), the peptide was obtained as a white foamy solid after preparative RP-HPLC purification (33 mg, 18.4%). Analytical RP-HPLC: t_R = 1.20 min (100% A to 100% D in 3.5 min, λ= 214 nm). MS (ESI+): $C_{73}H_{121}N_{23}O_{18}$ calc./obs. 1607.93/1607.93[M].

B19 (NWKKILGKVIDDMKM-NH_2) was obtained after manual synthesis from Rink Amide AM resin LL (300 mg, 0.29 mmol/g), the peptide was obtained as a white foamy solid after preparative RP-HPLC purification (40 mg, 22.5%). Analytical RP-HPLC: t_R = 1.56 min (100% A to 100% D in 3.5 min, λ= 214 nm). MS (ESI+): $C_{82}H_{140}N_{22}O_{20}S_2$ calc./obs. 1817.00/1817.00 [M].

B20 (DKFSEKLGKIIKIVK-NH_2) was obtained after manual synthesis from Rink Amide AM resin LL (300 mg, 0.29 mmol/g), the peptide was obtained as a white foamy solid after preparative RP-HPLC purification (30 mg, 16.5%). Analytical RP-HPLC: t_R = 1.42 min (100% A to 100% D in 3.5 min, λ= 214 nm). MS (ESI+): $C_{82}H_{145}N_{21}O_{20}$ calc./obs. 1744.01/1744.01 [M].

DA1 (fakkffkkfakfafk -NH_2) was obtained from D-enantiomeric amino acids after manual synthesis from Rink Amide AM resin LL (300 mg, 0.29 mmol/g), the peptide was obtained as a white foamy solid after preparative RP-HPLC purification (25.5 mg, 23.0%). Analytical RP-HPLC: t_R = 1.39 min (100% A to 100% D in 3.5 min, λ= 214 nm). MS (ESI+): $C_{99}H_{144}N_{22}O_{15}$ calc./obs. 1881.12/1881.12 [M].

DLL-III (vnwkkilgkiikvvk-NH_2) was obtained from D-enantiomeric amino acids after manual synthesis from Rink Amide AM resin LL (300 mg, 0.29 mmol/g), the peptide was obtained as a white foamy solid after preparative RP-HPLC purification (26 mg,17.0%). Analytical RP-HPLC: t_R = 1.53 min (100% A to 100% D in 3.5 min, λ= 214 nm). MS (ESI+): $C_{86}H_{153}N_{23}O_{16}$ calc./obs. 1764.19/1764.20 [M].

DB1 (vnwkkilgkiikvvk-NH_2) was obtained from D-enantiomeric amino acids after manual synthesis from Rink Amide AM resin LL (300 mg, 0.29 mmol/g), the peptide was obtained as a white foamy solid after preparative RP-HPLC purification (33 mg, 16.0%). Analytical RP-HPLC: t_R = 1.45 min (100% A to 100% D in 3.5 min, λ= 214 nm). MS (ESI+): $C_{89}H_{148}N_{24}O_{16}$ calc./obs. 1809.15/1809.16 [M].

FB1 was obtained from **B1** by procedure mentioned above. Rink Amide AM resin LL (100 mg, 0.29 mmol/g) was used, and the product was obtained as a bright yellow foamy solid after preparative RP-HPLC purification (16.8 mg, 27.6%). Analytical RP-HPLC: t_R = 1.70 min (100% A to 100% D in 3.5 min, λ= 214 nm). MS (ESI+): $C_{110}H_{158}N_{24}O_{22}$ calc./obs. 2167.20/2167.21[M].

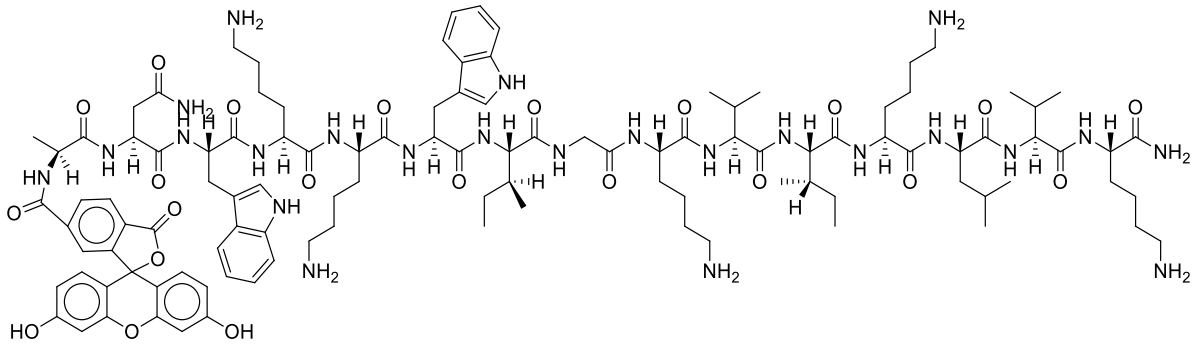

FDB1 was obtained from **DB1** by procedure mentioned above. Rink Amide AM resin LL (100 mg, 0.29 mmol/g) was used, and the product was obtained as a bright yellow foamy solid after preparative RP-HPLC purification (9.3 mg, 12.1%). Analytical RP-HPLC: t_R = 1.60 min (100% A to 100% D in 3.5 min, λ= 214 nm). MS (ESI+): $C_{110}H_{158}N_{24}O_{22}$ calc./obs. 2167.20/2167.22 [M].

FLL-III was obtained from **LL-III** by procedure mentioned above. Rink Amide AM resin LL (100 mg, 0.29 mmol/g) was used, and the product was obtained as a bright yellow foamy solid after preparative RP-HPLC purification (15.5 mg, 26.0%). Analytical RP-HPLC: t_R = 1.77 min (100% A to 100% D in 3.5 min, λ= 214 nm). MS (ESI+): $C_{107}H_{163}N_{23}O_{22}$ calc./obs. 2122.23/2122.25 [M].

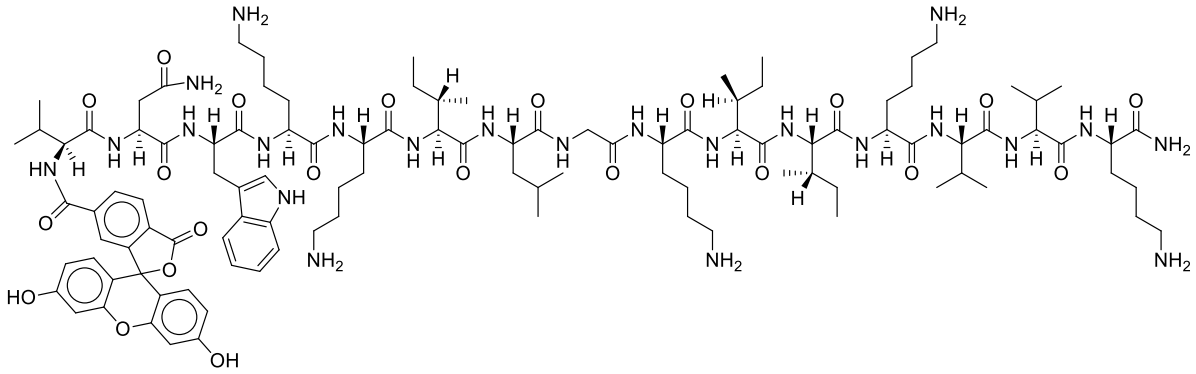

FDLL-III was obtained from **DL-III** by procedure mentioned above. Rink Amide AM resin LL (100 mg, 0.29 mmol/g) was used, and the product was obtained as a bright yellow foamy solid after preparative RP-HPLC purification (13 mg,17.2%). Analytical RP-HPLC: t_R = 1.68 min (100% A to 100% D in 3.5 min, λ= 214 nm). MS (ESI+): $C_{107}H_{163}N_{23}O_{22}$ calc./obs. 2122.23/2122.25 [M].

FA1 was obtained from **A1** by procedure mentioned above. Rink Amide AM resin LL (100 mg, 0.29 mmol/g) was used, and the product was obtained as a bright yellow foamy solid after preparative RP-HPLC purification (10.3 mg, 16.4%). Analytical RP-HPLC: t_R = 1.60 min (100% A to 100% D in 3.5 min, λ= 214 nm). MS (ESI+): $C_{120}H_{154}N_{22}O_{21}$ calc./obs. 2239.17/2239.16 [M].

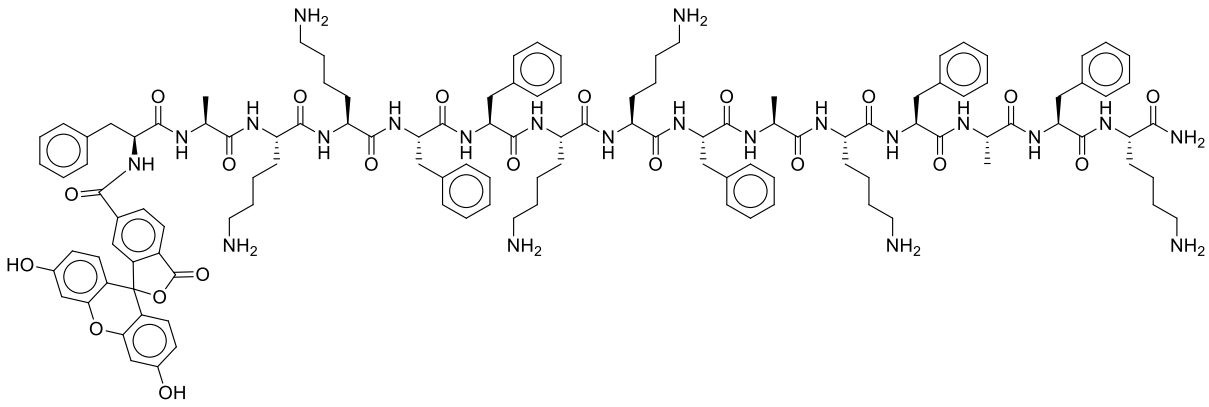

FDA1 was obtained from **DA1** by procedure mentioned above. Rink Amide AM resin LL (100 mg, 0.29 mmol/g) was used, and the product was obtained as a bright yellow foamy solid after preparative RP-HPLC purification (14.1 mg, 17.2%). Analytical RP-HPLC: t_R = 1.61 min (100% A to 100% D in 3.5 min, λ= 214 nm). MS (ESI+): $C_{120}H_{154}N_{22}O_{21}$ calc./obs. 2239.17/2239.16 [M].

G3KL $(KL)_8(KKL)_4(KKL)_2KKL$ was obtained after manual synthesis from Rink Amide AM resin LL (250 mg, 0.29 mmol/g), the compound was obtained as white solid after purification

on RP-HPLC (107 mg, 23.0%). Analytical RP-HPLC: t_R = 1.33 min (100% A to 100% D in 3.5 min, λ= 214 nm). HRMS (ESI+): $C_{222}H_{432}N_{60}O_{37}$ calc./obs. 4531.38/4531.38 [M].

T7 $(KL)_8(KKL)_4(KKLL)_2KKKL$ was obtained after manual synthesis from Rink Amide AM resin LL (300 mg, 0.29 mmol/g), the compound was obtained as white solid after purification on RP-HPLC (142 mg, 26.4%). Analytical RP-HPLC: t_R = 1.39 min (100% A to 100% D in 3.5 min, λ= 214 nm). HRMS (ESI+): $C_{240}H_{466}N_{64}O_{40}$ calc./obs. 4885.64/4885.65 [M].

EZ-209 $(KL)_8(KK^*L)_4(KK^*L)_2KLLL$ was obtained after automated synthesis from Rink Amide AM resin LL, the compound was obtained as white solid after purification on RP-HPLC (20 mg, 3.4%). Analytical RP-HPLC: t_R = 1.39 min (100% A to 100% D in 3.5 min, λ= 214 nm). HRMS (ESI+): $C_{228}H_{4442}N_{60}O_{38}$ calc./obs. 4629.45/4629.46 [M].

EZ-211 $(KL)_8(KK^*L)_4(KK^*L)_2KK^*L$ was obtained after automated synthesis from Rink Amide AM resin LL, the compound was obtained as white solid after purification on RP-HPLC (31 mg, 5.3%). Analytical RP-HPLC: t_R = 1.32 min (100% A to 100% D in 3.5 min, λ= 214 nm). HRMS (ESI+): $C_{222}H_{432}N_{60}O_{37}$ calc./obs. 4531.38/4531.38 [M].

EZ-212 $(KL)_8(KK^*L)_4(KK^*LL)_2KK^*K^*L$ was obtained after manual synthesis from Rink Amide AM resin LL (300 mg, 0.29 mmol/g), the compound was obtained as white solid after purification on RP-HPLC (85.9 mg, 12.9%). Analytical RP-HPLC: t_R = 1.32 min (100% A to 100% D in 3.5 min, λ= 214 nm). HRMS (ESI+): $C_{240}H_{466}N_{64}O_{40}$ calc./obs. 4885.64/4885.64 [M].

EZ-282 $(KL)_8(KKL)_4(KKL)_2KLLL$ was obtained after manual synthesis from Rink Amide AM resin LL (300 mg, 0.29 mmol/g), the compound was obtained as white solid after purification on RP-HPLC (131 mg, 21.1%). Analytical RP-HPLC: t_R = 1.39 min (100% A to 100% D in 3.5 min, λ= 214 nm). HRMS (ESI+): $C_{228}H_{442}N_{60}O_{38}$ calc./obs. 4629.45/4629.45 [M].

7.5. Synthesis and Characterization of small molecules, Dox-conjugates, and DACHPt conjugates

Z6 4-(pyridin-2-yldisulfanyl)phenyl)methanol

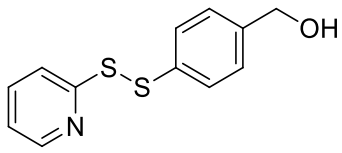

The reaction procedure was adapted from reference.[102]

To a stirred solution of 2,2'-dithiobispyridine (158 mg, 0.72 mmol, 2.0 eq) in 2 mL AcOH/EtOH (1/20 v/v, degassed by Argon for 5 min) 4-mercaptobenzyl alcohol (50 mg, 0.36 mmol, 1 eq) in 2 mL AcOH/EtOH (1:20 v/v, degassed by Argon for 5 min) was added dropwise at 4ºC. The mixture was slowly warmed up to room temperature and left overnight. After reaction completion the mixture was evaporated to dryness *in vacuo* to remove excess of AcOH and crude mixture was purified by a flash column chromatography (SiO_2, 0-40% ethyl acetate/hexane) to afford **Z6** (42.1 mg, 47%) as yellow oil.

Spectroscopic data are accordance with the literature.

^{1}H NMR (300 MHz, $CDCl_3$) δ 8.45 (d, *J* = 4.5 Hz, 1H), 7.68 – 7.59 (m, 2H), 7.52-7.48 (m, 2H), 7.30 (d, *J* = 8.2 Hz, 2H), 7.11 – 7.06 (m, 1H), 4.65 (s, 2H), 1.95 (br. s, 1H). ^{13}C NMR (75 MHz, CDCl3) δ 149.08, 142.71, 140.43, 137.41, 135.06, 127.99, 127.74, 120.80, 117.53, 64.41.Anal. RP-HPLC: t_R = 3.1 min (100% A to 100% D in 7.5 min, λ= 214 nm). HRMS (ESI+) $C_{12}H_{12}NOS_2$ calc./found 250.0355/250.0405 $[M+H]^+$.

Z7 4-nitrophenyl (4-(pyridin-2ylsulfanyl)benzyl) carbonate

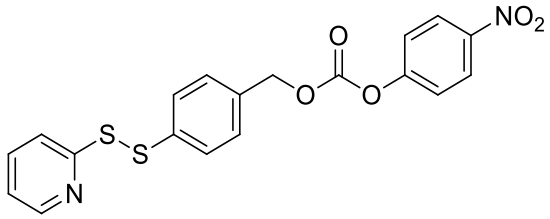

The reaction procedure was adapted from reference.[102]

To a solution of 4-nitrophenyl chloroformate (40.3 mg, 0.2 mmol, 1.2 eq) in 2 mL dry THF at 0°C under Ar atmosphere, a mixture of **Z6** (42.1 mg, 0.17 mmol, 1 eq), Et_3N (120 µL, 0.85 mmol, 5 eq) in 3 mL dry THF was added dropwise. The mixture was warmed slowly to room temperature and stirred overnight. After reaction completion THF was evaporated *in vacuo* and crude mixture was purified by flash chromatography (SiO_2, 0-40% ethyl acetate/hexane/1% AcOH) to afford **Z7** (38.0 mg, 54%) as a pale-yellow powder.

Spectroscopic data are accordance with the literature.

^{1}H NMR (300 MHz, $CDCl_3$) δ 8.49-8.45 (m, 1H), 8.26 (d, *J* = 9.2 Hz, 2H), 7.66 – 7.59 (m, 2H), 7.54 (t, *J* = 7.9 Hz, 2H), 7.38 (dd, *J* = 10.6, 5.7 Hz, 4H), 7.17 – 7.01 (m, 1H), 5.24 (s, 2H).

Anal. RP-HPLC: t_R = 4.46 min (100% A to 100% D in 7.5 min, λ= 214 nm). HRMS (ESI+): $C_{19}H_{15}N_2O_5S_2$ calc./found 415.0417/415.0420 $[M+H]^+$.

Z8

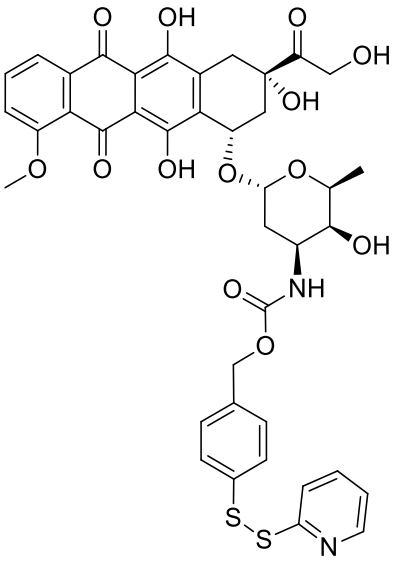

The linker **Z7** (23.0 mg, 0.055 mmol, 1 eq) in 2 mL anhydrous DMF was added to a solution of Doxorubicin hydrochloride (41.0 mg, 0.072 mmol, 1.3 eq), DIPEA (60 µL, 0.36 mmol, 6.5 eq) in 2 mL anhydrous DMF at 0°C , and stirred overnight. After reaction completion the mixture was evaporated *in vacuo* and crude was lyophilized and subjected to a flash column chromatography (SiO_2, DCM/MeOH, 30:1, v/v) to afford **Z8** (25.2 mg, 56%) as a red powder. Analytical RP-HPLC: t_R = 5.53 min (100% A to 100% D in 7.5 min, λ= 214 nm). HRMS (ESI+): $C_{40}H_{38}N_2O_{13}S_2$ calc./found 819.1888/819.1865 $[M+H]^+$.

Z9

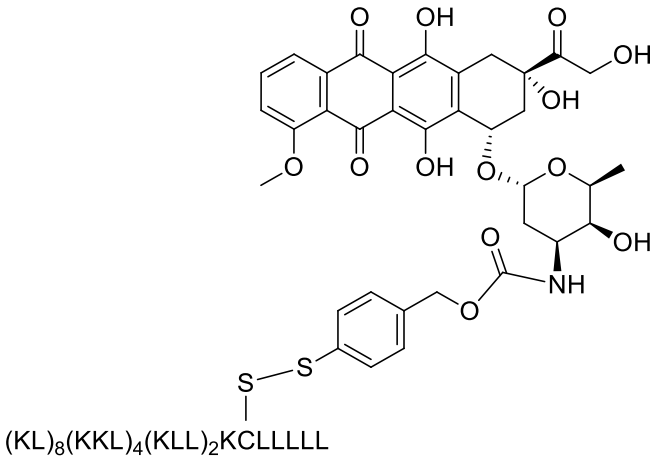

Z1 (2.78 μmol, 20 mg) in H_2O (300 μL) was added to **Z8** (4.2 mg, 5.06 μmol) in MeCN (600 μL) and stirred for 1 h. The final product **Z9** (4 mg, 18.5%) was purified by RP-HPLC to yield red powder. Analytical RP-HPLC: t_R = 3.84 min (100% A to 100% D in 7.5 min, λ= 214 nm). MS (ESI+): $C_{278}H_{500}N_{62}O_{54}S_2$ calc./found 5635.7726/5635.7810 [M] (M: monoisotopic reconstituted mass).

Z10

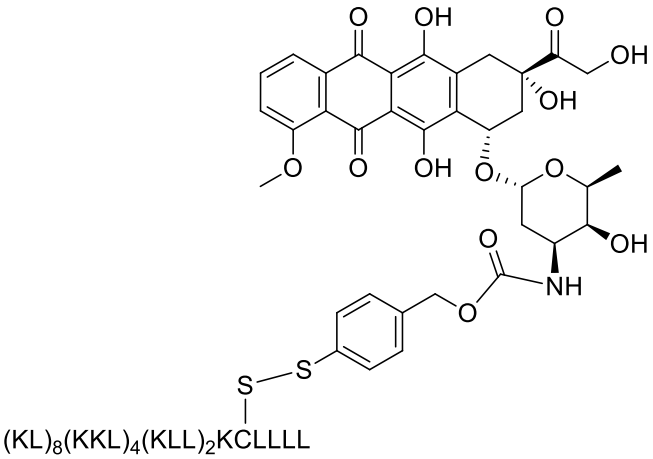

Z2 (2.82 μmol, 20 mg) in H_2O (300 μL) was added to **Z8** (4.6 mg, 5.64 mmol) in MeCN (600 μL) and stirred for 1 h. The final product **Z10** (7 mg, 32.5%) was purified by RP-HPLC to get red powder. Analytical RP-HPLC: t_R = 3.64 min (100% A to 100% D in 7.5 min, λ= 214 nm). MS (ESI+): $C_{272}H_{489}N_{61}O_{53}S_2$ calc./found 5522.6886/5522.6986 [M] (M: monoisotopic reconstituted mass).

Z13

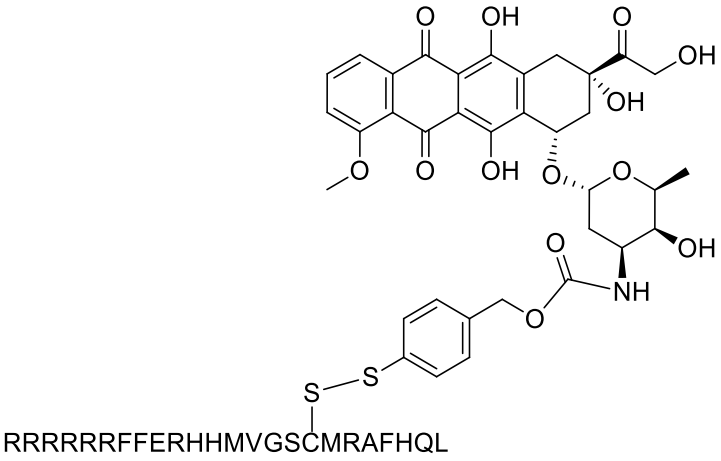

Z5 (4.9 μmol, 20 mg) in H_2O (500 μL) was added to **Z8** (8.0 mg, 9.8 mmol) in MeCN (1000 μL) and stirred for 1h. The final product **10** (5.8 mg, 24.6%) was purified by reverse phase

HPLC as red powder. Analytical RP-HPLC: t_R = 1.54 min (100% A to 100% D in 3.5 min, λ= 214 nm). MS (ESI+): $C_{170}H_{251}N_{57}O_{41}S_4$ calc./found 3874.8191/3874.8341 [M] (M: monoisotopic reconstituted mass).

Z21 pent-4-enal

The procedure was adapted from reference.[103]

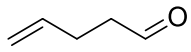

pent-4-ene-1-ol (1.0 mL, 10 mmol) was added to a suspension of pyridinium chlorochromate (3.2 g, 15 mmol) in 50 mL DCM. The reaction was stirred for 5 h, and the completion was monitored by TLC. The mixture was filtered through silica and celite (layered, 3:1 ratio), evaporated *in vacuo.* The product **Z21** as a colourless oil was processed without further purifications (0.8 g, 95%).

Spectroscopic data are accordance with the literature.

^{1}H NMR (300 MHz, $CDCl_3$) δ 9.77 (s, 1H), 6.02 – 5.66 (m, 1H), 5.17 – 4.89 (m, 2H), 2.54 (t, *J* = 7.5 Hz, 2H), 2.39 (q, *J* = 6.8 Hz, 2H).

Z22 hex-5-enal

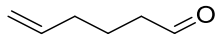

hex-5-enal was obtained with the same procedure as above (0.91 g, 10 mmol, 93 %).

Spectroscopic data are accordance with the literature.[186]

^{1}H NMR (300 MHz, $CDCl_3$) δ 9.77 (s, 1H), 5.92 – 5.62 (m, 1H), 5.18 – 4.83 (m, 2H), 2.45 (td, *J* = 7.3, 1.6 Hz, 2H), 2.10 (dd, *J* = 14.4, 6.9 Hz, 2H), 1.73 (p, *J* = 7.4 Hz, 2H).

Z23 pent-4-ene-1,1-diyl diacetate

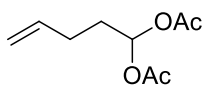

The procedure was adapted from patent.[187]

To a mixture of acetic anhydride (1.2 mL, 12.35 mmol, 1.3 eq) and $InCl_3$(105 mg, 0.475 mmol 0.05 eq) in 5 mL anhydrous DCM, pent-4-enal (0.8 g, 9.5 mmol, 1 eq). After 1 h the reaction was treated with 25% NaOAC (5 mL), extracted with DCM (2×5 mL), organic layers were

combined and washed with brine. The organic solvent was evaporated in *in vacuo* to dryness to remove excess of AcOH and to afford **Z23** as a colorless oil (1.72 g, quant.).

^{1}H NMR (300 MHz, $CDCl_3$) δ 6.78 (t, *J* = 5.5 Hz, 1H), 5.86-5.72 (m, 1H), 5.07 – 4.97 (m, 2H), 2.21 – 2.08 (m, 2H), 2.05 (s, 6H), 1.93 – 1.78 (m, 2H).

Z24 hex-5-ene-1,1-diyl diacetate

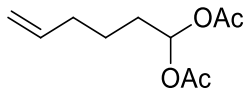

hex-5-ene-1,1-diyl diacetate was obtained with the same procedure as above (1.83 g, 9.3 mmol, quant.). Spectroscopic data are accordance with the literature.[97]

^{1}H NMR (300 MHz, $CDCl_3$) δ 6.78 (t, *J* = 5.6 Hz, 1H), 5.87 – 5.68 (m, 1H), 5.11 – 4.89 (m, 2H), 2.07 (s, 6H), 2.04 – 2.02 (m, 2H), 1.79 - 1.73 (m, 2H), 1.52- 1.42 (m, 2H).

Z17 5-oxopentane-1,1-diyl diacetate

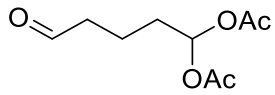

The procedure was adapted from reference.[96]

A solution of hex-5-ene-1,1-diyl diacetate (1 g, 5 mmol) in 15 mL DCM/MeOH (10:1, v/v) was placed in a long pear shaped flask with an inlet dispersion tube extending to the base. The flask was cooled to -72°C in a dry ice/acetone mixture, and ozone was applied. Ozonization was performed for 30 min until all of the compound had reacted (until the mixture turned blue). After the reaction completion Me_2S (1.55 mL, 20 mmol) was added, and the mixture was stirred overnight. The excess of Me_2S was evaporated *in vacuo*, and the crude was purified by column chromatography (SiO_2, 0-35% ethyl acetate/hexane) to afford **Z17** (0.44 g, 44%) as a colorless oil.

Spectroscopic data are accordance with the literature. [97]

^{1}H NMR (300 MHz, $CDCl_3$) δ 9.75 (t, *J* = 1.2 Hz, 1H), 6.76 (t, *J* = 5.1 Hz, 1H), 2.56 – 2.40 (m, 2H), 2.05 (s, 6H), 1.84 – 1.65 (m, 4H).

Z16 4-oxobutane-1,1-diyl diacetate

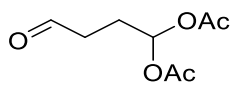

4-oxobutane-1,1-diyl diacetate was obtained with the same procedure as above (0.37 g, 5 mmol, 40%). Spectroscopic data are accordance with the literature.[97]

^{1}H NMR (300 MHz, $CDCl_3$) δ 9.77 (t, *J* = 1.1 Hz, 1H), 6.80 (t, *J* = 5.1 Hz, 1H), 2.58 (td, *J* = 7.3, 1.0 Hz, 2H), 2.12 (td, *J* = 7.3, 5.1 Hz, 2H), 2.06 (s, 6H).

Z25 2-(3-iodopropyl)-1,3-dioxolane

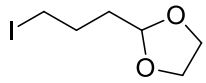

The procedure was adapted from reference.[18]

To the stirred mixture of NaI (5.0 g, 0.034 mol) and $NaHCO_3$ (0.4 g, 0.005 mol as a stabilizer) in 25 mL of acetone 2-(3-Chloropropyl)-1,3-dioxolane (2.5 g, 0.017 mol) was added. The solution was refluxed for 20 h, followed by evaporation *in vacuo*. The obtained solid was washed three times with 15 mL of diethyl ether, filtered off and the organic filtrate was stirred with 4 g of anhydrous Na_2SO_4, 0.25 g of $Na_2S_2O_3$ and 0.25 g of $NaHCO_3$ for 12 h. The mixture was filtered off and diethyl ether was evaporated *in vacuo* with addition of small portion of Na_2CO_3 (20 mg) during evaporation step. The crude oily product was purified by distillation under reduced pressure ($T_{boiling}$ = 70-75ºC at 1 mbar) to afford colorless liquid (2.6 g, 61%). The product was stored in the dark at -18ºC with a small amount of fine-grained Na_2CO_3 as a stabilizer.

Spectroscopic data are accordance with the literature.[18]

^{1}H NMR (300 MHz, $CDCl_3$) δ 4.86 (dd, *J* = 5.3, 3.3 Hz, 1H), 3.89 (ddd, *J* = 19.6, 14.0, 8.1 Hz, 4H), 3.27 – 3.10 (m, 2H), 2.02 – 1.82 (m, 2H), 1.80 – 1.64 (m, 2H).

Z26 4-iodobutanal

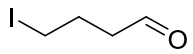

The procedure was adapted from reference.[18]

To the solution of 2-(3-iodopropyl)-1,3-dioxolane (1.0 g, 0.004 mol) in 40 mL THF the solution of 6 mL concentrated HCl in 130 mL H2O was added. An initially
cloudy reaction mixture was stirred in the dark at r.t. for 12 h until completion. The mixture was then extracted with DCM (5x8 mL). The combined organic layers were dried with anhydrous Na_2SO_4, and the solvent was evaporated *in vacuo* with addition of small portion of

Na_2CO_3. The product **Z26** as a colorless oil was processed without further purifications (0.7 g, 89%). The product was stored in the dark at -18ºC with a small amount of fine-grained $Na_2S_2O_3$ as a scavenger.

Spectroscopic data are accordance with the literature.[18]

^{1}H NMR (300 MHz, $CDCl_3$) δ 9.80 (s, 1H), 3.23 (t, *J* = 6.7 Hz, 2H), 2.67 – 2.56 (m, 2H), 2.13 (p, *J* = 6.8 Hz, 2H).

Z18 4-iodobutane-1,1-diyl diacetate

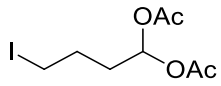

4-iodobutane-1,1-diyl diacetate was obtained with the same procedure as for **Z17** above (0.47 g, 1.7 mmol, 93%).

^{1}H NMR (300 MHz, $CDCl_3$) δ 6.78 (t, *J* = 4.5 Hz, 1H), 3.19 (t, *J* = 6.2 Hz, 2H), 2.06 (s, 6H), 1.95 – 1.84 (m, 4H). ^{13}C NMR (75 MHz, $CDCl_3$) δ 168.80, 89.44, 34.01, 27.36, 21.08, 5.34.

Z14a N-(5,5-Diacetoxybut-l-yl) doxorubicin trifluoroacetate

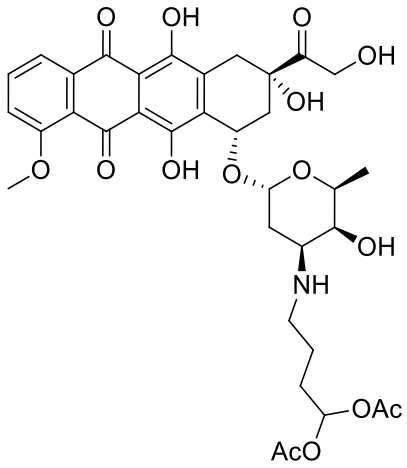

To a solution of Doxorubicin hydrochloride (58 mg, 0.1 mmol) in 5 mL DMF was added 4-iodobutane-1,1-diyl diacetate **Z18** (90 mg, 0.3 mmol) and $NaHCO_3$ (0.5 g, 6 mmol). The reaction mixture was stirred in the dark at room temperature for 5 h. After reaction completion the mixture was evaporated *in vacuo* and crude was lyophilized and subjected to purification by RP-HPLC (H_2O/MeCN, 1% TFA) to afford **Z14a** (23.6 mg, 33%).

Analytical RP-HPLC: t_R = 1.74 min (100% A to 100% D in 3.5 min, λ= 214 nm). MS (ESI+): $C_{35}H_{41}NO_{15}$ calc./found 716.2549/716.2543 $[M+H]^+$.

General procedure for Z15a, Z15b

The procedure was adapted from reference.[96]

To the solution of Doxorubicin hydrochloride (58 mg, 0.1mmol), 5-oxopentane-l,1-diacetate **X** (40,4 mg, 0.2 mmol) in 15 mL MeCN/H_2O (2:1, v/v) (5 mL) the solution of NaBH3CN (4.4 mg, 0.07 mmol) in 5 mL MeCN/H_2O (2:1, v/v) was added. The mixture was stirred under a nitrogen atmosphere at room temperature in the dark for 1 h. When reaction was complete, the solution was diluted with 20 mL H_2O, and extracted repeatedly with $CHCl_3$/MeOH (5:1, v/v, 10x20 mL). The combined organic layers were dried with anhydrous Na_2SO_4 and the solvent was evaporated *in vacuo*. The crude mixture was purified by RP-HPLC (H_2O/MeCN, 1% TFA) to afford **Z15a** (5.1 mg, 7%) and Z**15b** (15.0 mg, 20%).

Z15b N-(5,5-Diacetoxypent-l-yl) doxorubicinol trifluoroacetate

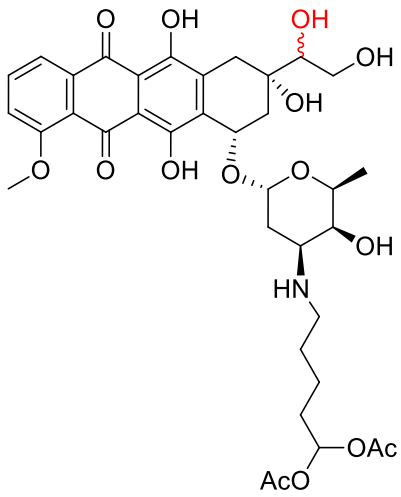

Analytical RP-HPLC: t_R = 1.68 min (100% A to 100% D in 3.5 min, λ= 214 nm). MS (ESI+): $C_{36}H_{46}NO_{15}$ calc./found 732.2862/732.2833 $[M+H]^+$. ^{1}H NMR (300 MHz, DMSO) δ 13.36 (t, *J* = 5.0 Hz, 1H), 12.57 (d, *J* = 1.8 Hz, 1H), 7.64 (br s, 1H), 7.23-7.17 (m, 1H), 7.04 – 6.88 (m, 1H), 5.95 (t, *J* = 5.5 Hz, 1H), 5.07 (s, 2H), 4.63 (br s, 1H), 4.23 (br s, 1H), 3.49 – 3.46 (m, 3H), 3.30 (s, 3H), 3.17 – 3.04 (m, 5H), 2.82 – 2.72 (m, 5H), 2.14 (br s, 2H), 1.85 – 1.83 (m, 2H), 1.33 (s, 6H), 1.05 – 0.98 (m, 2H), 0.92 – 0.86 (m, 2H), 0.69-0.60 (m, 2H), 0.52 (d, *J* = 6.2 Hz, 3H). ^{13}C NMR (101 MHz, DMSO) δ 186.43, 186.29, 168.88, 160.80, 156.24, 154.98, 136.20, 136.01, 135.61, 134.72, 119.97, 119.57, 118.98, 110.42, 110.37, 99.32, 89.46, 77.08 (C-13), 76.55, 70.72, 70.26, 66.05, 64.02, 61.86, 56.60, 39.52, 36.35, 31.90, 30.51, 25.03, 20.52, 20.10, 18.59, 16.68.

Z15a N-(5,5-Diacetoxypent-l-yl) doxorubicin trifluoroacetate

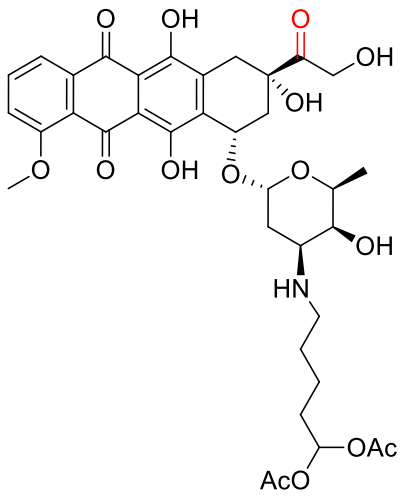

Analytical RP-HPLC: t_R = 1.78 min (100% A to 100% D in 3.5 min, λ= 214 nm). MS (ESI+): $C_{36}H_{43}NO_{15}$ calc./found 730.2705/730.2703 $[M+H]^+$.

Z27

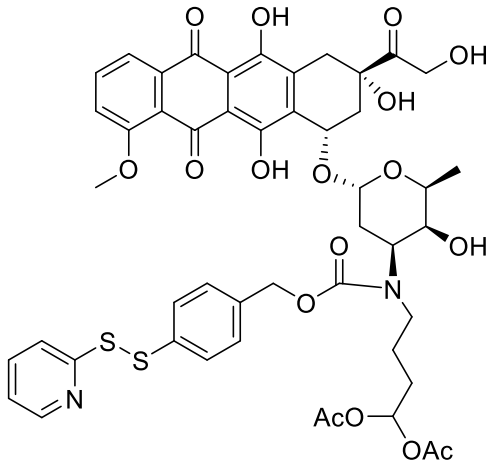

Z14a (23.6 mg, 0.033 mmol) and DMAP (20.1 mg, 0.165 mmol) were dissolved in DMF (2 mL), and then linker **Z7** (13.7 mg, 0.033 mmol) was added. The reaction was stirred at room temperature in the dark for 2 days. The mixture was evaporated *in vacuo* and crude was lyophilized and subjected to purification by RP-HPLC (H_2O/MeCN, 1% TFA) to afford **Z27** (1.7 mg, 5%).

Analytical RP-HPLC: t_R = 2.92 min (100% A to 100% D in 3.5 min, λ= 214 nm). MS (ESI+): $C_{48}H_{52}N_2O_{17}S_2$ calc./found 993.2780/993.2791 $[M+H]^+$.

pDox (2-Pyrrolino-Doxorubicin)

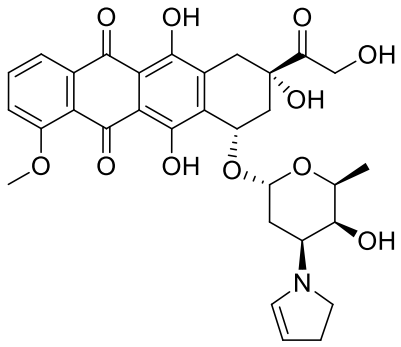

To a solution of Doxorubicin hydrochloride (58 mg, 0.1 mmol) in 5 mL DMF was added 4-iodobutyraldehyde (59.1 mg, 0.3 mmol) and $NaHCO_3$ (0.5 g, 6 mmol). The reaction mixture was stirred in the dark at room temperature for 4 h. After reaction completion the mixture was evaporated *in vacuo* and crude was lyophilized and subjected to purification by RP-HPLC (H_2O/MeCN, 1% TFA) to afford pDox (18.4 mg, 31%).

Analytical RP-HPLC: t_R = 1.65 min (100% A to 100% D in 3.5 min, λ= 214 nm). MS (ESI+): $C_{31}H_{33}NO_{11}$ calc./found 596.2126/596.2108 $[M+H]^+$.

Preparation of DACHPt-peptide dendrimer conjugates

The procedure was adapted from the literature.[115]

Dichloro(1,2-diaminocyclohexane)platinum(II) $DACHPtCl_2$ (Sigma Aldrich) was suspended in water (10 mM) and mixed with silver nitrate ($[AgNO_3]/[DACHPtCl_2]$ = 1.955) in the dark at r.t. for 12 h to form the aqueous complex $DACHPt(OH_2)_2^{2+}$. AgCl precipitate formed after reaction was removed by centrifugation at 4000 rpm for 10 min followed by filtration through a 0.22 μm filter.

To the solution of peptide dendrimer in water (0.0007 mmol, 0.35 mM), adjusted to pH 7.0 with NaOH, the aqueous solution of $DACHPt(OH_2)_2^{2+}$ was added (0.0035 mmol per each carboxylate group in the dendrimer structure). The reaction mixture was stirred at 25°C for 48 h. Unbound DACHPt was removed by dialysis (dilution factor 1000) at 4°C using Slide-A-Lyzer Dialysis Cassettes (MWCO 2000 Da, Thermo Scientific, USA) and the dialyzed solution was then freeze dried. Drug content was measured by Pt (Pt^{194}/Pt^{195}) assay on an ICP-MS (NexION 350, PerkinElmer), performed at external facilities (EPFL, Lausanne, Switzerland).

7.6. Cell- and bacteria-based assays

Stock solutions were prepated from corresponding TFA salts in H_2O if nothing specified.

7.6.1. Cell culture conditions

HeLa, HEK-293, MCF-7, MDA-MB-231 cells (ATCC, Manassas, USA) were cultured and maintained in DMEM high glucose (Dulbecco`s modified Eagle medium, Sigma Aldrich) medium, supplemented with 10% FBS (Sigma Aldrich) and 1% penicillin/streptomycin. A549, H69, H69 AR cells were cultured and maintained in RPMI-1640 medium (Sigma Aldrich), supplemented with 10% FBS (Sigma Aldrich) and 1% penicillin/streptomycin. MCF-10a cells (ATCC, Manassas, USA) were cultured and maintained in HuMEC ready medium (Thermo Fisher Scientific), contained epidermal growth factor, hydrocortisone, isoproterenol, transferrin, insulin, and bovine pituitary extract. The cells were handled and subcultured according to the manufacturer instructions. Cells were incubated in a humidified incubator at 37°C in the presence of 5% CO_2.

7.6.2. Cell viability assay by AlamarBlue®

The cells were seeded into 96 well plates, in appropriate Medium, the day before the experiment. HEK-293 were seeded into well plates, pretreated with solution of Polylysine (Merck Millipore, Schaffhausen CH). The medium was removed and the compounds at increasing concentration were added into the wells. The cells were incubated for 72 (24) hours in 200 μL/well at 37°C in corresponding medium in the presence of 5% CO2. After incubation time the medium was removed and replaced by 100 μL/well of medium containing 10% alamarBlue® (Sigma Aldrich). The cells were incubated for 3-5 hours at 37°C with 5% CO2 in a humidified atmosphere. The fluorescence was then measured on a Tecan Infinite M1000 Pro plate reader at λ_{ex} 560 nm and λ_{em} 590 nm. The value was normalized according to the untreated cells.

7.6.3. Hemolysis assay (MHC and HC_{50} determination)

HC_{50} determination

Compounds were subjected to a hemolysis assay to assess the hemolytic effect on human red blood cells (hRBCs). The blood was obtained from Interregionale Blutspende SRK AG, Bern, Switzerland. 1.5 mL of whole blood was centrifuged at 3000 rpm for 15 minutes at 4 °C. The plasma was discarded, and the hRBC pellet was re-suspended in 5 mL of PBS (pH 7.4) then centrifuged at 3000 rpm for 5 minutes at 4 °C. The washing of hRBC was repeated three times

and the remaining pellet was re-suspended in 10 mL of PBS. The samples were prepared as the initial concentration of 2000 µg/mL in PBS, added to the first well of 96-well microtiter plate (TPP, untreated) and diluted serially by ½, having 100 µL of sample in every well. Controls on each plate included a blank medium control (PBS 100 µL) and a hemolytic activity control (0.1% TritonTM X-100). 100 µL of hRBC suspension was incubated with 100 µL of each sample in PBS in V-shape 96-well plate (Nunc 96-Well Polystyrene Conical Bottom MicroWell Plates). After the plates were incubated for 4 h at room temperature, 100 µL of supernatant was carefully pipetted to a flat bottom, clear 96-wells plate (TPP® tissue culture plates, polystyrene). Hemolysis was measured by analyzing the absorbance of free hemoglobin leaked out of compromised in the supernatants at 540 nm with a plate reader (Tecan instrument Infinite M1000). The percentage of hemolysis at each concentration was detected and HC_{50} was determined.

MHC determination

To determine the minimal hemolytic concentration (MHC) stock solutions of 8 mg/mL of the peptide in H2O were prepared and 50 µL were diluted serially by l/2 in 50 µL PBS (pH 7.4) in 96-well plate (Costar or Nunc, polystyrene, untreated). Human red blood cells (hRBC) were prepared as explained above. The hRBC suspension (50 µL) was added to each well and the plate was incubated at room temperature for 4 hours. Minimal hemolytic concentration (MHC) end points were determined by visual determination of the wells after the incubation period. Controls on each plate included a blank medium control (50 µL PBS + 50 µL of hRBC suspension) and a hemolytic activity control (mQ-deionized water 50 µL + 50 µL hRBC suspension).

7.6.4. Antimicrobial activity and MIC determination

The minimal inhibitory concentration (MIC) was determined by using broth microdilution method. Mueller-Hinton (MH) medium was prepared at different pH. MH broth (Bio-Rad, 25 g) was dissolved in 1 L of mQ water, adjust with 1 M NaOH or 1 M HCl until final pH is 5.0, 7.4 or 8.0. Medium was sterilized by autoclaving at 121°C for 15 minutes.

Antimicrobial activity was assayed against *E. coli* W3110, *A. baumannii* (ACTT 19606), *P. aeruginosa* PAO1 (WT), *K. pneumoniae* (NCTC 418), methicillin-resistant *S. aureus* (COL). A colony of bacteria was picked and grown in Luria-Bertani (LB) medium overnight at 37°C. The compounds were prepared as stock solutions of 2 mg/mL in autoclaved mQ H_2O, diluted to the initial concentration of 64 µg/mL in 300 µL MH medium at right pH, added to the first

well of 96-well microtiter plate (Costar® ref 3879) and diluted serially by ½. After a 3-5 hours culture from the preculture grown overnight, the concentration of the bacteria was quantified by measuring OD_{600} and diluted to OD_{600} = 0.022 in MH medium at the right pH. Then 4 µL of the diluted bacterial solution was used to inoculate into the sample solutions (150 µL) with a final inoculation of about 5×10^5 CFU/mL. The plates were then incubated at 37°C for 18 h. For each assay, sterility (broth only) and growth control (broth with bacterial inoculum, without antibiotics) were checked with two columns in the plate. The next day, 15 µL of of 3-(4,5-dimethylthiazol-2-yl)-2,5-diphenyltetrazolium bromide (MTT) solution was added to each well of the plate, such a way that MIC was defined as the lowest concentration of the peptide that inhibited visible growth of the tested bacteria.

7.7. Circular dichroism (CD) spectroscopy and helix wheel evaluation

Circular dichroism (CD) spectra were recorded on a Jasco J-715 Spectropolarimeter. All the experiments were performed using Hellma Suprasil 110-QS 0.1 cm cuvettes. Stock solutions (1.00 mg/mL) of peptides were freshly prepared in 10 mM phosphate buffer (PB, pH 7.4); stock solution (1.00 mg/mL) of dendrimers were freshly prepared in 10 mM phosphate buffers at pH 5.0, 7.4 and 8.0 respectively.

The PB buffer was degassed for 10 min under high vacuum before each set of experiments. For the measurement, the peptides and dendrimers were diluted to 100 µg/mL with PB buffer at right pH and Dodecylphosphocholine (DPC, Avanti Polar Lipids, Inc., USA) was added to final concentration 5 mM if needed. The range of measurement was 185–260 nm, the scan rate was 20 nm/min, pitch 0.5 nm, response 16 sec and bandwidth 1.0 nm. The nitrogen flow was kept >8.5 L/min. After each measurement, the cuvettes were washed successively with 1 M HCl, milli-Q H_2O and PB buffer with selected pH. The baseline was recorded under the same conditions and subtracted manually. Percentage of different secondary structure types was calculated by DichroWeb.[188]

7.8. Lipid vesicle leakage assays

5(6)-carboxyfluorescein (CF) was purchased from Sigma. Egg Yolk Phosphatidylcholine (EYPC), Egg Yolk Phosphatidylglycerol (EYPG) and a Mini-Extruder were purchased from Avanti Polar Lipids. Egg PC or Egg PG thin lipid layers were prepared by evaporating a solution of 100 mg Egg PC or Egg PG in 4 mL MeOH/$CHCl_3$ (1:1) on a rotary evaporator at

room temperature and then dried in vacuo overnight. The resulting film was then hydrated with 4 mL *CF buffer B* (50 mM CF, 10 mM TRIS, 10 mM NaCl, pH 7.4) for 30 min, subjected to freeze-thaw cycles (7x) and extrusion (15x) through a polycarbonate membrane (pore size 100 nm). Extra vesicular components were removed by gel filtration (Sephadex G-50) with *buffer A* (10 mM TRIS, 107 mM NaCl, pH 7.4). Final conditions: ~ 2.5 mM Egg PC or Egg PG; inside: 50 mM CF, 10 mM TRIS, 10 mM NaCl, pH 7.4 buffer; outside: 10 mM TRIS, 107 mM NaCl, pH 7.4.

Egg PC or Egg PG stock solutions (37.5 µL) were diluted to 3000 µL with a *buffer A* (10 mM TRIS, 107 mM NaCl, pH 7.4) in a thermostated fluorescence cuvette (25°C) and gently stirred (final lipid concentration ~31 µM). CF efflux was monitored at λ_{em} 517 nm /λ_{ex} 492 nm as a function of time after addition at t = 45 sec of 30 µl of peptide stock solution (1 mg/mL stock in buffer A), having final concentration 10 µg/mL. Finally, 30 µL of 1.2% Triton X-100 was added to the cuvette (0.012% final concentration) at t = 240 sec to reach the maximum intensity. Fluorescence intensities were then normalized to the maximal emission intensity using $I(t) = (I_t - I_0) / (I_\infty - I_0)$ where $I_0 = I_t$ at peptide addition, $I_\infty = I_t$ at saturation of lysis.

7.9. Critical Micellar Concentration (CMC)

Nile red (Sigma Aldrich, Buchs, CH) was diluted in MeOH at a concentration of 2 µM and 5 µL of solution was added to each well of 96-well plate (Faust Laborbedarf AG, Schaffhausen), followed by solvent evaporation under the fumehood air flow at room temperature for 1 h. Serial dilution of the peptide dendrimers or conjugates, were performed in 10 mM phosphate buffer (pH 5 or pH 7.4) starting from 1(2) mg/mL to 0.5 µg/mL and 50 µL was added to the plate containing the dried Nile red fluorophore (final concentration 0.2 µM). The plates were incubated for 2 h before measurement of fluorescence at λ_{ex}= 540 nm and λ_{em}= 615 nm on a Tecan Infinite M1000 Pro plate reader.

7.10. Acid-base titration

Peptide dendrimer (0.7 µmol, 5 mg) was diluted in 10 mL Milli-Q water (Final concentration of 100 µM) and acidified to pH 3 with 1 M HCl. Then, 0.1 M NaOH was added by steps of 2 µL to the solution with a Dosimat plus (Metrohm, Zofingen, Switzerland) and pH measured on a 692 pH/ion meter (Metrohm).

7.11. Release kinetics

1mg/mL of conjugates and 5 mg/mL of TCEP were individually dissolved in PBS and adjusted to pH 7.0. TCEP was then added to the samples at a final concentration of 48 μg/mL (1.2 eq) and the mixture was incubated at 37°C. After 0, 5, 30, 60, 120, 180, 240 min, 30 μL of each sample was isolated, to which 3 μL of 10% TFA was added. Each aliquot was then analyzed by the analytical HPLC.

7.12. Confocal microscopy

7.12.1. Cellular uptake of Z13 and Doxorubicin

To 8-well chambered coverglass plates (Faust Laborbedarf AG, Schaffhausen, CH) HeLa cells were seeded at 2×10^4 cells per well and incubated overnight. Then the medium was removed, and cells were treated with **Z13** or **Doxorubicin** at 1 μM (in complete DMEM medium, 250 μL/well), and incubated for 3, 6, or 12 hours at 37°C. The medium was removed, and cells were washed with prewarmed PBS twice. Nucleus was stained with Hoechst 33258 in PBS (0.25 μL in 0.25 mL/well) for 30 min. After the staining cells were washed with prewarmed PBS twice and prewarmed Glycergel Mounting Medium was added. Images were taken on a Zeiss LSM 880 confocal microscope with Oil compatible lens x63/1.3.

7.12.2. Cellular uptake of fluorescein-labelled peptide

8-well chambered coverglass plates (Faust Laborbedarf AG, Schaffhausen) HeLa cells were plated at 2×10^4 cells per well. The medium was removed, and cells were treated with fluorescein-labelled peptides (10 μM in complete DMEM, 250 μL/well), incubated for 2 h at 37°C in a humidified atmosphere in 5% carbon dioxide following the removal of the complete growth medium. Then, cells were washed with prewarmed PBS twice and the cell membrane was labelled with CellMask Deep Red plasma membrane stain in PBS (0.25 μL in 0.25 mL/well) and nucleus was stained with Hoechst 33258 in PBS (0.25 μL in 0.25 mL/well) for 30 min at 37°C. After the incubation cells were washed with PBS twice and prewarmed Glycergel Mounting Medium was added. Images were taken on a Zeiss LSM 880 confocal microscope with Oil compatible lens x63/1.3.

7.12.3. Colocalization studies

To 8-well chambered coverglass plates (Faust Laborbedarf AG, Schaffhausen, CH) HeLa cells were seeded at 2×10^4 cells per well and incubated overnight. Then the medium was removed, and cells were treated with fluorescein-labelled peptides (10 μM in complete DMEM, 250

µL/well), incubated for 1 h at 37 °C in a humidified atmosphere in 5% carbon dioxide following the removal of the complete growth medium. Then cells were washed with prewarmed PBS twice and nucleus was stained with Hoechst 33258 in PBS (0.25 µL in 0.25 mL/well) for 30 min at 37°C. Mitochondria was stained with Mitotracker®Red according to manufacture protocol (100 nM) at 37°C for 30 min. Staining solution was replaced with fresh prewarmed FluoroBrite DMEM (Gibco) Medium. Images were taken on a Zeiss LSM 880 confocal microscope with Oil compatible lens x63/1.3. Colocalization was processed with coDDM Maker Software.[167]

7.13. Flow cytometry

7.13.1. Cellular uptake

HeLa cells were plated into 96 well plate, 3×10^4 cells/well, and allowed to adhere overnight. Medium was removed and cells were treated with Fluorescein-labelled peptides (200 µL of 10 µM solution in complete growth medium), following by incubation at 37ºC for 2 h. Untreated cells were used as a control. Then the cell medium was removed, cells were washed with PBS, trypsinized, and trypsinization was quenched with 100 µL of complete growth medium. Cells were centrifuged at 500g for 5 min at 20°C and supernatant was decanted. The cells were resuspended in 100 µL 2% FBS PBS solution and analyzed by Beckman Coulter CytoFLEX™ (CytoFLEX). CytExpert 2.0 (Beckman Coulter, Miami, FL, USA) was used for acquisition and FlowJo™ Software (Ashland, OR: Becton, Dickinson and Company; 2021) for data processing.

7.13.2. Propidium iodine (PI) internalization

HeLa cells were plated into 96 well plate, 3×10^4 cells/well, and allowed to adhere overnight. Medium was removed and cells were treated with selected peptides (10 µM in DMEM, 200 µL/well) and incubated for 10 min at 37°C in a humidified atmosphere in 5% carbon dioxide. Then the medium was removed, cells were trypsinized (30 µL/well, 0.025%), trypsinization was quenched by 100 µL of complete growth medium (DMEM, (-) Phenol Red, 10% FBS). Cells were directly stained with PI according to manufacture protocol for 10 min and analyzed by Beckman Coulter CytoFLEX™.

7.13.3. Mitochondrial membrane depolarization

HeLa cells were plated into 96 well plate, 3×10^4 cells/well, and allowed to adhere overnight. Medium was removed and cells were treated with selected peptides (1 and 15 µM in DMEM,

200 µL/well) and incubated for 120 and 15 min at 37°C in a humidified atmosphere in 5% carbon dioxide. Untreated cells and cells treated with 50 µM FCCP (15 min) were used as controls. Then the medium was removed, cells were washed with PBS, trypsinized, trypsinization was quenched by 100 µL of complete growth medium (DMEM, (-) Phenol Red, 10% FBS) and stained by TMRE-Mitochondrial Membrane Potential Assay Kit (Abcam, Cambridge, UK) according to manufacture protocol (100 nM) for 15 min. Right after cells were analyzed using Beckman Coulter CytoFLEX™.

7.13.4. Annexin V-FITC /Propidium iodine (PI) staining

A549 cells were plated into 96 well plate, 3×10^4 cells/well, and allowed to adhere overnight. Medium was removed and cells were treated with selected peptides (5 µM in RPMI full growth medium, 200 µL/well) and incubated for 3 h at 37°C in a humidified atmosphere in 5% CO_2. Then the medium was removed, cells were washed with PBS, gently trypsinized (30 µL/well, 0.025%), trypsinization was quenched by 100 µL of complete growth medium (RPMI, 10% FBS). The cells were centrifuged (5 min, 1500 rpm), followed by supernatant removal. Cells were directly stained with Annexin V and PI according to manufacture protocol for 10 min and analysed by Beckman Coulter CytoFLEX™.

FlowJo™ Software (Ashland, OR: Becton, Dickinson and Company; 2021) was used for data processing.

8. Supplementary data

8.1. Additional data for Chapter 2

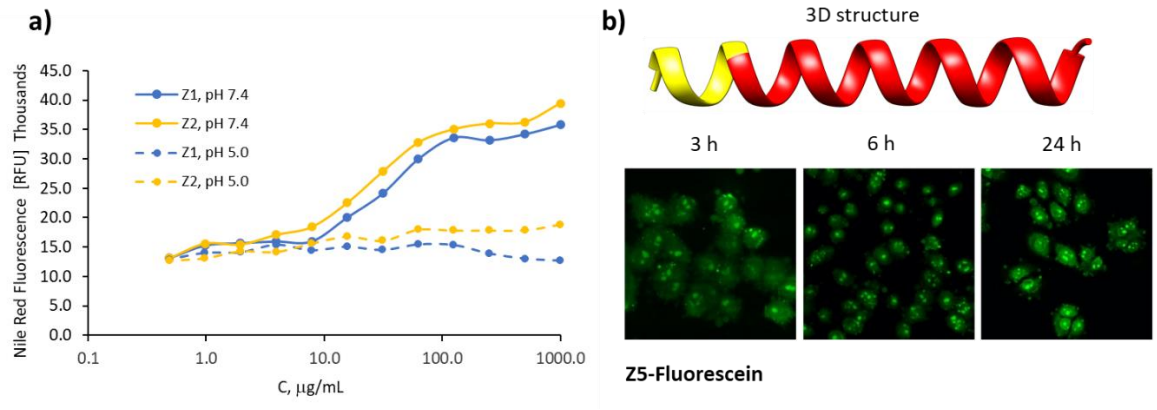

Figure S1. a) Critical aggregation concentration determination of Z1, Z2 in PB buffer at pH 7.4 and 5.0. Fluorescence measured at λ_{ex} = 540 nm and λ_{em} = 615 nm. RFU = relative fluorescence unit.

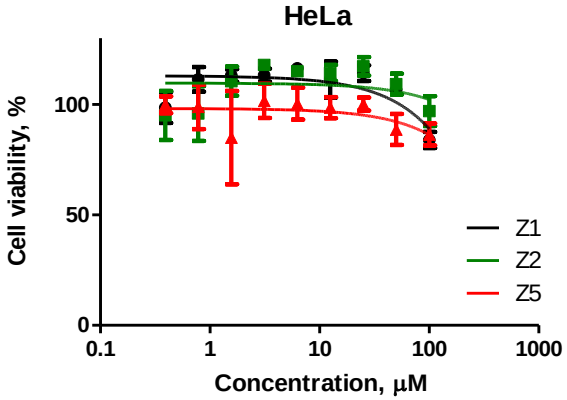

*Figure S2. Cell viability profiles for **Z1**,**Z2** and **Z5** in HeLa cells.The cells were incubated with compound at 37°C for 72 hours.*

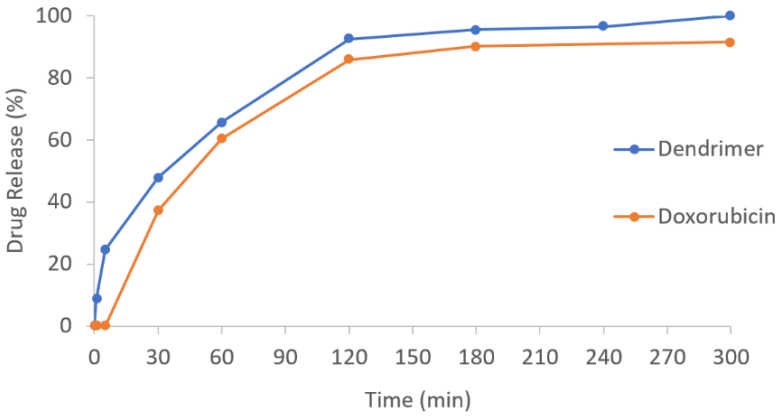

*Figure S3. Release kinetics of **Z10**, in the presence of 1.1 eq of TCEP at 37°C in PBS at pH 7 determined by HPLC.*

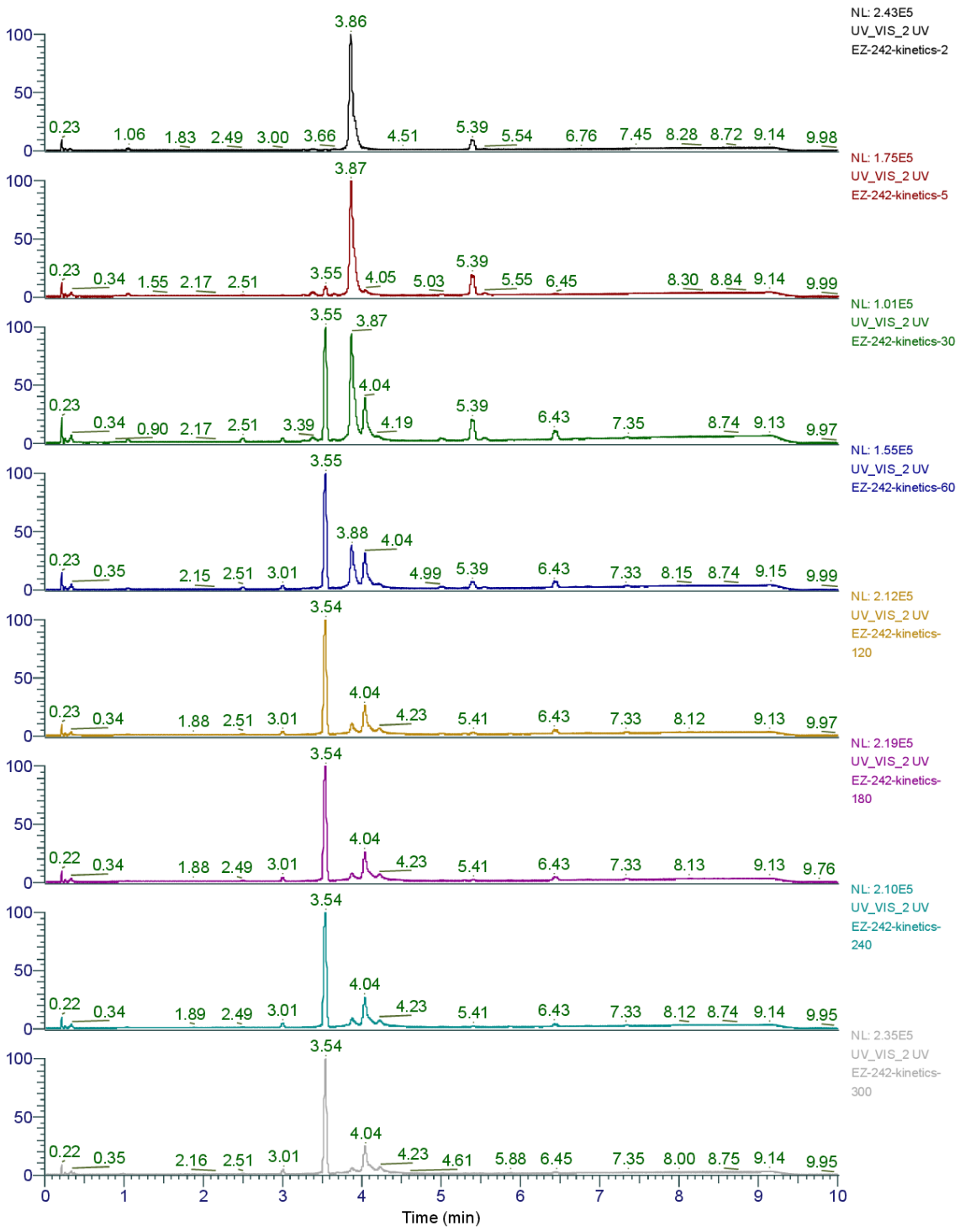

*Figure S4. Primary data for release kinetic of **Z10** in the presence of 1.2 eq TCEP at 37°C in PBS at pH 7 determined by HPLC. Retention times in 10 min run: starting **Z10** at 3.86 min, released dendrimer **Z2** at 3.54 min, released Doxorubicin at 4.04 min.*

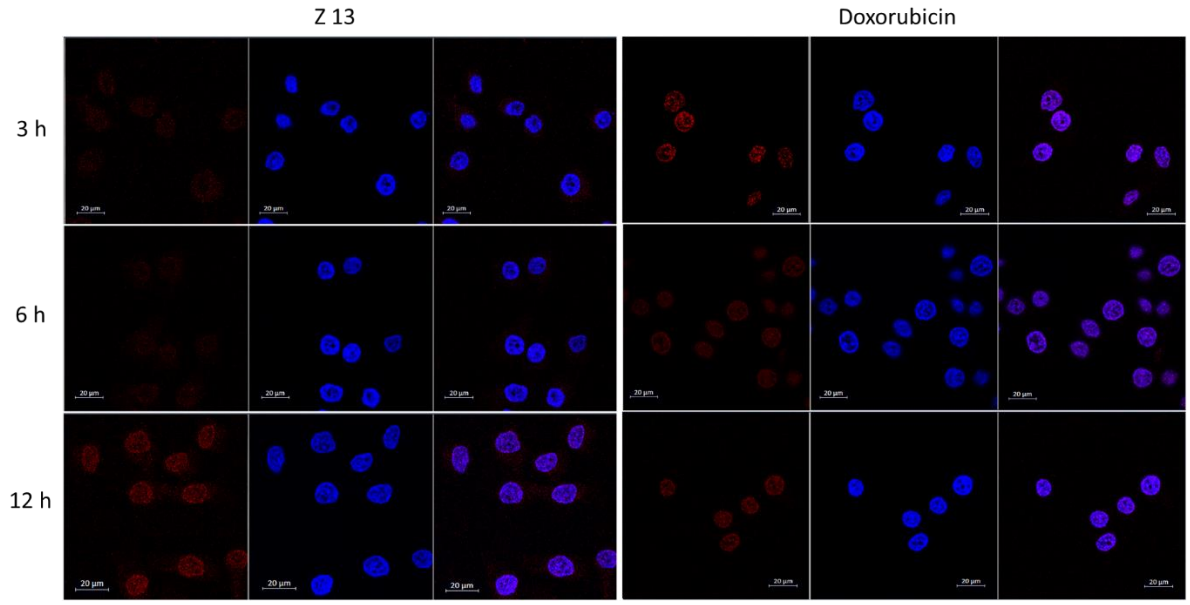

*Figure S5. Confocal microscopy of **Z13** and Doxorubicin in fixed HeLa cells after 3,6, 12 hour incubation at 37ºC with 1 μM of compound. Blue - Hoechst33258, red – compound (Doxorubicin). Scale bar 20 μm.*

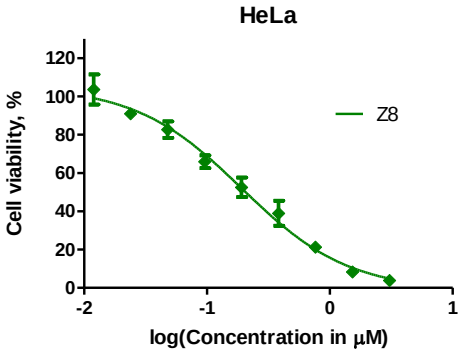

*Figure S6. Cytotoxicity of **Z8** in HeLa cell lines. The cells were incubated with compound at 37°C for 72 hours.*

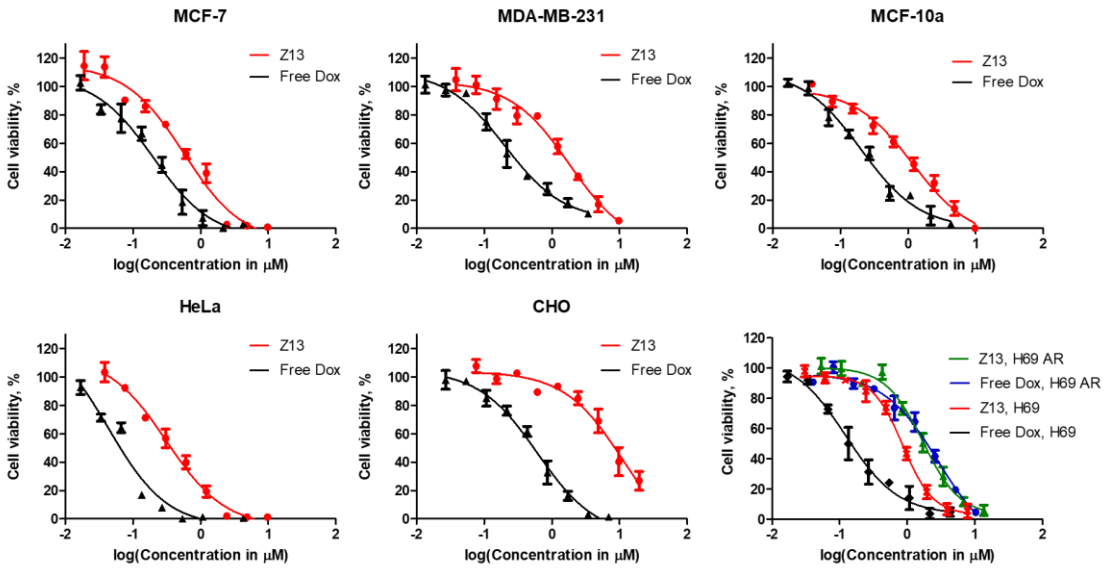

*Figure S7. Cytotoxicity of **Z13** and Doxorubicin, in MCF-7, MDA-MB-231, MCF-10a, HeLa, CHO, H69 and H69 AR cell lines. The cells were incubated with compounds at 37°C for 72 hours.*

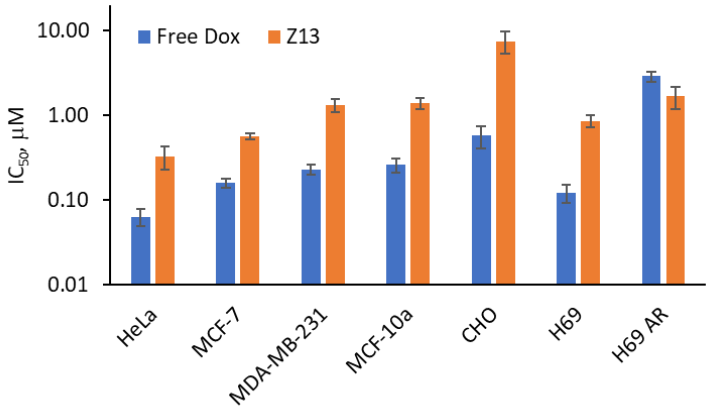

*Figure S8. Comparison of IC_{50} values of Doxorubicin and **Z13** among panel of cell lines.*

Table S1 Selectivity indices calculated as $(IC_{50}^{1}/IC_{50}^{2})$.

Selectivity index	**Z13**	Doxorubicin
CHO/HeLa	22.73	9.06
CHO/MCF-7	13.16	3.63
CHO/MDA-MB-231	5.64	2.52
CHO/H69	8.72	4.71
CHO/H69 AR	4.44	0.20
MCF-10a/HeLa	4.24	4.06
MCF-10a/MCF-7	2.46	1.63
MCF-10a/MDA-MB-231	1.05	1.13
MCF-10a/H69	1.63	2.11
MCF-10a/H69 AR	0.83	0.09

8.2. Additional data for Chapter 4

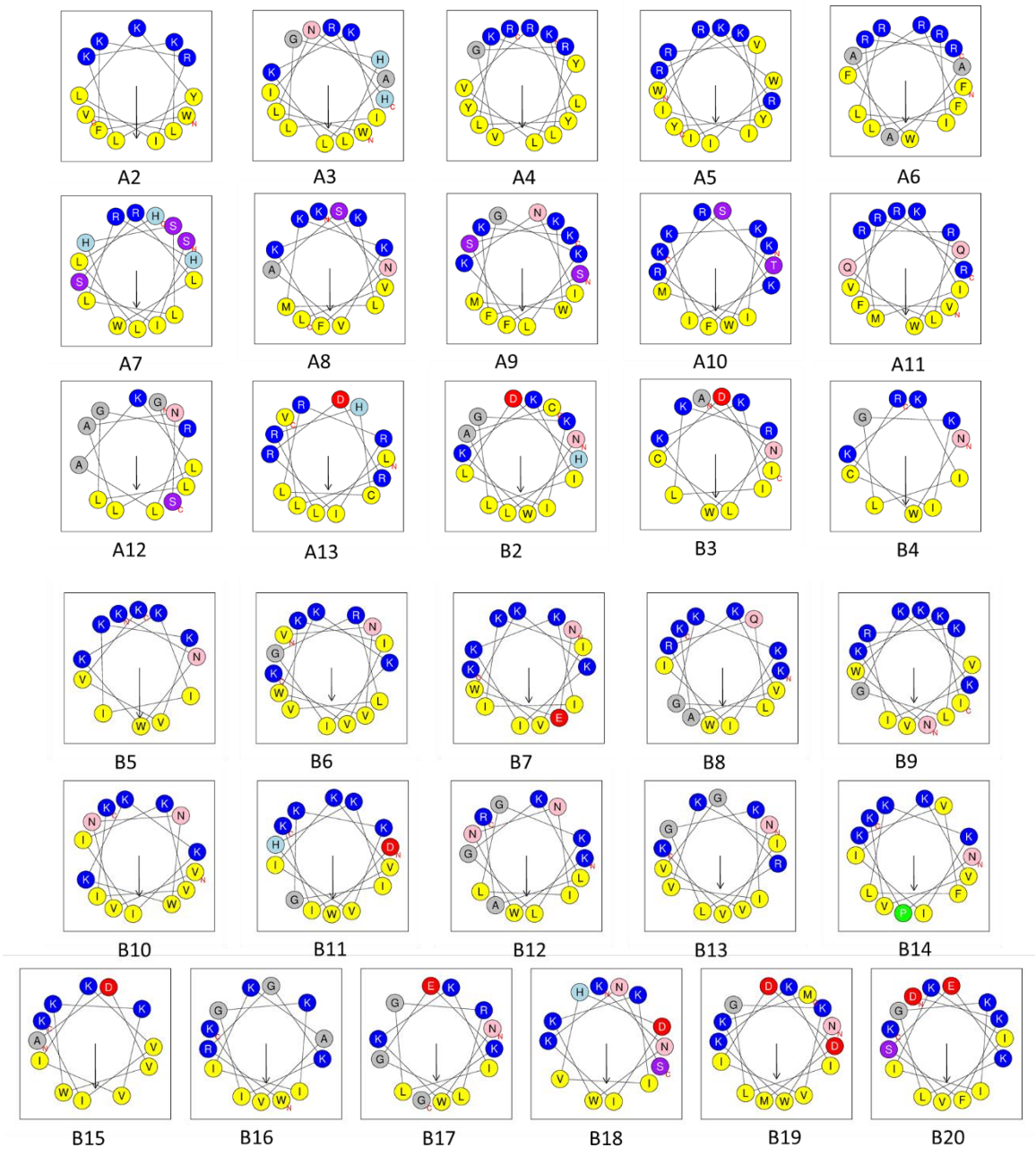

Figure S9. Helix wheels predicted by HeliQuest.[164] Circle size proportional to side-chain size, blue indicates cationic residues, red indicates anionic residues, yellow indicates hydrophobic residues, grey indicates alanine and glycine, pink indicates asparagine, light blue indicates histidine. Arrows represent the helical hydrophobic moment.

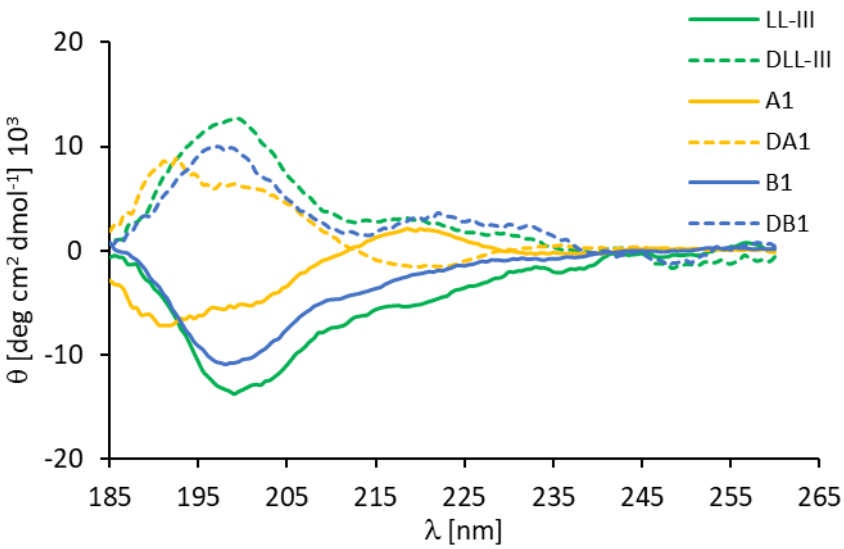

Figure S10. CD spectra of hit peptides (100 µg/mL) in 10 mM phosphate buffer pH 7.4.

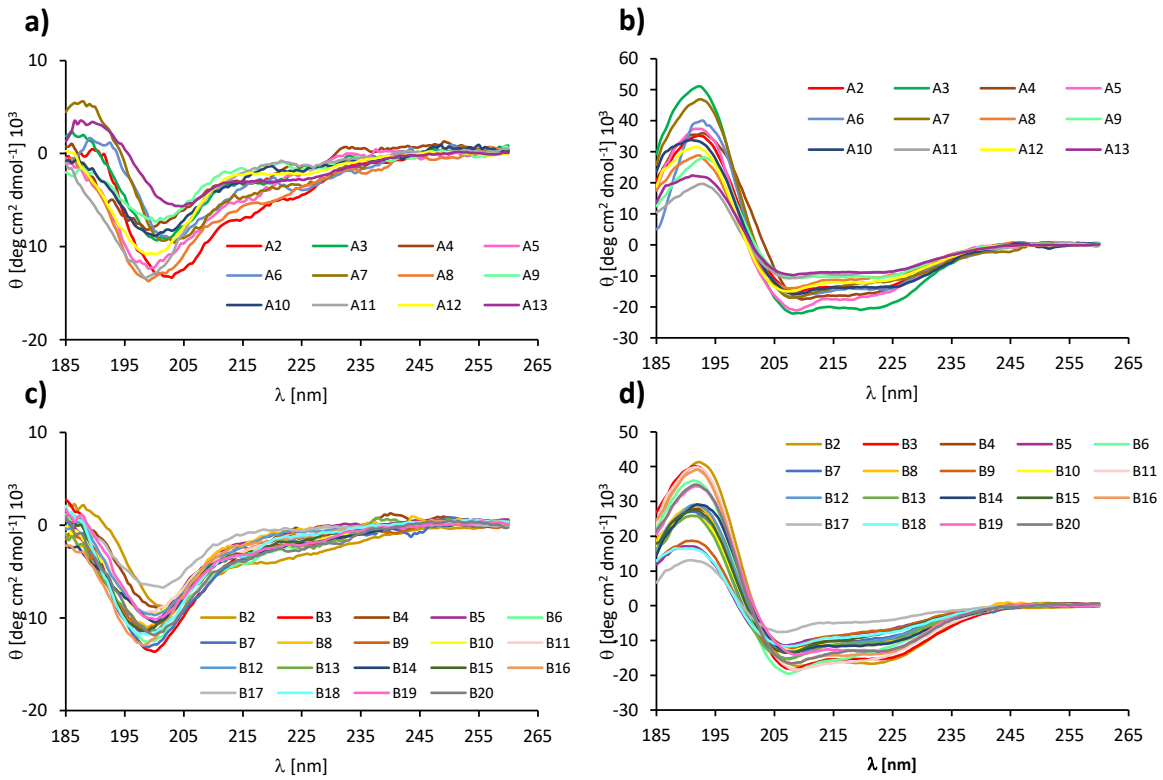

*Figure S11. CD spectra of A2-A13 (**a**), B2-B20 (**c**) at 100 µg/mL in 10 mM phosphate buffer pH 7.4 and (**b**), (**d**) in a presence of 5 mM DPC.*

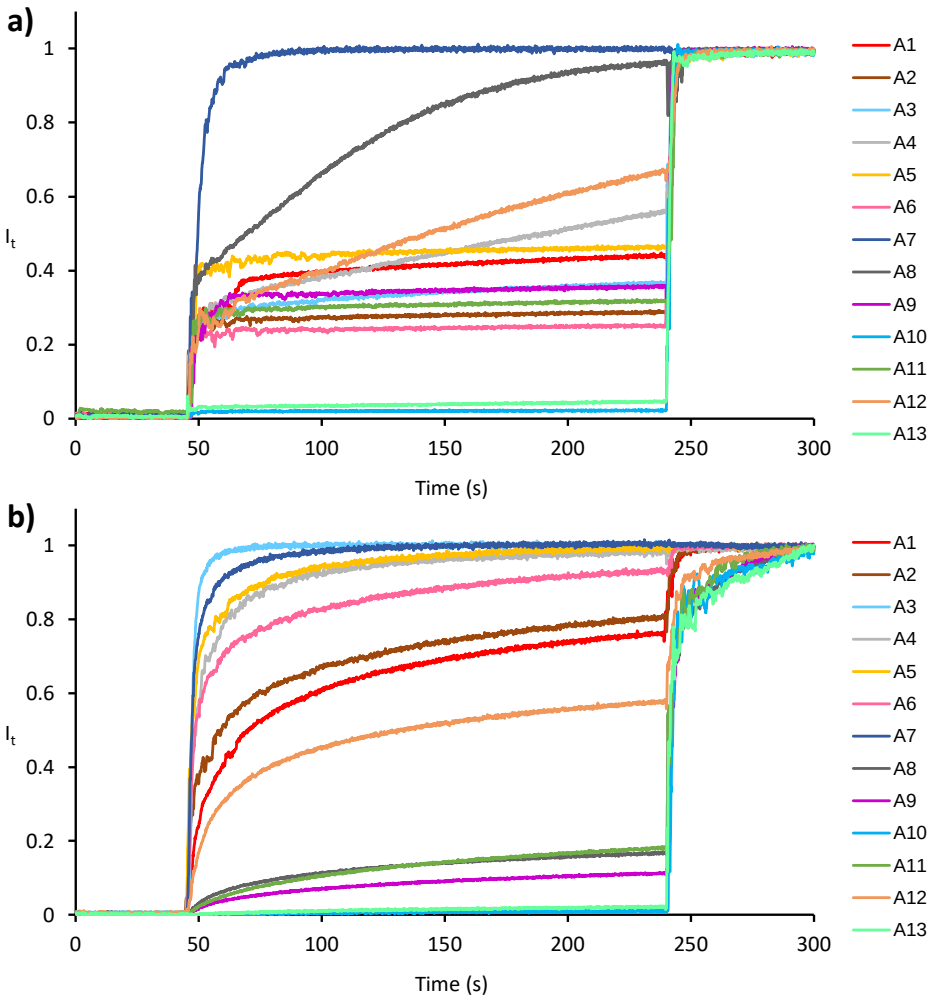

*Figure S12. (**a**) Vesicle leakage experiment of A1-A13 using 5(6)-carboxyfluorescein, at 10 µg/mL. Fluorescein leakage assay from egg yolk phosphatidyl glycerol (PG) lipid vesicles. (**b**) Fluorescein leakage assay from egg yolk phosphatidyl choline (PC) lipid vesicles. Vesicles were suspended in buffer (10 mM TRIS, 107 mM NaCl, pH 7.4) and compounds were added after 45 sec. After 240 seconds 1.2% Triton X-100 was added for full release of fluorescein.*

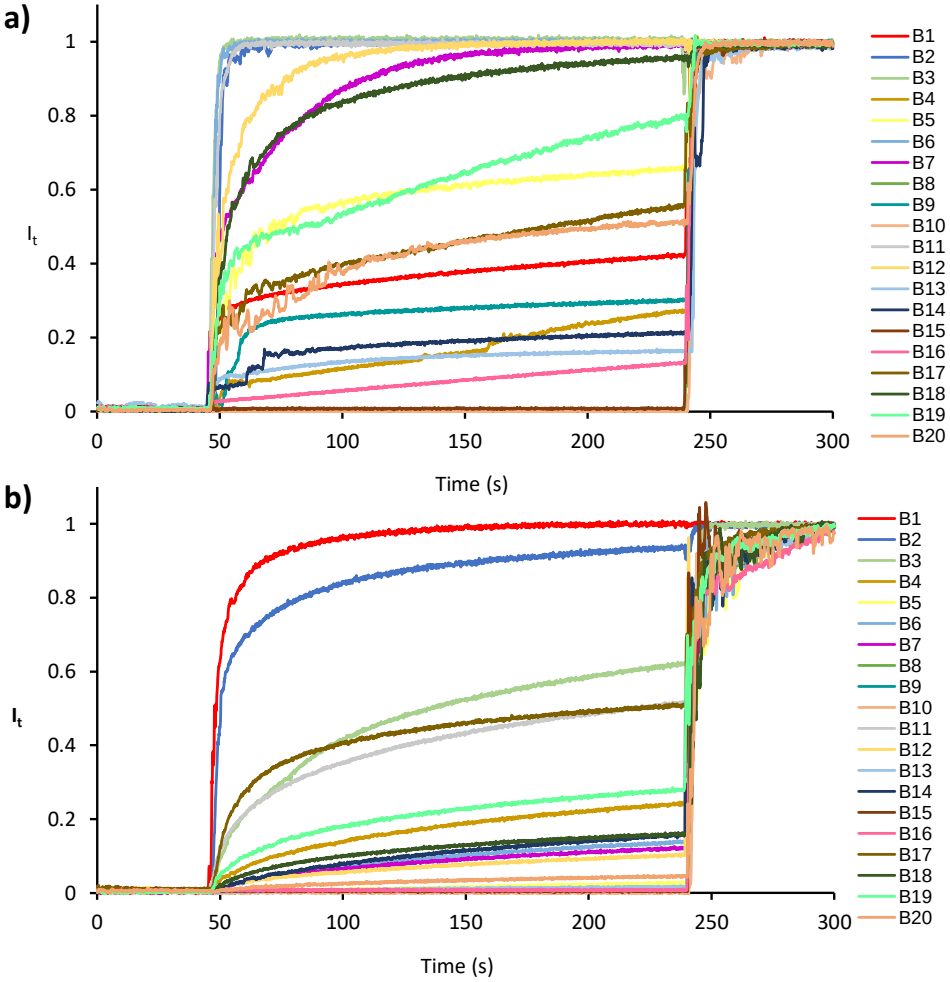

*Figure S13. (**a**) Vesicle leakage experiment of B1-B20 using 5(6)-carboxyfluorescein, at 10 μg/mL. Fluorescein leakage assay from egg yolk phosphatidyl glycerol (PG)* lipid vesicles. ***(b)*** *Fluorescein leakage assay from egg yolk phosphatidyl choline (PC)* lipid vesicles. *Vesicles were suspended in buffer (10 mM TRIS, 107 mM NaCl, pH 7.4) and compounds were added after 45 sec. After 240 seconds 1.2% Triton X-100 was added for full release of fluorescein.*

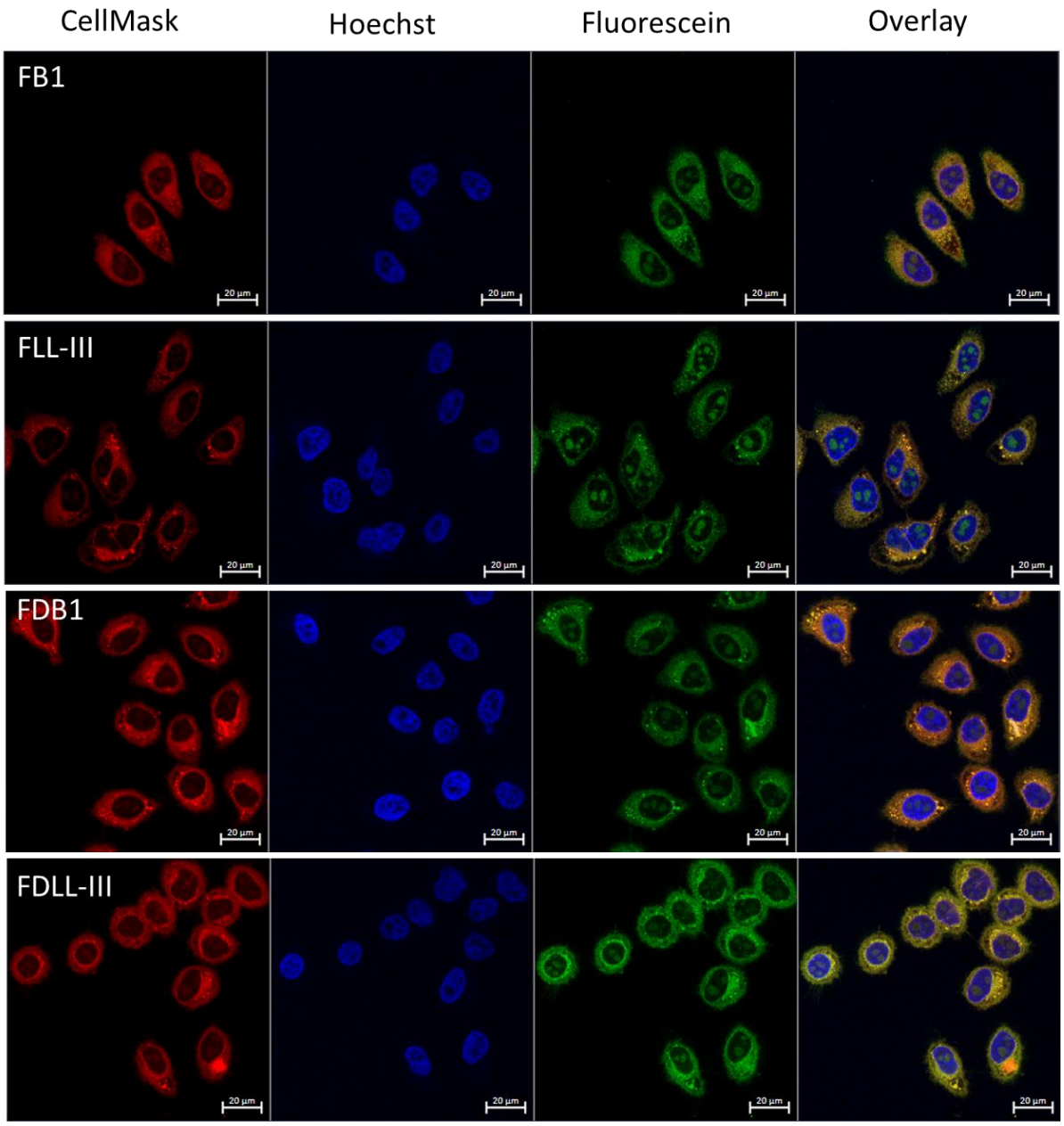

Figure S14. Confocal microscopy of HeLa cells, incubated for 2 h with 10 µM fluorescein-labelled ACPs; Cell plasma membrane is in red (CellMask), Nucleus is in blue (Hoechst33258), compounds are in green (Fluorescein). Scale bar 20 µm.

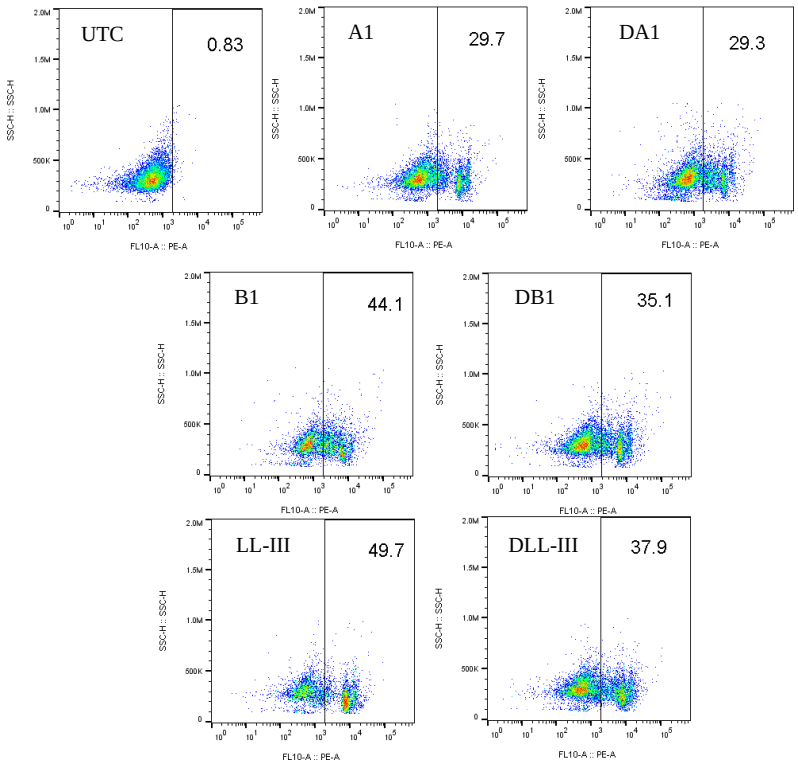

Figure S15. Propidium Iodine (PI) entrance to HeLa cells, treated by 10 μM of peptides and incubated for 10 min, was detected by FACS.

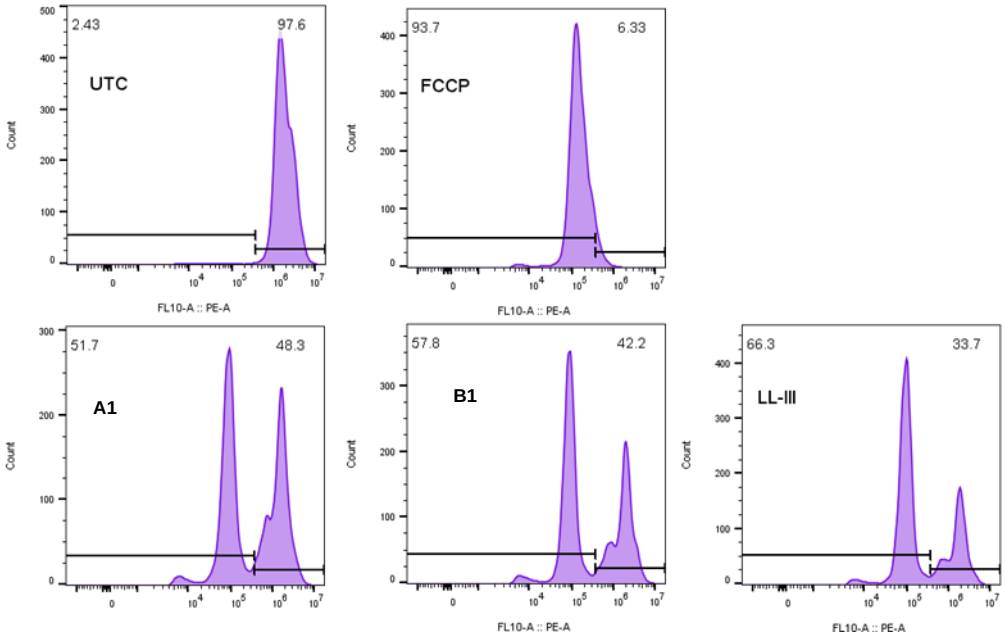

Figure S16. Mitochondrial Membrane Potential (MMP) depolarization as detected by FACS. HeLa cells were treated by 15 μM of ACPs and incubated for 15 min. UTC – untreated cells, Carbonyl cyanide-p-trifluoromethoxyphenylhydrazone (FCCP) 50 μM was used as a positive control.

8.3. Additional data for Chapter 5

Table S2. Dichroweb analysis of peptide and isopeptide dendrimers.

Cpd.	CD α/β/t/u (%)[a]					
	5 mM DPC			Buffer 10 mM		
	pH 5.0	pH 7.4	pH 8.0	pH 5.0	pH 7.4	pH 8.0
EZ-282	25/24/23/28	39/14/21/26	38/15/21/26	13/27/25/35	12/28/26/34	15/26/25/34
G3KL	16/28/24/32	25/20/25/30	31/18/22/29	12/28/24/36	12/28/25/35	14/25/26/35
T7	33/19/20/28	42/13/20/25	42/12/20/26	12/28/23/37	14/26/25/35	13/27/26/34
EZ-209	8/36/23/33	12/30/25/33	8/36/23/33	12/33/23/32	10/32/24/34	7/36/22/35
EZ-211	8/36//22/34	9/34/24/33	9/34/24/33	10/35/22/33	9/34/24/33	10/32/24/34
EZ-212	7/38/21/34	9/34/24/33	10/32/24/34	10/36/22/32	9/33/24/34	9/33/24/34

[a] CD spectra were recorded at 0.100 mg/mL in aqueous 10 mM phosphate buffer for pH 5.0, 7.4 and 8.0 with and without the addition of 5 mM DPC. The primary CD spectra were analyzed using DichroWeb, and percentages of α-helical (α), β-sheet (β), turns (t) and unordered (u) signals were extracted. The Contin-LL (Provencher and Glockner[189]) method and reference set 4 were used.[190]

Table S3. Preliminary data for peptide dendrimers on other cell lines.

Cpd.	Sequence[a]	IC_{50} (μM)[b]	
		HeLa	MCF-7
EZ-282	$(KL)_8(KKL)_4(KKL)_2KLLL$	≈60[c]	≈30[c]
G3KL	$(KL)_8(KKL)_4(KKL)_2KKL$	≈110[c]	≈50[c]
T7	$(KL)_8(KKL)_4(KKLL)_2KKKL$	≈80[c]	≈50[c]

[a] One-letter code for amino acids. *K* are representing branching lysines and K* indicates isopeptide residue. [b] IC_{50} was determined after 72 h incubation at 37°C in DMEM high glucose medium supplemented with 10% FBS. [c] Experiment was performed once in triplicate, the values are approximate.

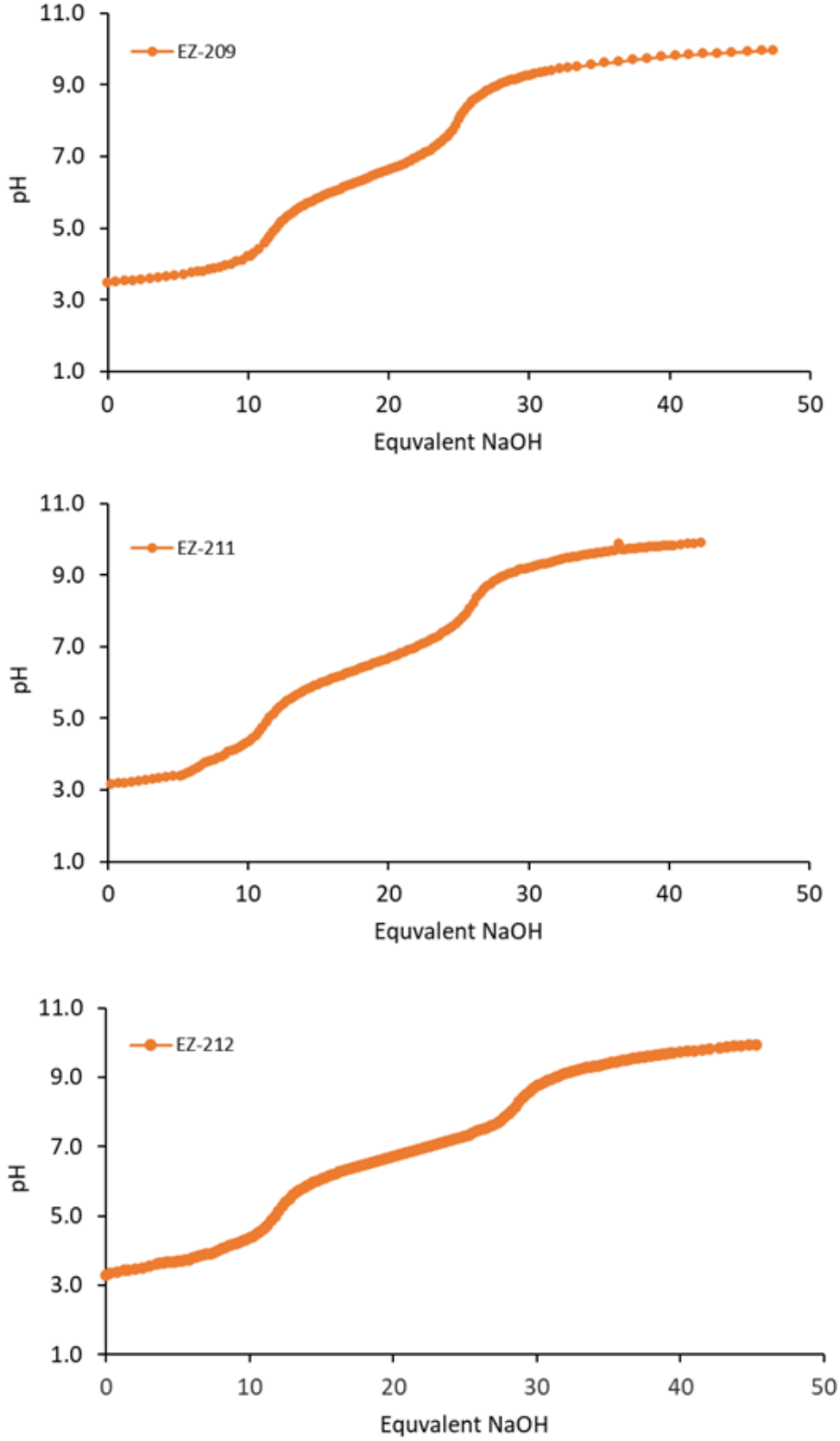

Figure S17. Acid-base titration curves of EZ-209, EZ-211, EZ-212

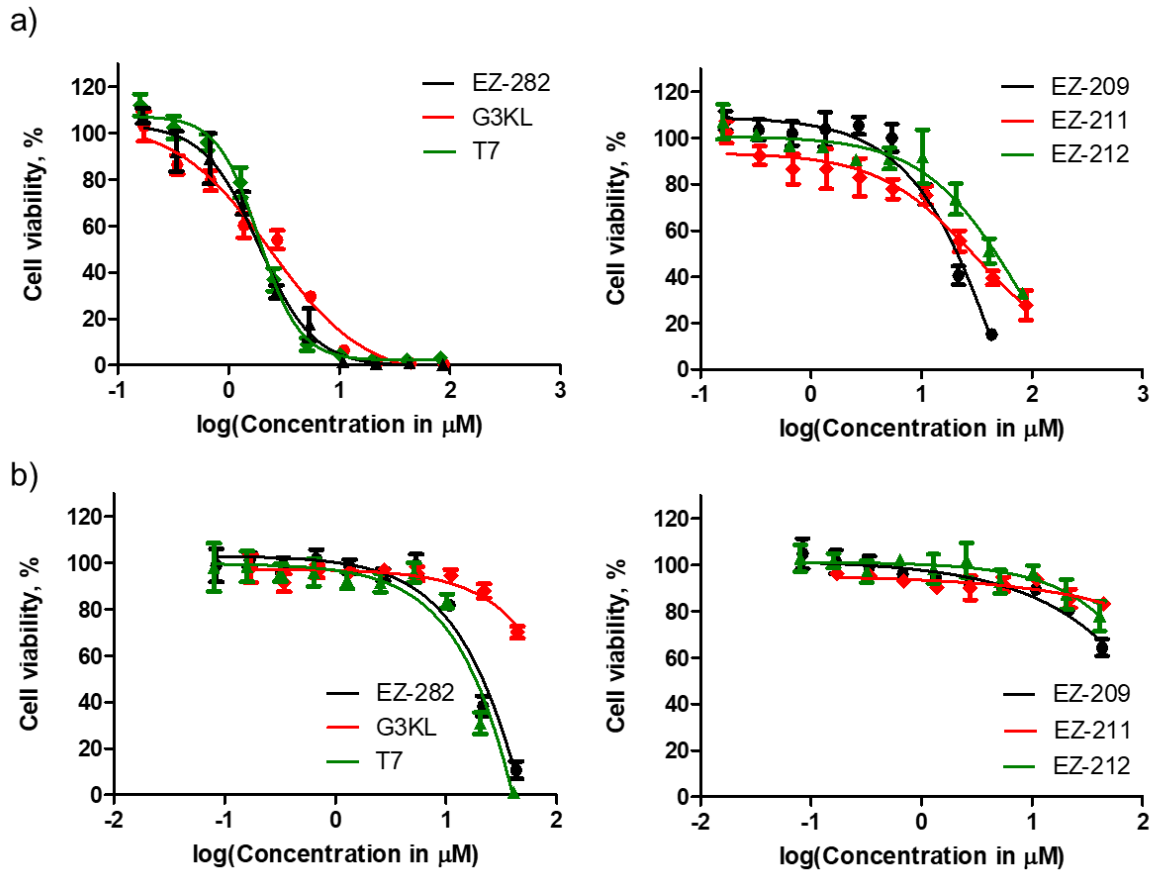

*Figure S18. Viability of (**a**) A549 and (**b**) HEK-293 cells after 72 hours of incubation in presence of the corresponding peptides in a range of concentrations.*

9. Bibliography

(1) Ferlay, J.; Ervik, M.; Lam, F.; Colombet, M.; Mery, L.; Piñeros, M. Global Cancer Observatory: Cancer Today. Lyon: International Agency for Research on Cancer; **2020** https://gco.iarc.fr/today

(2) Ward, R. A.; Fawell, S.; Floc'h, N.; Flemington, V.; McKerrecher, D.; Smith, P. D. Challenges and Opportunities in Cancer Drug Resistance. *Chem. Rev.* **2021**, *121* (6), 3297–3351. https://doi.org/10.1021/acs.chemrev.0c00383.

(3) Zhong, L.; Li, Y.; Xiong, L.; Wang, W.; Wu, M.; Yuan, T.; Yang, W.; Tian, C.; Miao, Z.; Wang, T.; Yang, S. Small Molecules in Targeted Cancer Therapy: Advances, Challenges, and Future Perspectives. *Sig Transduct Target Ther* **2021**, *6* (1), 1–48. https://doi.org/10.1038/s41392-021-00572-w.

(4) Housman, G.; Byler, S.; Heerboth, S.; Lapinska, K.; Longacre, M.; Snyder, N.; Sarkar, S. Drug Resistance in Cancer: An Overview. *Cancers* **2014**, *6* (3), 1769–1792. https://doi.org/10.3390/cancers6031769.

(5) Robey, R. W.; Pluchino, K. M.; Hall, M. D.; Fojo, A. T.; Bates, S. E.; Gottesman, M. M. Revisiting the Role of ABC Transporters in Multidrug-Resistant Cancer. *Nat. Rev. Cancer* **2018**, *18* (7), 452–464. https://doi.org/10.1038/s41568-018-0005-8.

(6) Joyce, H.; McCann, A.; Clynes, M.; Larkin, A. Influence of Multidrug Resistance and Drug Transport Proteins on Chemotherapy Drug Metabolism. *Expert Opin. Drug. Metab. Toxicol.* **2015**, *11* (5), 795–809. https://doi.org/10.1517/17425255.2015.1028356.

(7) Michael, M.; Doherty, M. M. Tumoral Drug Metabolism: Overview and Its Implications for Cancer Therapy. *J. Clin. Oncol.* **2005**, *23* (1), 205–229.

(8) Bonanno, L.; Favaretto, A.; Rosell, R. Platinum Drugs and DNA Repair Mechanisms in Lung Cancer. *Anticancer Res.* **2014**, *34* (1), 493–501.

(9) Kandoth, C.; McLellan, M. D.; Vandin, F.; Ye, K.; Niu, B.; Lu, C.; Xie, M.; Zhang, Q.; McMichael, J. F.; Wyczalkowski, M. A.; Leiserson, M. D. M.; Miller, C. A.; Welch, J. S.; Walter, M. J.; Wendl, M. C.; Ley, T. J.; Wilson, R. K.; Raphael, B. J.; Ding, L. Mutational Landscape and Significance across 12 Major Cancer Types. *Nature* **2013**, *502* (7471), 333–339. https://doi.org/10.1038/nature12634.

(10) Pommier, Y.; Sordet, O.; Antony, S.; Hayward, R. L.; Kohn, K. W. Apoptosis Defects and Chemotherapy Resistance: Molecular Interaction Maps and Networks. *Oncogene* **2004**, *23* (16), 2934–2949. https://doi.org/10.1038/sj.onc.1207515.

(11) Arcamone, F.; Cassinelli, G.; Fantini, G.; Grein, A.; Orezzi, P.; Pol, C.; Spalla, C. Adriamycin, 14-Hydroxydaimomycin, a New Antitumor Antibiotic from S. Peucetius Var. Caesius. *Biotechnol. Bioeng.* **1969**, *11* (6), 1101–1110. https://doi.org/10.1002/bit.260110607.

(12) Tacar, O.; Sriamornsak, P.; Dass, C. R. Doxorubicin: An Update on Anticancer Molecular Action, Toxicity and Novel Drug Delivery Systems. *J. Pharm. Pharmacol.* **2013**, *65* (2), 157–170. https://doi.org/10.1111/j.2042-7158.2012.01567.x.

(13) Speelmans, G.; Staffhorst, R. W. H. M.; de Kruijff, B.; de Wolf, F. A. Transport Studies of Doxorubicin in Model Membranes Indicate a Difference in Passive Diffusion across and Binding at the Outer and Inner Leaflet of the Plasma Membrane. *Biochemistry* **1994**, *33* (46), 13761–13768. https://doi.org/10.1021/bi00250a029.

(14) Faraji, A.; Manshadi, H. R. D.; Mobaraki, M.; Zare, M.; Houshmand, M. Association of ABCB1 and SLC22A16 Gene Polymorphisms with Incidence of Doxorubicin-Induced Febrile Neutropenia: A Survey of Iranian Breast Cancer Patients. *PLOS ONE* **2016**, *11* (12), 1–10. https://doi.org/10.1371/journal.pone.0168519.

(15) Yang, F.; Teves, S. S.; Kemp, C. J.; Henikoff, S. Doxorubicin, DNA Torsion, and Chromatin Dynamics. *Biochim. Biophys. Acta Rev. Cancer* **2014**, *1845* (1), 84–89. https://doi.org/10.1016/j.bbcan.2013.12.002.

(16) Nagy, A.; Armatis, P.; Schally, A. V. High Yield Conversion of Doxorubicin to 2-Pyrrolinodoxorubicin, an Analog 500-1000 Times More Potent: Structure-Activity Relationship of Daunosamine-Modified Derivatives of Doxorubicin. *Proc. Natl. Acad. Sci. U. S. A.* **1996**, *93* (6), 2464–2469. https://doi.org/10.1073/pnas.93.6.2464.

(17) Nagy, A.; Armatis, P.; Cai, R.-Z.; Szepeshazi, K.; Halmos, G.; Schally, A. V. Design, Synthesis, and in Vitro Evaluation of Cytotoxic Analogs of Bombesin-like Peptides Containing Doxorubicin or Its Intensely Potent Derivative, 2-Pyrrolinodoxorubicin. *Proc. Natl. Acad. Sci. U. S. A.* **1997**, *94* (2), 652–656. https://doi.org/10.1073/pnas.94.2.652.

(18) Studenovsky, M.; Ulbrich, K.; Ibrahimova, M.; Rihova, B. Polymer Conjugates of the Highly Potent Cytostatic Drug 2-Pyrrolinodoxorubicin. *Eur. J. Pharm. Sci.* **2011**, *42* (1), 156–163. https://doi.org/10.1016/j.ejps.2010.11.006.

(19) Stepankova, J.; Studenovsky, M.; Malina, J.; Kasparkova, J.; Liskova, B.; Novakova, O.; Ulbrich, K.; Brabec, V. DNA Interactions of 2-Pyrrolinodoxorubicin, a Distinctively More Potent Daunosamine-Modified Analogue of Doxorubicin. *Biochem. Pharmacol.* **2011**, *82* (3), 227–235. https://doi.org/10.1016/j.bcp.2011.04.010.

(20) Koch, T. H.; Barthel, B. L.; Kalet, B. T.; Rudnicki, D. L.; Post, G. C.; Burkhart, D. J. Anthracycline–Formaldehyde Conjugates and Their Targeted Prodrugs. In *Anthracycline Chemistry and Biology II: Mode of Action, Clinical Aspects and New Drugs*; Krohn, K., Ed.; Topics in Current Chemistry; Springer: Berlin, Heidelberg, 2008; pp 141–170. https://doi.org/10.1007/128_2007_4.

(21) Arnesano, F.; Natile, G. Mechanistic Insight into the Cellular Uptake and Processing of Cisplatin 30 Years after Its Approval by FDA. *Coord. Chem. Rev.* **2009**, *253* (15), 2070–2081. https://doi.org/10.1016/j.ccr.2009.01.028.

(22) Gately, D. P.; Howell, S. B. Cellular Accumulation of the Anticancer Agent Cisplatin: A Review. *Br. J. Cancer* **1993**, *67* (6), 1171–1176. https://doi.org/10.1038/bjc.1993.221.

(23) Johnstone, T. C.; Suntharalingam, K.; Lippard, S. J. Third Row Transition Metals for the Treatment of Cancer. *Philos. Trans. Royal Soc. A* **2015**, *373* (2037), 20140185. https://doi.org/10.1098/rsta.2014.0185.

(24) Johnstone, T. C.; Suntharalingam, K.; Lippard, S. J. The Next Generation of Platinum Drugs: Targeted Pt(II) Agents, Nanoparticle Delivery, and Pt(IV) Prodrugs. *Chem. Rev.* **2016**, *116* (5), 3436–3486. https://doi.org/10.1021/acs.chemrev.5b00597.

(25) Voland, C.; Bord, A.; Péleraux, A.; Pénarier, G.; Carrière, D.; Galiègue, S.; Cvitkovic, E.; Jbilo, O.; Casellas, P. Repression of Cell Cycle–Related Proteins by Oxaliplatin but Not Cisplatin in Human Colon Cancer Cells. *Mol. Cancer Ther.* **2006**, *5* (9), 2149–2157. https://doi.org/10.1158/1535-7163.MCT-05-0212.

(26) Zhang, S.; Lovejoy, K. S.; Shima, J. E.; Lagpacan, L. L.; Shu, Y.; Lapuk, A.; Chen, Y.; Komori, T.; Gray, J. W.; Chen, X.; Lippard, S. J.; Giacomini, K. M. Organic Cation Transporters Are Determinants of Oxaliplatin Cytotoxicity. *Cancer Res.* **2006**, *66* (17), 8847–8857. https://doi.org/10.1158/0008-5472.CAN-06-0769.

(27) Li, X.; Liu, Y.; Tian, H. Current Developments in Pt(IV) Prodrugs Conjugated with Bioactive Ligands. *Bioinorg. Chem. Appl.* **2018**, *2018*, e8276139. https://doi.org/10.1155/2018/8276139.

(28) Hanušová, V.; Boušová, I.; Skálová, L. Possibilities to Increase the Effectiveness of Doxorubicin in Cancer Cells Killing. *Drug Metab. Rev.* **2011**, *43* (4), 540–557. https://doi.org/10.3109/03602532.2011.609174.

(29) Gavas, S.; Quazi, S.; Karpiński, T. M. Nanoparticles for Cancer Therapy: Current Progress and Challenges. *Nanoscale Res. Lett.* **2021**, *16*, 173. https://doi.org/10.1186/s11671-021-03628-6.

(30) Hu, C.-M. J.; Zhang, L. Therapeutic Nanoparticles to Combat Cancer Drug Resistance. *Curr. Drug Metab.* **2009**, *10* (8), 836–841. https://doi.org/10.2174/138920009790274540.

(31) Duan, X.; He, C.; Kron, S. J.; Lin, W. Nanoparticle Formulations of Cisplatin for Cancer Therapy. *Wiley Interdiscip. Rev. Nanomed. Nanobiotechnol.* **2016**, *8* (5), 776–791. https://doi.org/10.1002/wnan.1390.

(32) Duggan, S. T.; Keating, G. M. Pegylated Liposomal Doxorubicin. *Drugs* **2011**, *71* (18), 2531–2558. https://doi.org/10.2165/11207510-000000000-00000.

(33) Chan, S.; Davidson, N.; Juozaityte, E.; Erdkamp, F.; Pluzanska, A.; Azarnia, N.; Lee, L. W. Phase III Trial of Liposomal Doxorubicin and Cyclophosphamide Compared with Epirubicin and Cyclophosphamide as First-Line Therapy for Metastatic Breast Cancer. *Ann. Oncol.* **2004**, *15* (10), 1527–1534. https://doi.org/10.1093/annonc/mdh393.

(34) Celsion. *A Phase III, Randomized, Double Blind, Dummy-Controlled Study of ThermoDox® (Lyso-Thermosensitive Liposomal Doxorubicin-LTLD) in Hepatocellular Carcinoma (HCC) Using Standardized Radiofrequency Ablation (RFA) Treatment Time ≥ 45 Minutes for Solitary Lesions ≥ 3 Cm to ≤ 7 Cm*; Clinical trial registration NCT02112656; clinicaltrials.gov, 2018.

(35) Gong, J.; Yan, J.; Forscher, C.; Hendifar, A. Aldoxorubicin: A Tumor-Targeted Doxorubicin Conjugate for Relapsed or Refractory Soft Tissue Sarcomas. *Drug Des. Devel. Ther.* **2018**, *12*, 777–786. https://doi.org/10.2147/DDDT.S140638.

(36) AEterna Zentaris. *Randomized Controlled Study Comparing AEZS-108 With Doxorubicin as Second Line Therapy for Locally Advanced, Recurrent or Metastatic Endometrial Cancer.*; Clinical trial registration NCT01767155; clinicaltrials.gov, 2018.

(37) Stathopoulos, G. P.; Antoniou, D.; Dimitroulis, J.; Stathopoulos, J.; Marosis, K.; Michalopoulou, P. Comparison of Liposomal Cisplatin versus Cisplatin in Non-Squamous Cell Non-Small-Cell Lung Cancer. *Cancer Chemother. Pharmacol.* **2011**, *68* (4), 945–950. https://doi.org/10.1007/s00280-011-1572-5.

(38) Boulikas, T. Clinical Overview on Lipoplatin™: A Successful Liposomal Formulation of Cisplatin. *Expert Opin. Investig. Drugs.* **2009**, *18* (8), 1197–1218. https://doi.org/10.1517/13543780903114168.

(39) Jehn, C. F.; Boulikas, T.; Kourvetaris, A.; Kofla, G.; Possinger, K.; Lüftner, D. First Safety and Response Results of a Randomized Phase III Study with Liposomal Platin in the Treatment of Advanced Squamous Cell Carcinoma of the Head and Neck (SCCHN). *Anticancer Res.* **2008**, *28* (6B), 3961–3964.

(40) Uchino, H.; Matsumura, Y.; Negishi, T.; Koizumi, F.; Hayashi, T.; Honda, T.; Nishiyama, N.; Kataoka, K.; Naito, S.; Kakizoe, T. Cisplatin-Incorporating Polymeric Micelles (NC-6004) Can Reduce Nephrotoxicity and Neurotoxicity of Cisplatin in Rats. *Br. J. Cancer* **2005**, *93* (6), 678–687. https://doi.org/10.1038/sj.bjc.6602772.

(41) Perez-Soler, R.; Shin, D. M.; Siddik, Z. H.; Murphy, W. K.; Huber, M.; Lee, S. J.; Khokhar, A. R.; Hong, W. K. Phase I Clinical and Pharmacological Study of Liposome-Entrapped NDDP Administered Intrapleurally in Patients with Malignant Pleural Effusions. *Clin. Cancer Res.* **1997**, *3* (3), 373–379.

(42) Working, P. K.; Newman, M. S.; Sullivan, T.; Brunner, M.; Podell, M.; Sahenk, Z.; Turner, N. Comparative Intravenous Toxicity of Cisplatin Solution and Cisplatin Encapsulated in Long-Circulating, Pegylated Liposomes in Cynomolgus Monkeys. *Toxicol. Sci.* **1998**, *46* (1), 155–165. https://doi.org/10.1006/toxs.1998.2555.

(43) Newman, M. S.; Colbern, G. T.; Working, P. K.; Engbers, C.; Amantea, M. A. Comparative Pharmacokinetics, Tissue Distribution, and Therapeutic Effectiveness of Cisplatin Encapsulated in Long-Circulating, Pegylated Liposomes (SPI-077) in Tumor-Bearing Mice. *Cancer Chemother. Pharmacol.* **1999**, *43* (1), 1–7. https://doi.org/10.1007/s002800050855.

(44) Campone, M.; Rademaker-Lakhai, J. M.; Bennouna, J.; Howell, S. B.; Nowotnik, D. P.; Beijnen, J. H.; Schellens, J. H. M. Phase I and Pharmacokinetic Trial of AP5346, a DACH–Platinum–Polymer Conjugate, Administered Weekly for Three out of Every 4 Weeks to Advanced Solid Tumor Patients. *Cancer Chemother. Pharmacol.* **2007**, *60* (4), 523–533. https://doi.org/10.1007/s00280-006-0397-0.

(45) Anselmo, A. C.; Mitragotri, S. Nanoparticles in the Clinic: An Update. *Bioeng. Transl. Med.* **2019**, *4* (3), e10143. https://doi.org/10.1002/btm2.10143.

(46) Wang, L.; Wang, N.; Zhang, W.; Cheng, X.; Yan, Z.; Shao, G.; Wang, X.; Wang, R.; Fu, C. Therapeutic Peptides: Current Applications and Future Directions. *Sig Transduct Target Ther* **2022**, *7* (1), 1–27. https://doi.org/10.1038/s41392-022-00904-4.

(47) Cruciani, R. A.; Barker, J. L.; Zasloff, M.; Chen, H. C.; Colamonici, O. Antibiotic Magainins Exert Cytolytic Activity against Transformed Cell Lines through Channel Formation. *Proc. Natl. Acad. Sci. U. S. A.* **1991**, *88* (9), 3792–3796. https://doi.org/10.1073/pnas.88.9.3792.

(48) Lichtenstein, A.; Ganz, T.; Selsted, M. E.; Lehrer, R. I. In Vitro Tumor Cell Cytolysis Mediated by Peptide Defensins of Human and Rabbit Granulocytes. *Blood* **1986**, *68* (6), 1407–1410. https://doi.org/10.1182/blood.V68.6.1407.1407.

(49) Brady, D.; Grapputo, A.; Romoli, O.; Sandrelli, F. Insect Cecropins, Antimicrobial Peptides with Potential Therapeutic Applications. *Int. J. Mol. Sci.* **2019**, *20* (23), 5862. https://doi.org/10.3390/ijms20235862.

(50) Mader, J. S.; Salsman, J.; Conrad, D. M.; Hoskin, D. W. Bovine Lactoferricin Selectively Induces Apoptosis in Human Leukemia and Carcinoma Cell Lines. *Mol. Cancer Ther.* **2005**, *4* (4), 612–624. https://doi.org/10.1158/1535-7163.MCT-04-0077.

(51) Mader, J. S.; Hoskin, D. W. Cationic Antimicrobial Peptides as Novel Cytotoxic Agents for Cancer Treatment. *Expert Opin. Investig. Drugs.* **2006**, *15* (8), 933–946. https://doi.org/10.1517/13543784.15.8.933.

(52) Harris, F.; Dennison, S. R.; Singh, J.; Phoenix, D. A. On the Selectivity and Efficacy of Defense Peptides with Respect to Cancer Cells. *Med. Res. Rev.* **2013**, *33* (1), 190–234. https://doi.org/10.1002/med.20252.

(53) Gaspar, D.; Veiga, A. S.; Castanho, M. A. R. B. From Antimicrobial to Anticancer Peptides. A Review. *Front. Microbiol.* **2013**, *4*, 1–15.

(54) Izzi, V.; Heljasvaara, R.; Pihlajaniemi, T. Understanding the Extracellular Matrix in Acute Myeloid Leukemia. *Haematologica* **2017**, *102* (11), 1807–1809. https://doi.org/10.3324/haematol.2017.174847.

(55) Li, X.; Shen, B.; Chen, Q.; Zhang, X.; Ye, Y.; Wang, F.; Zhang, X. Antitumor Effects of Cecropin B-LHRH' on Drug-Resistant Ovarian and Endometrial Cancer Cells. *BMC Cancer* **2016**, *16* (1), 251. https://doi.org/10.1186/s12885-016-2287-0.

(56) Barceló-Coblijn, G.; Martin, M. L.; de Almeida, R. F. M.; Noguera-Salvà, M. A.; Marcilla-Etxenike, A.; Guardiola-Serrano, F.; Lüth, A.; Kleuser, B.; Halver, J. E.; Escribá, P. V. Sphingomyelin and Sphingomyelin Synthase (SMS) in the Malignant Transformation of Glioma Cells and in 2-Hydroxyoleic Acid Therapy. *Proc. Natl. Acad. Sci. U. S. A.* **2011**, *108* (49), 19569–19574. https://doi.org/10.1073/pnas.1115484108.

(57) Logozzi, M.; Spugnini, E.; Mizzoni, D.; Di Raimo, R.; Fais, S. Extracellular Acidity and Increased Exosome Release as Key Phenotypes of Malignant Tumors. *Cancer Metastasis Rev.* **2019**, *38* (1), 93–101. https://doi.org/10.1007/s10555-019-09783-8.

(58) Chiangjong, W.; Chutipongtanate, S.; Hongeng, S. Anticancer Peptide: Physicochemical Property, Functional Aspect and Trend in Clinical Application (Review). *Int. J. Oncol.* **2020**, *57* (3), 678–696. https://doi.org/10.3892/ijo.2020.5099.

(59) Brown, L.; Wolf, J. M.; Prados-Rosales, R.; Casadevall, A. Through the Wall: Extracellular Vesicles in Gram-Positive Bacteria, Mycobacteria and Fungi. *Nat. Rev. Microbiol.* **2015**, *13* (10), 620–630. https://doi.org/10.1038/nrmicro3480.

(60) Malanovic, N.; Lohner, K. Gram-Positive Bacterial Cell Envelopes: The Impact on the Activity of Antimicrobial Peptides. *Biochimica et Biophysica Acta (BBA) - Biomembranes* **2016**, *1858* (5), 936–946. https://doi.org/10.1016/j.bbamem.2015.11.004.

(61) Teixeira, V.; Feio, M. J.; Bastos, M. Role of Lipids in the Interaction of Antimicrobial Peptides with Membranes. *Prog. Lipid Res.* **2012**, *51* (2), 149–177. https://doi.org/10.1016/j.plipres.2011.12.005.

(62) Riedl, S.; Zweytick, D.; Lohner, K. Membrane-Active Host Defense Peptides – Challenges and Perspectives for the Development of Novel Anticancer Drugs. *Chem. Phys. Lipids* **2011**, *164* (8), 766–781. https://doi.org/10.1016/j.chemphyslip.2011.09.004.

(63) Leuschner, C.; Hansel, W. Membrane Disrupting Lytic Peptides for Cancer Treatments. *Curr. Pharm. Des. 10* (19), 2299–2310.

(64) Shai, Y. Mode of Action of Membrane Active Antimicrobial Peptides. *Peptide Science* **2002**, *66* (4), 236–248. https://doi.org/10.1002/bip.10260.

(65) Gabernet, G.; Müller, A. T.; Hiss, J. A.; Schneider, G. Membranolytic Anticancer Peptides. *Med. Chem. Commun.* **2016**, *7* (12), 2232–2245. https://doi.org/10.1039/C6MD00376A.

(66) Sui, S.-F.; Wu, H.; Guo, Y.; Chen, K.-S. Conformational Changes of Melittin upon Insertion into Phospholipid Monolayer and Vesicle. *J. Biochem.* **1994**, *116* (3), 482–487.

(67) Gazit, E.; Boman, A.; Boman, H. G.; Shai, Y. Interaction of the Mammalian Antibacterial Peptide Cecropin P1 with Phospholipid Vesicles. *Biochemistry* **1995**, *34* (36), 11479–11488. https://doi.org/10.1021/bi00036a021.

(68) Ludtke, S. J.; He, K.; Heller, W. T.; Harroun, T. A.; Yang, L.; Huang, H. W. Membrane Pores Induced by Magainin. *Biochemistry* **1996**, *35* (43), 13723–13728. https://doi.org/10.1021/bi9620621.

(69) Zasloff, M. Antimicrobial Peptides of Multicellular Organisms. *Nature* **2002**, *415* (6870), 389–395. https://doi.org/10.1038/415389a.

(70) Hilchie, A. L.; Doucette, C. D.; Pinto, D. M.; Patrzykat, A.; Douglas, S.; Hoskin, D. W. Pleurocidin-Family Cationic Antimicrobial Peptides Are Cytolytic for Breast Carcinoma Cells and Prevent Growth of Tumor Xenografts. *Breast Cancer Res.* **2011**, *13* (5), R102. https://doi.org/10.1186/bcr3043.

(71) Risso, A.; Braidot, E.; Sordano, M. C.; Vianello, A.; Macrì, F.; Skerlavaj, B.; Zanetti, M.; Gennaro, R.; Bernardi, P. BMAP-28, an Antibiotic Peptide of Innate Immunity,

Induces Cell Death through Opening of the Mitochondrial Permeability Transition Pore. *Mol. Cell. Biol.* **2002**, *22* (6), 1926–1935. https://doi.org/10.1128/MCB.22.6.1926-1935.2002.

(72) Eliassen, L. T.; Berge, G.; Leknessund, A.; Wikman, M.; Lindin, I.; Løkke, C.; Ponthan, F.; Johnsen, J. I.; Sveinbjørnsson, B.; Kogner, P.; Flægstad, T.; Rekdal, Ø. The Antimicrobial Peptide, Lactoferricin B, Is Cytotoxic to Neuroblastoma Cells in Vitro and Inhibits Xenograft Growth in Vivo. *Int. J. Cancer* **2006**, *119* (3), 493–500. https://doi.org/10.1002/ijc.21886.

(73) Wang, Y.; Li, D.; Shi, H.; Wen, Y.; Yang, L.; Xu, N.; Chen, X.; Chen, X.; Chen, P.; Li, J.; Deng, H.; Wang, C.; Xie, G.; Huang, S.; Mao, Y.; Chen, L.; Zhao, X.; Wei, Y. Intratumoral Expression of Mature Human Neutrophil Peptide-1 Mediates Antitumor Immunity in Mice. *Clin. Cancer Res.* **2009**, *15* (22), 6901–6911. https://doi.org/10.1158/1078-0432.CCR-09-0484.

(74) Leuschner, C.; Hansel, W. Targeting Breast and Prostate Cancers Through Their Hormone Receptors1. *Biol. Reprod.* **2005**, *73* (5), 860–865. https://doi.org/10.1095/biolreprod.105.043471.

(75) Kuriyama, I.; Miyazaki, A.; Tsuda, Y.; Yoshida, H.; Mizushina, Y. Inhibitory Effect of Novel Somatostatin Peptide Analogues on Human Cancer Cell Growth Based on the Selective Inhibition of DNA Polymerase β. *Bioorg. Med. Chem.* **2013**, *21* (2), 403–411. https://doi.org/10.1016/j.bmc.2012.11.024.

(76) Ourth, D. D. Antitumor Cell Activity in Vitro by Myristoylated-Peptide. *Biomed. Pharmacother.* **2011**, *65* (4), 271–274. https://doi.org/10.1016/j.biopha.2011.02.015.

(77) Koskimaki, J. E.; Karagiannis, E. D.; Rosca, E. V.; Vesuna, F.; Winnard, P. T.; Raman, V.; Bhujwalla, Z. M.; Popel, A. S. Peptides Derived from Type IV Collagen, CXC Chemokines, and Thrombospondin-1 Domain-Containing Proteins Inhibit Neovascularization and Suppress Tumor Growth in MDA-MB-231 Breast Cancer Xenografts. *Neoplasia* **2009**, *11* (12), 1285-IN2. https://doi.org/10.1593/neo.09620.

(78) Lee, H. S.; Park, C. B.; Kim, J. M.; Jang, S. A.; Park, I. Y.; Kim, M. S.; Cho, J. H.; Kim, S. C. Mechanism of Anticancer Activity of Buforin IIb, a Histone H2A-Derived Peptide. *Cancer Lett.* **2008**, *271* (1), 47–55. https://doi.org/10.1016/j.canlet.2008.05.041.

(79) Chan, Y. R.; Gallo, R. L. PR-39, a Syndecan-Inducing Antimicrobial Peptide, Binds and Affects P130Cas*. *J. Biol. Chem.* **1998**, *273* (44), 28978–28985. https://doi.org/10.1074/jbc.273.44.28978.

(80) Rérole, A.-L.; Gobbo, J.; De Thonel, A.; Schmitt, E.; Pais de Barros, J. P.; Hammann, A.; Lanneau, D.; Fourmaux, E.; Deminov, O.; Micheau, O.; Lagrost, L.; Colas, P.; Kroemer, G.; Garrido, C. Peptides and Aptamers Targeting HSP70: A Novel Approach for Anticancer Chemotherapy. *Cancer Res.* **2011**, *71* (2), 484–495. https://doi.org/10.1158/0008-5472.CAN-10-1443.

(81) González-Montoya, M.; Cano-Sampedro, E.; Mora-Escobedo, R. Bioactive Peptides from Legumes as Anticancer Therapeutic Agents. *Int. J. Cancer Clin. Res.* **2017**, *4*, 1-10. https://doi.org/10.23937/2378-3419/1410081.

(82) Wang, G.; Li, X.; Wang, Z. APD3: The Antimicrobial Peptide Database as a Tool for Research and Education. *Nucleic Acids Res.* **2016**, *44* (Database issue), D1087–D1093. https://doi.org/10.1093/nar/gkv1278.

(83) Tyagi, A.; Tuknait, A.; Anand, P.; Gupta, S.; Sharma, M.; Mathur, D.; Joshi, A.; Singh, S.; Gautam, A.; Raghava, G. P. S. CancerPPD: A Database of Anticancer Peptides and Proteins. *Nucleic Acids Res.* **2015**, *43* (Database issue), D837–D843. https://doi.org/10.1093/nar/gku892.

(84) Gogoladze, G.; Grigolava, M.; Vishnepolsky, B.; Chubinidze, M.; Duroux, P.; Lefranc, M.-P.; Pirtskhalava, M. Dbaasp: Database of Antimicrobial Activity and Structure of Peptides. *FEMS Microbiol. Lett.* **2014**, *357* (1), 63–68. https://doi.org/10.1111/1574-6968.12489.

(85) Wollowitz, S. Managing High-Potency Active Pharmaceutical Ingredients—A Drug Sponsor's Guide. *Drug Dev. Res.* **2010**, *71* (7), 420–428. https://doi.org/10.1002/ddr.20385.

(86) Reymond, J.-L. Peptide Dendrimers: From Enzyme Models to Antimicrobials and Transfection Reagents. *CHIMIA* **2021**, *75* (6), 535–535. https://doi.org/10.2533/chimia.2021.535.

(87) Eggimann, G. A.; Blattes, E.; Buschor, S.; Biswas, R.; Kammer, S. M.; Darbre, T.; Reymond, J.-L. Designed Cell Penetrating Peptide Dendrimers Efficiently Internalize Cargo into Cells. *Chem. Commun.* **2014**, *50* (55), 7254–7257. https://doi.org/10.1039/C4CC02780A.

(88) Johansson, E. M. V.; Dubois, J.; Darbre, T.; Reymond, J.-L. Glycopeptide Dendrimer Colchicine Conjugates Targeting Cancer Cells. *Bioorg. Med. Chem.* **2010**, *18* (17), 6589–6597. https://doi.org/10.1016/j.bmc.2010.04.026.

(89) Lagnoux, D.; Darbre, T.; Schmitz, M. L.; Reymond, J.-L. Inhibition of Mitosis by Glycopeptide Dendrimer Conjugates of Colchicine. *Eur. J. Chem.* **2005**, *11* (13), 3941–3950. https://doi.org/10.1002/chem.200401294.

(90) Heitz, M.; Javor, S.; Darbre, T.; Reymond, J.-L. Stereoselective PH Responsive Peptide Dendrimers for SiRNA Transfection. *Bioconjugate Chem.* **2019**, *30* (8), 2165–2182. https://doi.org/10.1021/acs.bioconjchem.9b00403.

(91) Zheng, Y.; Shen, Y.; Meng, X.; Wu, Y.; Zhao, Y.; Wu, C. Stabilizing P-Dithiobenzyl Urethane Linkers without Rate-Limiting Self-Immolation for Traceless Drug Release. *ChemMedChem* **2019**, *14* (12), 1196–1203. https://doi.org/10.1002/cmdc.201900248.

(92) Such, G. K.; Yan, Y.; Johnston, A. P. R.; Gunawan, S. T.; Caruso, F. Interfacing Materials Science and Biology for Drug Carrier Design. *Adv. Mater.* **2015**, *27* (14), 2278–2297. https://doi.org/10.1002/adma.201405084.

(93) Dupart, P. S.; Mitra, K.; Lyons, C. E.; Hartman, M. C. T. Photo-Controlled Delivery of a Potent Analogue of Doxorubicin. *Chem. Commun.* **2019**, *55* (39), 5607–5610. https://doi.org/10.1039/C9CC02050K.

(94) Sinha, S. C.; Li, L.-S.; Watanabe, S.; Kaltgrad, E.; Tanaka, F.; Rader, C.; Lerner, R. A.; Barbas III, C. F. Aldolase Antibody Activation of Prodrugs of Potent Aldehyde-Containing Cytotoxics for Selective Chemotherapy. *Eur. J. Chem.* **2004**, *10* (21), 5467–5472. https://doi.org/10.1002/chem.200400419.

(95) Jeffrey, S. C.; Nguyen, M. T.; Andreyka, J. B.; Meyer, D. L.; Doronina, S. O.; Senter, P. D. Dipeptide-Based Highly Potent Doxorubicin Antibody Conjugates. *Bioorg. Med. Chem. Lett.* **2006**, *16* (2), 358–362. https://doi.org/10.1016/j.bmcl.2005.09.081.

(96) Cherif, A.; Farquhar, D. N-(5,5-Diacetoxypent-1-Yl)Doxorubicin: A New Intensely Potent Doxorubicin Analog. *J. Med. Chem.* **1992**, *35* (17), 3208–3214. https://doi.org/10.1021/jm00095a017.

(97) Farquhar, D.; Cherif, A.; Bakina, E.; Nelson, J. A. Intensely Potent Doxorubicin Analogues: Structure−Activity Relationship. *J. Med. Chem.* **1998**, *41* (6), 965–972. https://doi.org/10.1021/jm9706980.

(98) Kumari, R.; Majumder, M. M.; Lievonen, J.; Silvennoinen, R.; Anttila, P.; Nupponen, N. N.; Lehmann, F.; Heckman, C. A. Prognostic Significance of Esterase Gene Expression in Multiple Myeloma. *Br. J. Cancer* **2021**, *124* (8), 1428–1436. https://doi.org/10.1038/s41416-020-01237-1.

(99) Torchilin, V. Tumor Delivery of Macromolecular Drugs Based on the EPR Effect. *Adv. Drug Deliv. Rev.* **2011**, *63* (3), 131–135. https://doi.org/10.1016/j.addr.2010.03.011.

(100) Bargh, J. D.; Isidro-Llobet, A.; Parker, J. S.; Spring, D. R. Cleavable Linkers in Antibody–Drug Conjugates. *Chem. Soc. Rev.* **2019**, *48* (16), 4361–4374. https://doi.org/10.1039/C8CS00676H.

(101) Deng, Z.; Hu, J.; Liu, S. Disulfide-Based Self-Immolative Linkers and Functional Bioconjugates for Biological Applications. *Macromolecular Rapid Communications* **2020**, *41* (1), 1900531. https://doi.org/10.1002/marc.201900531.

(102) Sun, T.; Morger, A.; Castagner, B.; Leroux, J.-C. An Oral Redox-Sensitive Self-Immolating Prodrug Strategy. *Chem. Commun.* **2015**, *51* (26), 5721–5724. https://doi.org/10.1039/C5CC00405E.

(103) Davies, A. T.; Slawin, A. M. Z.; Smith, A. D. Enantioselective NHC-Catalyzed Redox [2+2] Cycloadditions with Perfluoroketones: A Route to Fluorinated Oxetanes. *Eur. J. Chem.* **2015**, *21* (52), 18944–18948. https://doi.org/10.1002/chem.201504256.

(104) Yao, X.; Panichpisal, K.; Kurtzman, N.; Nugent, K. Cisplatin Nephrotoxicity: A Review. *Am. J. Med. Sci.* **2007**, *334* (2), 115–124. https://doi.org/10.1097/MAJ.0b013e31812dfe1e.

(105) Reymond, J.-L.; Darbre, T. Peptide and Glycopeptide Dendrimer Apple Trees as Enzyme Models and for Biomedical Applications. *Org. Biomol. Chem.* **2012**, *10* (8), 1483–1492. https://doi.org/10.1039/C2OB06938E.

(106) Śmiłowicz, D.; Metzler-Nolte, N. Synthesis of Monofunctional Platinum(IV) Carboxylate Precursors for Use in Pt(IV)–Peptide Bioconjugates. *Dalton Trans.* **2018**, *47* (43), 15465–15476. https://doi.org/10.1039/C8DT03082K.

(107) Ndinguri, M. W.; Solipuram, R.; Gambrell, R. P.; Aggarwal, S.; Hammer, R. P. Peptide Targeting of Platinum Anti-Cancer Drugs. *Bioconjugate Chem.* **2009**, *20* (10), 1869–1878. https://doi.org/10.1021/bc900065r.

(108) Lee, M.; Simpson, J.; Burns, A.; Kupchinsky, S.; Brooks, N.; Hartley, J.; Kelland, L. Novel Platinum(II) Derivatives of Analogues of Netropsin and Distamycin: Synthesis, DNA Binding and Cytotoxic Properties. *Chem. Med. Res.* **1996**, *6*, 365−371.

(109) Wisnovsky, S. P.; Wilson, J. J.; Radford, R. J.; Pereira, M. P.; Chan, M. R.; Laposa, R. R.; Lippard, S. J.; Kelley, S. O. Targeting Mitochondrial DNA with a Platinum-Based Anticancer Agent. *Chemistry & Biology* **2013**, *20* (11), 1323–1328. https://doi.org/10.1016/j.chembiol.2013.08.010.

(110) Abramkin, S.; Valiahdi, S. M.; Jakupec, M. A.; Galanski, M.; Metzler-Nolte, N.; Keppler, B. K. Solid-Phase Synthesis of Oxaliplatin–TAT Peptide Bioconjugates. *Dalton Trans.* **2012**, *41* (10), 3001–3005. https://doi.org/10.1039/C2DT12024K.

(111) Kulhari, H.; Pooja, D.; Singh, M. K.; Chauhan, A. S. Optimization of Carboxylate-Terminated Poly(Amidoamine) Dendrimer-Mediated Cisplatin Formulation. *Drug Dev. Ind. Pharm.* **2015**, *41* (2), 232–238. https://doi.org/10.3109/03639045.2013.858735.

(112) Song, W.; Li, M.; Tang, Z.; Li, Q.; Yang, Y.; Liu, H.; Duan, T.; Hong, H.; Chen, X. Methoxypoly(Ethylene Glycol)-Block-Poly(L-Glutamic Acid)-Loaded Cisplatin and a Combination With IRGD for the Treatment of Non-Small-Cell Lung Cancers. *Macromol. Biosci.* **2012**, *12* (11), 1514–1523. https://doi.org/10.1002/mabi.201200145.

(113) Shirbin, S. J.; Ladewig, K.; Fu, Q.; Klimak, M.; Zhang, X.; Duan, W.; Qiao, G. G. Cisplatin-Induced Formation of Biocompatible and Biodegradable Polypeptide-Based Vesicles for Targeted Anticancer Drug Delivery. *Biomacromolecules* **2015**, *16* (8), 2463–2474. https://doi.org/10.1021/acs.biomac.5b00692.

(114) Nishiyama, N.; Kataoka, K. Preparation and Characterization of Size-Controlled Polymeric Micelle Containing Cis-Dichlorodiammineplatinum(II) in the Core. *J. Control. Release* **2001**, *74* (1), 83–94. https://doi.org/10.1016/S0168-3659(01)00314-5.

(115) Oberoi, H. S.; Nukolova, N. V.; Zhao, Y.; Cohen, S. M.; Kabanov, A. V.; Bronich, T. K. Preparation and In Vivo Evaluation of Dichloro(1,2-Diaminocyclohexane)Platinum(II)-Loaded Core Cross-Linked Polymer Micelles. *Chemother. Res. Pract.* **2012**, *2012*, 905796. https://doi.org/10.1155/2012/905796.

(116) Quan, X.-Q.; Kang, L.; Yin, X.-Z.; Jin, Z.-H.; Gao, Z.-G. Synthesis of PEGylated Hyaluronic Acid for Loading Dichloro(1,2-Diaminocyclohexane)Platinum(II) (DACHPt) in Nanoparticles for Cancer Treatment. *Chin. Chem. Lett.* **2015**, *26* (6), 695–699. https://doi.org/10.1016/j.cclet.2015.04.024.

(117) Cabral, H.; Nishiyama, N.; Okazaki, S.; Koyama, H.; Kataoka, K. Preparation and Biological Properties of Dichloro(1,2-Diaminocyclohexane)Platinum(II) (DACHPt)-Loaded Polymeric Micelles. *J. Control. Release* **2005**, *101* (1), 223–232. https://doi.org/10.1016/j.jconrel.2004.08.022.

(118) Ueno, T.; Endo, K.; Hori, K.; Ozaki, N.; Tsuji, A.; Kondo, S.; Wakisaka, N.; Murono, S.; Kataoka, K.; Kato, Y.; Yoshizaki, T. Assessment of Antitumor Activity and Acute Peripheral Neuropathy of 1,2-Diaminocyclohexane Platinum (II)-Incorporating Micelles (NC-4016). *Int. J. Nanomedicine* **2014**, *9* (1), 3005–3012. https://doi.org/10.2147/IJN.S60564.

(119) Knop, K.; Hoogenboom, R.; Fischer, D.; Schubert, U. S. Poly(Ethylene Glycol) in Drug Delivery: Pros and Cons as Well as Potential Alternatives. *Angew. Chem. Int. Ed.* **2010**, *49* (36), 6288–6308. https://doi.org/10.1002/anie.200902672.

(120) Hang, Z.; Cooper, M. A.; Ziora, Z. M. Platinum-Based Anticancer Drugs Encapsulated Liposome and Polymeric Micelle Formulation in Clinical Trials. *Biochem. Comp.* **2016**, *4* (1), 2. http://dx.doi.org/10.7243/2052-9341-4-2.

(121) Anthony, E. J.; Bolitho, E. M.; Bridgewater, H. E.; Carter, O. W. L.; Donnelly, J. M.; Imberti, C.; Lant, E. C.; Lermyte, F.; Needham, R. J.; Palau, M.; Sadler, P. J.; Shi, H.; Wang, F.-X.; Zhang, W.-Y.; Zhang, Z. Metallodrugs Are Unique: Opportunities and Challenges of Discovery and Development. *Chem. Sci.* **2020**, *11* (48), 12888–12917. https://doi.org/10.1039/D0SC04082G.

(122) Giannini, F.; Bartoloni, M.; Paul, L. E. H.; Süss-Fink, G.; Reymond, J.-L.; Furrer, J. Cytotoxic Peptide Conjugates of Dinuclear Arene Ruthenium Trithiolato Complexes. *Med. Chem. Commun.* **2015**, *6* (2), 347–350. https://doi.org/10.1039/C4MD00433G.

(123) Stuart, M. C. A.; van de Pas, J. C.; Engberts, J. B. F. N. The Use of Nile Red to Monitor the Aggregation Behavior in Ternary Surfactant–Water–Organic Solvent Systems. *J. Phys. Org. Chem.* **2005**, *18* (9), 929–934. https://doi.org/10.1002/poc.919.

(124) Holohan, C.; Van Schaeybroeck, S.; Longley, D. B.; Johnston, P. G. Cancer Drug Resistance: An Evolving Paradigm. *Nat. Rev. Cancer* **2013**, *13* (10), 714–726. https://doi.org/10.1038/nrc3599.

(125) Vlieghe, P.; Lisowski, V.; Martinez, J.; Khrestchatisky, M. Synthetic Therapeutic Peptides: Science and Market. *Drug Discov. Today* **2010**, *15* (1), 40–56. https://doi.org/10.1016/j.drudis.2009.10.009.

(126) Thundimadathil, J. Cancer Treatment Using Peptides: Current Therapies and Future Prospects. *J. Amino Acids* **2012**, *2012*, e967347. https://doi.org/10.1155/2012/967347.

(127) Carola, L.; William, H. Membrane Disrupting Lytic Peptides for Cancer Treatments. *Curr. Pharm. Des.* **2004**, *10* (19), 2299–2310.

(128) Papo, N.; Shahar, M.; Eisenbach, L.; Shai, Y. A Novel Lytic Peptide Composed of Dl-Amino Acids Selectively Kills Cancer Cells in Culture and in Mice*. *J. Biol. Chem.* **2003**, *278* (23), 21018–21023. https://doi.org/10.1074/jbc.M211204200.

(129) Papo, N.; Shai, Y. Host Defense Peptides as New Weapons in Cancer Treatment. *Cell. Mol. Life Sci.* **2005**, *62* (7), 784–790. https://doi.org/10.1007/s00018-005-4560-2.

(130) Huang, Y.; Wang, X.; Wang, H.; Liu, Y.; Chen, Y. Studies on Mechanism of Action of Anticancer Peptides by Modulation of Hydrophobicity Within a Defined Structural Framework. *Mol. Cancer Ther.* **2011**, *10* (3), 416–426. https://doi.org/10.1158/1535-7163.MCT-10-0811.

(131) Lo, Y.-C.; Rensi, S. E.; Torng, W.; Altman, R. B. Machine Learning in Chemoinformatics and Drug Discovery. *Drug Discov. Today* **2018**, *23* (8), 1538–1546. https://doi.org/10.1016/j.drudis.2018.05.010.

(132) Chen, H.; Engkvist, O.; Wang, Y.; Olivecrona, M.; Blaschke, T. The Rise of Deep Learning in Drug Discovery. *Drug Discov. Today* **2018**, *23* (6), 1241–1250. https://doi.org/10.1016/j.drudis.2018.01.039.

(133) Schneider, G. Automating Drug Discovery. *Nat. Rev. Drug. Discov.* **2018**, *17* (2), 97–113. https://doi.org/10.1038/nrd.2017.232.

(134) Xu, L.; Liang, G.; Wang, L.; Liao, C. A Novel Hybrid Sequence-Based Model for Identifying Anticancer Peptides. *Genes* **2018**, *9* (3), 158. https://doi.org/10.3390/genes9030158.

(135) Vijayakumar, S.; PTV, L. ACPP: A Web Server for Prediction and Design of Anti-Cancer Peptides. *Int. J. Pept. Res. Ther.* **2015**, *21* (1), 99–106. https://doi.org/10.1007/s10989-014-9435-7.

(136) Wei, L.; Zhou, C.; Chen, H.; Song, J.; Su, R. ACPred-FL: A Sequence-Based Predictor Using Effective Feature Representation to Improve the Prediction of Anti-Cancer Peptides. *Bioinformatics* **2018**, *34* (23), 4007–4016. https://doi.org/10.1093/bioinformatics/bty451.

(137) Schaduangrat, N.; Nantasenamat, C.; Prachayasittikul, V.; Shoombuatong, W. ACPred: A Computational Tool for the Prediction and Analysis of Anticancer Peptides. *Molecules* **2019**, *24* (10), 1973. https://doi.org/10.3390/molecules24101973.

(138) Akbar, S.; Hayat, M.; Iqbal, M.; Jan, M. A. IACP-GAEnsC: Evolutionary Genetic Algorithm Based Ensemble Classification of Anticancer Peptides by Utilizing Hybrid Feature Space. *Artif. Intell. Med.* **2017**, *79*, 62–70. https://doi.org/10.1016/j.artmed.2017.06.008.

(139) Chen, W.; Ding, H.; Feng, P.; Lin, H.; Chou, K.-C. IACP: A Sequence-Based Tool for Identifying Anticancer Peptides. *Oncotarget* **2016**, *7* (13), 16895–16909. https://doi.org/10.18632/oncotarget.7815.

(140) Li, F.-M.; Wang, X.-Q. Identifying Anticancer Peptides by Using Improved Hybrid Compositions. *Sci. Rep.* **2016**, *6* (1), 33910. https://doi.org/10.1038/srep33910.

(141) Kabir, M.; Arif, M.; Ahmad, S.; Ali, Z.; Swati, Z. N. K.; Yu, D.-J. Intelligent Computational Method for Discrimination of Anticancer Peptides by Incorporating Sequential and Evolutionary Profiles Information. *Chemom. Intell. Lab. Syst.* **2018**, *182*, 158–165. https://doi.org/10.1016/j.chemolab.2018.09.007.

(142) Manavalan, B.; Basith, S.; Shin, T. H.; Choi, S.; Kim, M. O.; Lee, G. MLACP: Machine-Learning-Based Prediction of Anticancer Peptides. *Oncotarget* **2017**, *8* (44), 77121–77136. https://doi.org/10.18632/oncotarget.20365.

(143) Hajisharifi, Z.; Piryaiee, M.; Mohammad Beigi, M.; Behbahani, M.; Mohabatkar, H. Predicting Anticancer Peptides with Chou′s Pseudo Amino Acid Composition and Investigating Their Mutagenicity via Ames Test. *J. Theor. Biol.* **2014**, *341*, 34–40. https://doi.org/10.1016/j.jtbi.2013.08.037.

(144) Wu, C.; Gao, R.; Zhang, Y.; De Marinis, Y. PTPD: Predicting Therapeutic Peptides by Deep Learning and Word2vec. *BMC Bioinform.* **2019**, *20* (1), 456. https://doi.org/10.1186/s12859-019-3006-z.

(145) Grisoni, F.; Neuhaus, C. S.; Gabernet, G.; Müller, A. T.; Hiss, J. A.; Schneider, G. Designing Anticancer Peptides by Constructive Machine Learning. *ChemMedChem* **2018**, *13* (13), 1300–1302. https://doi.org/10.1002/cmdc.201800204.

(146) Gabernet, G.; Gautschi, D.; Müller, A. T.; Neuhaus, C. S.; Armbrecht, L.; Dittrich, P. S.; Hiss, J. A.; Schneider, G. In Silico Design and Optimization of Selective Membranolytic Anticancer Peptides. *Sci. Rep.* **2019**, *9* (1), 11282. https://doi.org/10.1038/s41598-019-47568-9.

(147) Gogoladze, G.; Grigolava, M.; Vishnepolsky, B.; Chubinidze, M.; Duroux, P.; Lefranc, M.-P.; Pirtskhalava, M. Dbaasp: Database of Antimicrobial Activity and Structure of Peptides. *FEMS Microbiol. Lett.* **2014**, *357* (1), 63–68. https://doi.org/10.1111/1574-6968.12489.

(148) Pirtskhalava, M.; Amstrong, A. A.; Grigolava, M.; Chubinidze, M.; Alimbarashvili, E.; Vishnepolsky, B.; Gabrielian, A.; Rosenthal, A.; Hurt, D. E.; Tartakovsky, M. DBAASP v3: Database of Antimicrobial/Cytotoxic Activity and Structure of Peptides as a Resource for Development of New Therapeutics. *Nucleic Acids Res.* **2021**, *49* (D1), D288–D297. https://doi.org/10.1093/nar/gkaa991.

(149) Bian, Y.; Xie, X.-Q. Generative Chemistry: Drug Discovery with Deep Learning Generative Models. *J. Mol. Model.* **2021**, *27* (3), 71. https://doi.org/10.1007/s00894-021-04674-8.

(150) Capecchi, A.; Zhang, A.; Reymond, J.-L. Populating Chemical Space with Peptides Using a Genetic Algorithm. *J. Chem. Inf. Model.* **2020**, *60* (1), 121–132. https://doi.org/10.1021/acs.jcim.9b01014.

(151) Čeřovský, V.; Buděšínský, M.; Hovorka, O.; Cvačka, J.; Voburka, Z.; Slaninová, J.; Borovičková, L.; Fučík, V.; Bednárová, L.; Votruba, I.; Straka, J. Lasioglossins: Three

Novel Antimicrobial Peptides from the Venom of the Eusocial Bee Lasioglossum Laticeps (Hymenoptera: Halictidae). *ChemBioChem* **2009**, *10* (12), 2089–2099. https://doi.org/10.1002/cbic.200900133.

(152) Capecchi, A.; Cai, X.; Personne, H.; Köhler, T.; Delden, C. van; Reymond, J.-L. Machine Learning Designs Non-Hemolytic Antimicrobial Peptides. *Chem. Sci.* **2021**, *12* (26), 9221–9232. https://doi.org/10.1039/D1SC01713F.

(153) Heffernan, R.; Paliwal, K.; Lyons, J.; Singh, J.; Yang, Y.; Zhou, Y. Single-Sequence-Based Prediction of Protein Secondary Structures and Solvent Accessibility by Deep Whole-Sequence Learning. *J. Comput. Chem.* **2018**, *39* (26), 2210–2216. https://doi.org/10.1002/jcc.25534.

(154) Eisenberg, D.; Weiss, R. M.; Terwilliger, T. C. The Helical Hydrophobic Moment: A Measure of the Amphiphilicity of a Helix. *Nature* **1982**, *299* (5881), 371–374. https://doi.org/10.1038/299371a0.

(155) Slaninová, J.; Mlsová, V.; Kroupová, H.; Alán, L.; Tůmová, T.; Monincová, L.; Borovičková, L.; Fučík, V.; Čeřovský, V. Toxicity Study of Antimicrobial Peptides from Wild Bee Venom and Their Analogs toward Mammalian Normal and Cancer Cells. *Peptides* **2012**, *33* (1), 18–26. https://doi.org/10.1016/j.peptides.2011.11.002.

(156) Kašperová, A.; Turánek, J.; Čeřovský, V.; Raška, M. *In Vitro* and *in Vivo* Antimicrobial Effect of Lasioglossins on the *Candida Albicans*. *Collect. Czech. Chem. Commun.* **2015**, *13*, 54–57. https://doi.org/10.1135/css201113054.

(157) Vrablikova, A.; Czernekova, L.; Cahlikova, R.; Novy, Z.; Petrik, M.; Imran, S.; Novak, Z.; Krupka, M.; Cerovsky, V.; Turanek, J.; Raska, M. Lasioglossins LLIII Affect the Morphogenesis of Candida Albicans and Reduces the Duration of Experimental Vaginal Candidiasis in Mice. *Microbiol. Immunol.* **2017**, *61* (11), 474–481. https://doi.org/10.1111/1348-0421.12538.

(158) Capecchi, A.; Probst, D.; Reymond, J.-L. One Molecular Fingerprint to Rule Them All: Drugs, Biomolecules, and the Metabolome. *J. Cheminf.* **2020**, *12* (1), 43. https://doi.org/10.1186/s13321-020-00445-4.

(159) Owen, D. R. Short Bioactive Peptides and Methods for Their Use. EP1379265A2, January 14, **2004.**

(160) Sanches, P. R. S.; Carneiro, B. M.; Batista, M. N.; Braga, A. C. S.; Lorenzón, E. N.; Rahal, P.; Cilli, E. M. A Conjugate of the Lytic Peptide Hecate and Gallic Acid: Structure, Activity against Cervical Cancer, and Toxicity. *Amino Acids* **2015**, *47* (7), 1433–1443. https://doi.org/10.1007/s00726-015-1980-7.

(161) Gawronska, B.; Leuschner, C.; Enright, F. M.; Hansel, W. Effects of a Lytic Peptide Conjugated to β HCG on Ovarian Cancer: Studies in Vitro and in Vivo. *Gynecol. Oncol.* **2002**, *85* (1), 45–52. https://doi.org/10.1006/gyno.2001.6558.

(162) Slaninová, J.; Putnová, H.; Borovičková, L.; Šácha, P.; Čeřovský, V.; Monincová, L.; Fučík, V. The Antifungal Effect of Peptides from Hymenoptera Venom and Their Analogs. *Open Life Sci.* **2011**, *6* (2), 150–159. https://doi.org/10.2478/s11535-010-0111-4.

(163) Riedl, S.; Zweytick, D.; Lohner, K. Membrane-Active Host Defense Peptides – Challenges and Perspectives for the Development of Novel Anticancer Drugs. *Chem. Phys. Lipids* **2011**, *164* (8), 766–781. https://doi.org/10.1016/j.chemphyslip.2011.09.004.

(164) Gautier, R.; Douguet, D.; Antonny, B.; Drin, G. HELIQUEST: A Web Server to Screen Sequences with Specific α-Helical Properties. *Bioinformatics* **2008**, *24* (18), 2101–2102. https://doi.org/10.1093/bioinformatics/btn392.

(165) Bandyopadhyay, S.; Lee, M.; Sivaraman, J.; Chatterjee, C. Model Membrane Interaction and DNA-Binding of Antimicrobial Peptide Lasioglossin II Derived from Bee Venom. *Biochem. Biophys. Res. Commun.* **2013**, *430* (1), 1–6. https://doi.org/10.1016/j.bbrc.2012.11.015.

(166) Battista, F.; Oliva, R.; Del Vecchio, P.; Winter, R.; Petraccone, L. Insights into the Action Mechanism of the Antimicrobial Peptide Lasioglossin III. *Int. J. Mol. Sci.* **2021**, *22* (6), 2857. https://doi.org/10.3390/ijms22062857.

(167) De Santis, I.; Lorenzini, L.; Moretti, M.; Martella, E.; Lucarelli, E.; Calzà, L.; Bevilacqua, A. Co-Density Distribution Maps for Advanced Molecule Colocalization and Co-Distribution Analysis. *Sensors* **2021**, *21* (19), 6385. https://doi.org/10.3390/s21196385.

(168) Kwok, A.; Eggimann, G. A.; Heitz, M.; Reymond, J.-L.; Hollfelder, F.; Darbre, T. Efficient Transfection of SiRNA by Peptide Dendrimer–Lipid Conjugates. *ChemBioChem* **2016**, *17* (23), 2223–2229. https://doi.org/10.1002/cbic.201600485.

(169) Zamolo, S. J.; Darbre, T.; Reymond, J.-L. Transfecting Tissue Models with CRISPR/Cas9 Plasmid DNA Using Peptide Dendrimers. *Chem. Commun.* **2020**, *56* (80), 11981–11984. https://doi.org/10.1039/D0CC04750C.

(170) Erzina, D.; Capecchi, A.; Javor, S.; Reymond, J.-L. An Immunomodulatory Peptide Dendrimer Inspired from Glatiramer Acetate. *Angew. Chem. Int. Ed.* **2021**, *60* (50), 26403–26408. https://doi.org/10.1002/anie.202113562.

(171) Clouet, A.; Darbre, T.; Reymond, J.-L. A Combinatorial Approach to Catalytic Peptide Dendrimers. *Angew. Chem. Int. Ed.* **2004**, *43* (35), 4612–4615. https://doi.org/10.1002/anie.200460177.

(172) Clouet, A.; Darbre, T.; Reymond, J.-L. Combinatorial Synthesis, Selection, and Properties of Esterase Peptide Dendrimers. *Peptide Sci.* **2006**, *84* (1), 114–123. https://doi.org/10.1002/bip.20394.

(173) Javor, S.; Delort, E.; Darbre, T.; Reymond, J.-L. A Peptide Dendrimer Enzyme Model with a Single Catalytic Site at the Core. *J. Am. Chem. Soc.* **2007**, *129* (43), 13238–13246. https://doi.org/10.1021/ja074115f.

(174) Uhlich, N. A.; Darbre, T.; Reymond, J.-L. Peptide Dendrimer Enzyme Models for Ester Hydrolysis and Aldolization Prepared by Convergent Thioether Ligation. *Org. Biomol. Chem.* **2011**, *9* (20), 7071–7084. https://doi.org/10.1039/C1OB05877K.

(175) Kofoed, J.; Reymond, J.-L. Dendrimers as Artificial Enzymes. *Curr. Opin. Chem. Biol.* **2005**, *9* (6), 656–664. https://doi.org/10.1016/j.cbpa.2005.10.013.

(176) Stach, M.; Siriwardena, T. N.; Köhler, T.; van Delden, C.; Darbre, T.; Reymond, J.-L. Combining Topology and Sequence Design for the Discovery of Potent Antimicrobial Peptide Dendrimers against Multidrug-Resistant Pseudomonas Aeruginosa. *Angew. Chem. Int. Ed.* **2014**, *53* (47), 12827–12831. https://doi.org/10.1002/anie.201409270.

(177) Siriwardena, T. N.; Stach, M.; He, R.; Gan, B.-H.; Javor, S.; Heitz, M.; Ma, L.; Cai, X.; Chen, P.; Wei, D.; Li, H.; Ma, J.; Köhler, T.; van Delden, C.; Darbre, T.; Reymond, J.-L. Lipidated Peptide Dendrimers Killing Multidrug-Resistant Bacteria. *J. Am. Chem. Soc.* **2018**, *140* (1), 423–432. https://doi.org/10.1021/jacs.7b11037.

(178) Siriwardena, T. N.; Capecchi, A.; Gan, B.-H.; Jin, X.; He, R.; Wei, D.; Ma, L.; Köhler, T.; van Delden, C.; Javor, S.; Reymond, J.-L. Optimizing Antimicrobial Peptide Dendrimers in Chemical Space. *Angew. Chem. Int. Ed.* **2018**, *57* (28), 8483–8487. https://doi.org/10.1002/anie.201802837.

(179) Pires, J.; Siriwardena, T. N.; Stach, M.; Tinguely, R.; Kasraian, S.; Luzzaro, F.; Leib, S. L.; Darbre, T.; Reymond, J.-L.; Endimiani, A. In Vitro Activity of the Novel Antimicrobial Peptide Dendrimer G3KL against Multidrug-Resistant Acinetobacter Baumannii and Pseudomonas Aeruginosa. *Antimicrob. Agents Chemother.* *59* (12), 7915–7918. https://doi.org/10.1128/AAC.01853-15.

(180) Siriwardena, T. N.; Gan, B.-H.; Köhler, T.; van Delden, C.; Javor, S.; Reymond, J.-L. Stereorandomization as a Method to Probe Peptide Bioactivity. *ACS Cent. Sci.* **2021**, *7* (1), 126–134. https://doi.org/10.1021/acscentsci.0c01135.

(181) Baeriswyl, S.; Personne, H.; Bonaventura, I. D.; Köhler, T.; Delden, C. van; Stocker, A.; Javor, S.; Reymond, J.-L. A Mixed Chirality α-Helix in a Stapled Bicyclic and a Linear Antimicrobial Peptide Revealed by X-Ray Crystallography. *RSC Chem. Biol.* **2021**, *2* (6), 1608–1617. https://doi.org/10.1039/D1CB00124H.

(182) Cai, X.; Javor, S.; Gan, B. H.; Köhler, T.; Reymond, J.-L. The Antibacterial Activity of Peptide Dendrimers and Polymyxin B Increases Sharply above PH 7.4. *Chem. Commun.* **2021**, *57* (46), 5654–5657. https://doi.org/10.1039/D1CC01838H.

(183) Casares, D.; Escribá, P. V.; Rosselló, C. A. Membrane Lipid Composition: Effect on Membrane and Organelle Structure, Function and Compartmentalization and Therapeutic Avenues. *Int. J. Mol. Sci.* **2019**, *20* (9), 2167. https://doi.org/10.3390/ijms20092167.

(184) Szlasa, W.; Zendran, I.; Zalesińska, A.; Tarek, M.; Kulbacka, J. Lipid Composition of the Cancer Cell Membrane. *J. Bioenerg. Biomembr.* **2020**, *52* (5), 321–342. https://doi.org/10.1007/s10863-020-09846-4.

(185) He, M.; Guo, S.; Ren, J.; Li, Z. In Situ Characterizing Membrane Lipid Phenotype of Human Lung Cancer Cell Lines Using Mass Spectrometry Profiling. *J. Cancer* **2016**, *7* (7), 810–816. https://doi.org/10.7150/jca.14310.

(186) Rosillo, M.; Arnáiz, E.; Abdi, D.; Blanco-Urgoiti, J.; Domínguez, G.; Pérez-Castells, J. Combination of RCM and the Pauson–Khand Reaction: One-Step Synthesis of Tricyclic Structures. *Eur. J. Org. Chem.* **2008**, *2008* (23), 3917–3927. https://doi.org/10.1002/ejoc.200800332.

(187) Govindan, S. V.; McBride, W. J.; Sathyanarayan, N.; Mazza-Ferreira C. Pro-Drug Form (P2pdox) of the Highly Potent 2-Pyrrolinodoxorubicin Conjugated to Antibodies for Targeted Therapy of Cancer. US20140219956A1, December 30, **2015**.

(188) Whitmore, L.; Wallace, B. A. DICHROWEB, an Online Server for Protein Secondary Structure Analyses from Circular Dichroism Spectroscopic Data. *Nucleic Acids Res.* **2004**, *32* (suppl_2), W668–W673. https://doi.org/10.1093/nar/gkh371.

(189) Provencher, S. W.; Gloeckner, J. Estimation of Globular Protein Secondary Structure from Circular Dichroism. *Biochemistry* **1981**, *20* (1), 33–37. https://doi.org/10.1021/bi00504a006.

(190) Sreerama, N.; Woody, R. W. Estimation of Protein Secondary Structure from Circular Dichroism Spectra: Comparison of CONTIN, SELCON, and CDSSTR Methods with an Expanded Reference Set. *Anal. Biochem.* **2000**, *287* (2), 252–260. https://doi.org/10.1006/abio.2000.4880.